THEORETICAL MODELLING OF TWO WAVE-POWER DEVICES

by

Stéphanie Lovas

Submitted to the Department of Civil and Environmental Engineering
in partial fulfillment of the requirements for the degree of

Master of Science in Civil and Environmental Engineering

at the

MASSACHUSETTS INSTITUTE OF TECHNOLOGY

February 2010

Author .....
Department of Civil and Environmental Engineering
December 15, 2009

Certified by .....
Prof. Chiang C. Mei
Ford Professor of Engineering
Department of Civil and Environmental Engineering
Thesis Supervisor

Accepted by .....
Prof. Daniele Veneziano
Chairman, Departmental Committee for Graduate Students

THEORETICAL MODELLING OF TWO WAVE-POWER DEVICES

by

Stéphanie Lovas

Submitted to the Department of Civil and Environmental Engineering
on December 15, 2009, in partial fulfillment of the
requirements for the degree of
Master of Science in Civil and Environmental Engineering

Abstract

Many wave energy devices are currently studied. In this thesis we focus on two specific devices: the Oscillating Water Column (OWC), and the buoys.
In the first part of this thesis we examine the effects of coastline geometry on the performance of an OWC. Under the assumption of inviscid irrotationnal flow, we develop a linear theory for the velocity potential for the case of a coastline of arbitrary apex angle. Scattering and radiation problems are solved separately using eigenfunctions expansions, and are then combined to study the energy extraction rate. Numerical simulations for a convex and a concave corner are considered and comparison with an OWC at the tip of a thin breakwater and on a straight coast are discussed. Assuming that the multiple-turbine system can be controlled over a wide range of frequencies, we study the effects of fixed chamber size and air compressibility on the optimal power extraction. A simpler way of optimization is then develop and we show that this simpler scheme can achieve almost as high an efficiency as the idealized many-frequency optimization.
In the second part of this thesis, we first model theoretically an array of cylinders and then apply the theory developped to an array of buoys. However, numerical difficulties encountered for the array of cylinders have led to the conclusion that the theory developed is numerically inefficient, although it is accurate.

Thesis Supervisor: Prof. Chiang C. Mei
Title: Ford Professor of Engineering
Department of Civil and Environmental Engineering

Acknowledgments

This research has been supported by a Scholter Fellowship and the MIT-Portugal Alliance Grant.

I am grateful to Professor Chiang C. Mei for his guidance and wonderful availability.

I am also grateful to Doctor Yuming Liu for his precious advices.

Finally I would like to thank Rémi Vallerent for his help with Matlab.

Contents

List of Figures

List of Tables

Chapter 1

Introduction

As the world is facing the challenge to reduce its gaz emmission and to find new renewable source of energy, wave power extraction can provide a viable solution. The interest for wave power extraction is not new and the first machine to be taken out was probably by Girard, father and son in 1799 (see Charlier and Finkl (2009))and proposed to take out mechanical energy using a raft. However systematic studies began only in the seventies (see Evans (1981), McCormick (1981)). Many devices have been invented so far, for example the Cockerell's raft (see Haren (1978)) and Salte's duck (see Salter (1976)). However at the present time wave power generation is not a widely employed commercial technology and a lot of research is done to determine which will be the winning device.

Most of the systems use either a movable body (for example buoys) or an oscillating column to extract the energy. The first three chapters of the present thesis concentrate on the oscillating water column (OWC) and on the effect of coastline on its energy extraction performance. OWC geometries have been studied intensively in the past decades. Smith (1958) and then Evans and Porter (1995) have derived methods for simple two-dimensionnal geometries. Three-dimensionnal OWC geometry has been studied by Fernandes (1983).

Recently a pilot OWC plant has been constructed in the 90's in the island of Azores, Portugal, (see picture 1-1a) with a rated power of 400kW (see Falcão (2000) and more recently Neumann et al. (2008)). Lately a new project in Portugal plans

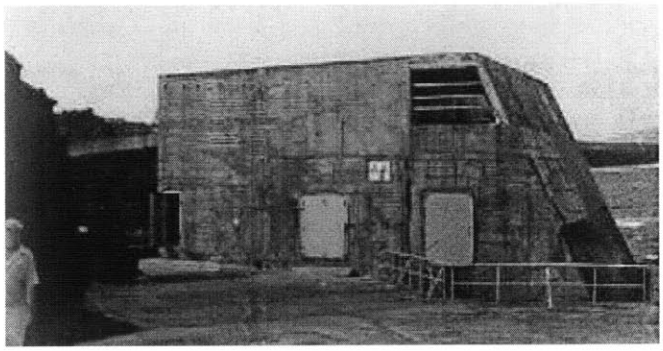

(a) OWC at Pico, island of Azores. Image taken from PI-OWC project.

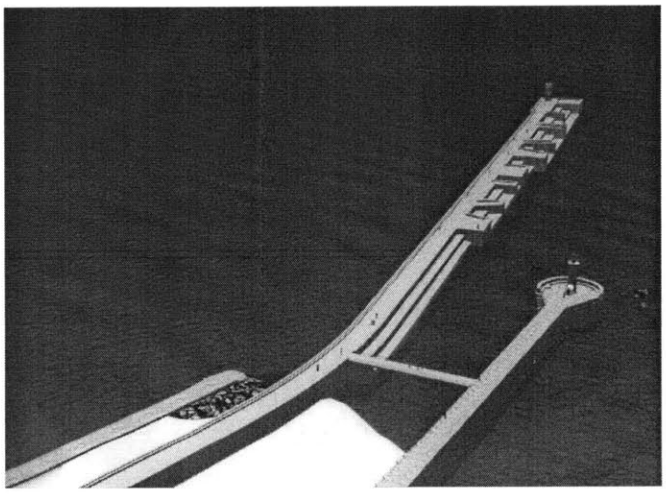

(b) OWC in a breakwater. Mouth of Foz do Douro River, Portugal. Image taken from Martins et al. (2005)

Figure 1-1: Oscillating water column device

to integrate an OWC plant into the head of a new breakwater at the mouth of Douro River in Porto (see figure 1-1b). Ultimately, the installation would include three OWCs, which together would generate 750 kilowatts (see Martins et al. (2005)). Stimulated by this project, two simplified coastline models have already been studied: the case of a thin breakwater has been studied by Martin-Rivas and Mei (2008) and the case of a straight coastline by Martin-Rivas and Mei (2009).

In chapter 2 of the present thesis we develop a general theory for any arbitrary apex angle of the coastline. Scattering problem and radiation problem are solved using eigenfunction expansion and matching conditions. The two problems are then combined to examine the energy extraction rate. We first assume that the power take-off system can be controlled over a wide range of frequencies and study the energy extraction rate. We then develop a new and simpler way of optimization. Numerical computations are then considered for two specific cases: an OWC at the convex corner of right angle coast in chapter 3 and an OWC at the concave corner of right angle coast in chapter 4. In particular we show that the simpler scheme of optimization can achieve almost as high an efficiency as the many-frequency idealized optimization.

In chapter 5 we consider an array of vertical circular cylinders extending to the bottom and in staggered rows. We want to find a new method to find an explicit analytical solution for this problem so that the method can then be applied in chapter 6 to an array of buoys in staggered row as represented in figure 1-2. Many studies have been conducted on array of cylinder, as they are of interest for off-shore structures as oil rigs. A general situation of an arbitrary configuration of N vertical cylinders has been studied by Linton and Evans (1990) who improved the multiple scattering method used by Spring and Monkmeyer (1974). They associate with each cylinder a general wave potential describing wave radiating away from that cylinder, which, together wih the incident wave potential, describes the total wave field.

By the method of images the situation we are focusing on is formally equivalent to the one of three half cylinders in a rectangular channel. The case of a vertical circular cylinder placed at the centreline of a channel has been examined by Linton and Evans

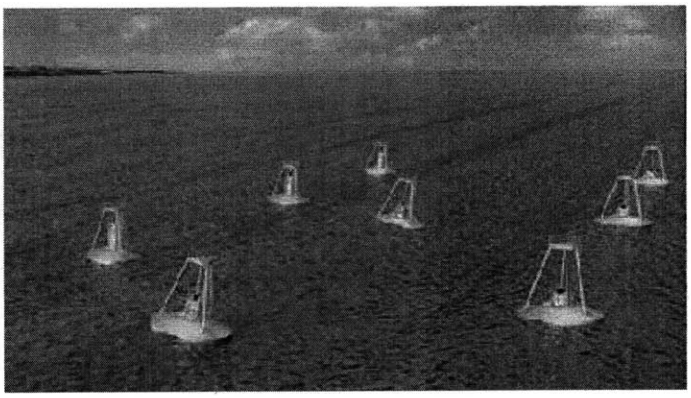

Figure 1-2: Array of buoys. Image taken from Ocean Power Technologies Inc.

(1992a). The method used is based around the construction of suitable multipoles for channel problems. The key to the construction of these multipoles is the derivation of suitable integral representations for solutions to Laplace's equation in the laterally unbounded fluid which can then be modified to take account of the channel walls using a technique similar to that used by Thorne (1953). The procedure is fairly complicated but picks out the correct far-field behaviour. Linton and Evans (1992b) have used Green's functions suitable for a two-dimensional waveguide to construct a homogeneous integral for the case of a obstacle of arbitrary shape, where the cross-section is symmetric with respect to the centreline of the channel. The problem of the scattering of a plane incident wave for a circular cylinder is then considered in detail.

In the present thesis, we first derive the solution that satisies the Laplace equation in the channel and the boundary condition on the laterral walls. We then impose the remaining boundary conditions and derive an infinite system of linear algebraic equations that are truncated and solved numerically. Computational difficulties have been encountered and investigations have led to the conclusion that the theory developed is numerically unefficient, although it is accurate.

Chapter 2

OWC at the tip of a wedge of $\nu\pi$ degree

We consider an oscillating water column (OWC) at the tip of a wedge of $\nu\pi$ degree as shown in figure 2-1 where ν is a real number comprised between 0 and 2. The OWC is composed by a cylinder of radius a, open to the sea at the bottom. The water can enter the cylinder and rises to a certain level. A Wells' turbine is installed at the top of the cylinder at some height above the water surface. It rotates in only one direction and converts mechanical energy to electricity. We consider the sea depth to be constant and equal to h. The opening of the OWC is at a depth d. We consider that the walls of the cylinder and the wedge are vertical.

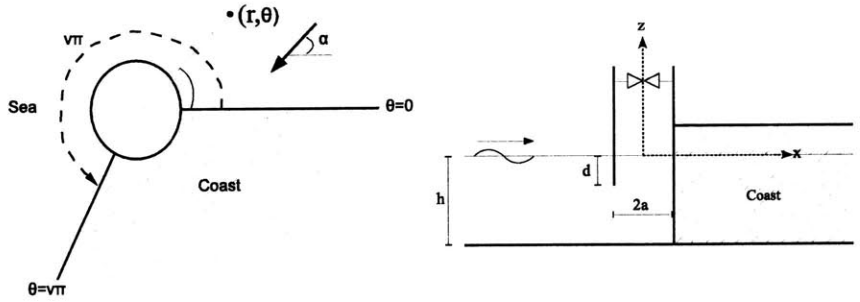

(a) Up view (b) Side view

Figure 2-1: OWC at the tip of a wedge, up view (left) and side view (right)

Let the tip of the wedge be the z axis. The still water surface is the (x, y) plane.

In the cylindrical polar coordinate system (r, θ, z) the walls are given by $\theta = 0$ and $\theta = \nu\pi$. In all this study we consider simple harmonic motion with frequency ω. We will also assume that the amplitude of the waves is small enough so that the linearized theory applies. The problem will be decomposed into the sum of a radiation problem and a diffraction problem.

2.1 Model of energy extraction

Let us consider one or more Wells'turbine installed at the top of the OWC. We consider a linear turbine model and thus the mass flux through the Wells' turbines is proportional to the chamber air pressure. We assume the air pressure p_a inside the chamber is uniform in space. This assumption is relevant due to the high sound speed in air and the low frequency of sea waves. Following Saramento and Falcao (1985) we relate the mass flux of air M through the chamber to the turbine characteristics:

$$\frac{dM}{dt} = \frac{d(\rho_a V)}{dt} = \frac{KD}{N} p_a \tag{2.1.1}$$

where ρ_a is the air density, V is the volume of the chamber, N the rotational speed of turbine blades, D the turbine rotor outer diameter and K an empirical factor that depends of the design, numbers and setup of the Wells'turbine. Taking into account the air compressibility, we have

$$\frac{d(\rho_a V)}{dt} = \rho_a \frac{dV}{dt} + V \frac{d\rho_a}{dt} \tag{2.1.2}$$

Let us denote by Q the rate of total upward displacement of the water surface:

$$Q = \frac{dV}{dt} = \int_0^a \int_0^{2\pi} w(r, \theta, z = 0) r dr d\theta = \int\int_{S_c} w \, dS \tag{2.1.3}$$

where S_c is the water surface in the chamber. Let us assume isentropy. Thus

$$c_A^2 \frac{d\rho_a}{dt} = \frac{dp_a}{dt} \tag{2.1.4}$$

where c_a is the sound velocity in air. Substituting the two previous equalities in (2.1.2) gives

$$\frac{dM}{dt} = \rho_a Q - \frac{V_0}{c_a^2}\frac{dp_a}{dt} \tag{2.1.5}$$

Let us consider simple harmonic motion so that $Q = \mathrm{Re}\left(\widehat{Q}e^{-i\omega t}\right)$ and $p_a = \mathrm{Re}\left(\widehat{p_a}e^{-i\omega t}\right)$. Equations (2.1.1) and (2.1.5) give then

$$\widehat{Q} = \left(\frac{KD}{N\rho_a} - \frac{i\omega V_0}{c_a^2\rho_a}\right)\widehat{p_a} \tag{2.1.6}$$

The vertical flux can be decomposed into two parts: a contribution from the diffraction problem $\widehat{Q}^D$ and a contribution from the radiation problem $\widehat{Q}^R$:

$$\widehat{Q} = \widehat{Q}^D + \widehat{Q}^R \tag{2.1.7}$$

Following Evans (1982) we express the volume flux due to the radiation potential as

$$\widehat{Q}^R = -\left(\mathcal{B} - i\mathcal{C}\right)\widehat{p_a} \tag{2.1.8}$$

where $\mathcal{B}$ and $\mathcal{C}$ are real. These coefficients are analogous respectively to the damping coefficient and the added mass for a rigid body system: indeed $\mathcal{C}$ is in phase with the flux acceleration whereas $\mathcal{B}$ is in phase with the flux velocity. We also write

$$\widehat{Q}^D = \Gamma A_0 \tag{2.1.9}$$

where A_0 is the amplitude of the plane incident wave. Γ will be further called the scattering coefficient. Substituting (2.1.8) and (2.1.9) into (2.1.6) gives

$$\frac{\widehat{p_a}}{A_0} = \frac{\Gamma}{\left(\frac{KD}{N\rho_a} + \mathcal{B}\right) - i\left(\mathcal{C} + \frac{\omega V_0}{c_a^2\rho_a}\right)} \tag{2.1.10}$$

Using (2.1.1), the time-averaged power output to the turbine is equal to

$$P_{\text{out}} = \overline{\frac{d\left(\rho_a V\right)}{dt}\frac{p_a}{\rho_a}} = \frac{KD}{N\rho_a}\overline{p_a^2} = \frac{KD}{2N\rho_a}\left|\widehat{p_a}\right|^2 \tag{2.1.11}$$

Thus replacing $\widehat{p_a}$ by its expression given in (2.1.10) we have

$$P_{\text{out}} = \frac{KD}{2N\rho_a}\frac{A_0^2\left|\Gamma\right|^2}{\left(\frac{KD}{N\rho_a}+\mathcal{B}\right)^2+\left(\mathcal{C}+\frac{\omega V_0}{c_a^2\rho_a}\right)^2} \tag{2.1.12}$$

We will define the normalized capture length, kL to be the fraction of available power per unit crest length of the incident wave which is extracted from the OWC:

$$kL = \frac{P_{\text{out}}}{\frac{\rho g A_0^2 C_g}{2k}} = \frac{KD}{N\rho_a}\frac{k}{\rho g C_g}\frac{\left|\Gamma\right|^2}{\left(\frac{KD}{N\rho_a}+\mathcal{B}\right)^2+\left(\mathcal{C}+\frac{\omega V_0}{c_a^2\rho_a}\right)^2} \tag{2.1.13}$$

Let us introduce dimensionless variables $\tilde{\mathcal{B}}$, $\tilde{\mathcal{C}}$ and $\tilde{\Gamma}$. We shall use here a different normalisation as the one used by Martin-Rivas and Mei (2008) for the study of an OWC at the tip of a thin breakwater or Martin-Rivas and Mei (2009) for the case of an OWC in a straight coastline. Indeed to study the effect of column radius a and frequence ω, we should not immerse them as scales. Otherwise the effects of varying a or ω are not pure and only partially accounted for. For this reason we will use h for length scale and $\sqrt{h/g}$ as time scale, and introduce the following dimensionless variables:

$$\begin{aligned}\mathcal{B} &= \tilde{\mathcal{B}}\frac{h}{\rho_\omega\sqrt{g/h}}, \quad \mathcal{C} = \tilde{\mathcal{C}}\frac{h}{\rho_\omega\sqrt{g/h}} \\ \Gamma &= \tilde{\Gamma}\frac{hg}{\sqrt{g/h}}\end{aligned} \tag{2.1.14}$$

With these definitions, (2.1.13) becomes

$$kL = \frac{khg}{C_g\sqrt{g/h}}\frac{\chi\left|\tilde{\Gamma}\right|^2}{\left(\chi+\tilde{\mathcal{B}}\right)^2+\left(\tilde{\mathcal{C}}-\beta\right)^2} \tag{2.1.15}$$

where

$$\chi = \frac{\rho_w K D \sqrt{g/h}}{\rho_a N h}, \quad \beta = -\frac{\omega V_o \rho_w \sqrt{g/h}}{C_a^2 \rho_a h} \tag{2.1.16}$$

The parameter χ represents the effects of power takeoff and characterizes the turbines. We shall assume that its magnitude can be controlled by proper design. Coefficient β is analogous to a negative spring constant, which varies with ω and is finite only because air is compressible. As noted by Saramento and Falcao (1985), this springlike effect of air compressibility is equivalent to adding an imaginary term to the turbine proportinality constant K, thus introducing a phase difference between the pressure and the mass flow rate.

2.2 Diffraction problem

2.2.1 Analysis

We consider an incident wave from infinity at the angle $\theta = \alpha$ with respect to the wedge. Inside the water the potential is governed by:

$$\nabla^2 \varphi = 0 \tag{2.2.1}$$

The boundary conditions are:

$$\frac{\partial \varphi}{\partial n} = 0 \text{ on the bottom and the walls} \tag{2.2.2}$$

$$\frac{\partial \varphi}{\partial z} - \frac{\omega^2}{g}\varphi = 0 \quad \text{at z=0} \tag{2.2.3}$$

Let k be the positive real root of the dispersion relation:

$$\omega^2 = gk \tanh(kh) \tag{2.2.4}$$

and k_l, $l = 1, 2, 3, ...$ the positive real roots of:

$$\omega^2 = -gk_l \tanh(k_l h) \quad l = 1, 2, 3, ... \tag{2.2.5}$$

Let $Z_0(z)$ and $Z_l(z), l = 1, 2, 3...$ be the corresponding eigenfunctions:

$$Z_0(z) = \frac{\cosh(k(z+h))}{\sqrt{N_0}}, \; N_0 = \frac{1}{2}\left(1 + \frac{\sinh(2kh)}{2kh}\right) \tag{2.2.6}$$

and

$$Z_l(z) = \frac{\cos(k_l(z+h))}{\sqrt{N_l}}, \; N_l = \frac{1}{2}\left(1 + \frac{\sin(2k_l h)}{2k_l h}\right) \quad l = 1, 2, 3... \tag{2.2.7}$$

The eigenfunctions are orthogonal for $-h \leq z \leq 0$:

$$\int_{-h}^{0} Z_l(z) Z_p(z) = h\delta_{lp} \tag{2.2.8}$$

For simplicity we denote $k = ik_0$ and include $Z_0(z)$ in the set of (2.2.5) with $l = 0$. All Z_l satisfy (2.2.3) and the no flux boundary condition at the bottom.

Potential outside The potential outside the cylinder ($r > a$) can be expressed as the sum of two potentials:

$$\varphi_{ext} = \varphi_1 + \varphi_2 \tag{2.2.9}$$

where φ_1 is the potential due to a cylinder extending to the bottom at the end of a wedge and φ_2 is a correction due to the opening. φ_1 is solved exactly by Martin-Rivas and Mei (2008). The calculation is reported in Appendix A with the following result:

$$\varphi_1 = -\frac{igA}{\omega}\sum_{n=0}^{\infty}\frac{\epsilon_n}{\nu\pi}\frac{2\pi i \cos(\frac{n\alpha}{\nu})e^{-i\frac{n\pi}{2\nu}}Y'_{\frac{n}{\nu}}(ka)}{H'_{\frac{n}{\nu}}(ka)}\left(J_{\frac{n}{\nu}}(kr) - \frac{J'_{\frac{n}{\nu}}(ka)}{Y'_{\frac{n}{\nu}}(ka)}Y_{\frac{n}{\nu}}(kr)\right)cos\left(\frac{n\theta}{\nu}\right)\frac{Z_0(z)}{Z_0(0)} \tag{2.2.10}$$

where $\epsilon_0 = 1$ and $\epsilon_n = 2$ for $n \geq 1$. φ_2 can be written as the infinite serie of modified Bessel functions vanishing at infinity:

$$\varphi_2 = -\frac{igA}{\omega} \sum_{n=0}^{\infty} \sum_{l=0}^{\infty} A_{nl} \frac{K_{\frac{n}{\nu}}(k_l r)}{k_l a K'_{\frac{n}{\nu}}(k_l a)} \cos\left(\frac{n\theta}{\nu}\right) Z_l(z) \tag{2.2.11}$$

where A_{nl} are unknown coefficients. φ_2 satifies the no flux condition on the two walls of the wedge. The coefficient for $l = 0$ corresponds to the outgoing wave (Abramowitz and Stegun (1964), formula 9.6.4):

$$K_{\frac{n}{\nu}}(k_0 r) = K_{\frac{n}{\nu}}(-ikr) = \frac{\pi}{2} i e^{\frac{in\pi}{2\nu}} H^{(1)}_{\frac{n}{\nu}}(kr) \tag{2.2.12}$$

For all $l \neq 0$, $K_{\frac{n}{\nu}}(k_l r)$ dies out at infinity.

Potential inside. Inside the cylinder ($r \leq a$) the potential is due only to the opening and can be expressed as an infinite serie of modified Bessel functions finite at the origin $r = 0$:

$$\varphi_C = -\frac{igA}{\omega} \sum_{n=0}^{\infty} \sum_{l=0}^{\infty} \left(B_{nl} \cos(n\theta) + C_{nl} \sin(n\theta)\right) \frac{I_n(k_l r)}{k_l a I'_n(k_l a)} Z_l(z) \tag{2.2.13}$$

where B_{nl} and C_{nl} are unknown coefficients. For $l = 0$ we have:

$$I_n(k_0 r) = I_n(-ikr) = (-i)^n J_n(kr) \tag{2.2.14}$$

Flux continuity at the opening Since φ_1 satisfies the condition of no flux on the surface $r = a$, continuity of the radial flux at $r = a$ leads to:

$$\frac{\partial \varphi_2}{\partial r} = \frac{\partial \varphi_C}{\partial r} = U(\theta, z), \quad 0 \leq \theta \leq \nu\pi, \ -h \leq z \leq -d \tag{2.2.15}$$

In addition, the no flux condition on the wall of the cylinder imposes at $r = a$:

$$\frac{\partial \varphi_2}{\partial r} = 0, \quad 0 \leq \theta \leq \nu\pi, \ -d \leq z \leq 0 \tag{2.2.16}$$

$$\frac{\partial \varphi_C}{\partial r} = 0, \quad \text{for} \quad \begin{cases} \nu\pi \leq \theta \leq 2\pi \ -h \leq z \leq -d \\ 0 \leq \theta \leq 2\pi \ -d \leq z \leq 0 \end{cases} \tag{2.2.17}$$

Combining (2.2.15), (2.2.16) and (2.2.17) we finally get:

$$\frac{\partial \varphi_2}{\partial r} = \begin{cases} 0 & \text{for } 0 \leq \theta \leq \nu\pi \ -d \leq z \leq 0 \\ U(\theta, z) & \text{for } 0 \leq \theta \leq \nu\pi \ -h \leq z \leq -d \end{cases} \tag{2.2.18}$$

and:

$$\frac{\partial \varphi_C}{\partial r} = \begin{cases} 0 & \text{for } 0 \leq \theta \leq 2\pi, \ -d \leq z \leq 0 \\ U(\theta, z) & \text{for } 0 \leq \theta \leq \nu\pi, \ -h \leq z \leq -d \\ 0 & \text{for } \nu\pi \leq \theta \leq 2\pi, -h \leq z \leq -d \end{cases} \tag{2.2.19}$$

Equation (2.2.18) gives:

$$-\frac{igA}{a\omega} \sum_{n=0}^{\infty} \sum_{l=0}^{\infty} A_{nl} \cos\left(\frac{n\theta}{\nu}\right) Z_l(z) = \begin{cases} 0, & 0 \leq \theta \leq \nu\pi, \ -d \leq z \leq 0 \\ U(\theta, z), & 0 \leq \theta \leq \nu\pi, \ -h \leq z \leq -d \end{cases} \tag{2.2.20}$$

Using orthogonality we obtain:

$$\frac{\nu\pi}{\epsilon_n} A_{nl} = \frac{ia\omega}{ghA} \int_{-h}^{-d} \int_{0}^{\nu\pi} U(\theta, z) Z_l(z) \cos\left(\frac{n\theta}{\nu}\right) d\theta dz \tag{2.2.21}$$

Similarly equation (2.2.19) gives:

$$-\frac{igA}{a\omega} \sum_{n=0}^{\infty} \sum_{l=0}^{\infty} \left(B_{nl} \cos(n\theta) + C_{nl} \sin(n\theta)\right) Z_l(z) = \begin{cases} 0 & \text{for } 0 \leq \theta \leq 2\pi, \ -d \leq z \leq 0 \\ U(\theta, z) & \text{for } 0 \leq \theta \leq \nu\pi, \ -h \leq z \leq -d \\ 0 & \text{for } \ \nu\pi \leq \theta \leq 2\pi, -h \leq z \leq -d \end{cases} \tag{2.2.22}$$

Using orthogonality we obtain for any l and any n:

$$\frac{2\pi}{\epsilon_n} B_{nl} = \frac{ia\omega}{ghA} \int_{-h}^{-d} \int_{0}^{\nu\pi} U(\theta, z) Z_l(z) \cos(n\theta) d\theta dz \tag{2.2.23}$$

$$\frac{2\pi}{\epsilon_n}C_{nl} = \frac{ia\omega}{ghA}\int_{-h}^{-d}\int_{0}^{\nu\pi} U(\theta,z)Z_l(z)\sin(n\theta)d\theta dz \tag{2.2.24}$$

Continuity of the pressure At the opening $r = a$ the continuity of the pressure requires:

$$\varphi_1 + \varphi_2 = \varphi_C \quad \text{for} \quad 0 \le \theta \le \nu\pi \;\; -h \le z \le -d \tag{2.2.25}$$

For brievety we shall use the following notation:

$$\mathcal{E}_n = \frac{\epsilon_n}{\nu\pi}\frac{2\pi i\cos(\frac{n\alpha}{\nu})e^{-i\frac{n\pi}{2\nu}}Y'_{\frac{n}{\nu}}(ka)}{Z_0(0)H'_{\frac{n}{\nu}}(ka)}\left(J_{\frac{n}{\nu}}(kr) - \frac{J'_{\frac{n}{\nu}}(ka)}{Y'_{\frac{n}{\nu}}(ka)}Y_{\frac{n}{\nu}}(kr)\right) \tag{2.2.26}$$

Thus equation (2.2.25) can be written as:

$$\begin{aligned}\sum_{n=0}^{\infty}\mathcal{E}_n\cos\left(\frac{n\theta}{\nu}\right)Z_0(z) + \sum_{n=0}^{\infty}\sum_{l=0}^{\infty}A_{nl}\frac{K_{\frac{n}{\nu}}(k_la)}{k_laK'_{\frac{n}{\nu}}(k_la)}\cos\left(\frac{n\theta}{\nu}\right)Z_l(z)\\ = \sum_{n=0}^{\infty}\sum_{l=0}^{\infty}\left(B_{nl}\cos(n\theta) + C_{nl}\sin(n\theta)\right)\frac{I_n(k_la)}{k_laI'_n(k_la)}Z_l(z)\end{aligned} \tag{2.2.27}$$

A_{nl}, B_{nl} and C_{nl} can be replaced by their expression in equation (2.2.21), (2.2.23) and (2.2.24). This leads to:

$$\begin{aligned}&\sum_{n=0}^{\infty}\mathcal{E}_n cos\left(\frac{n\theta}{\nu}\right)Z_0(z) =\\ &\sum_{n=0}^{\infty}\sum_{l=0}^{\infty}\frac{\epsilon_n ia\omega}{2\pi ghA}\int_{-h}^{-d}\int_{0}^{\nu\pi}U(\theta',z')Z_l(z')\cos(n\theta')d\theta' dz'\frac{I_n(k_la)}{k_laI'_n(k_la)}\cos(n\theta)Z_l(z) +\\ &\sum_{n=0}^{\infty}\sum_{l=0}^{\infty}\frac{\epsilon_n ia\omega}{2\pi ghA}\int_{-h}^{-d}\int_{0}^{\nu\pi}U(\theta',z')Z_l(z')\sin(n\theta')d\theta' dz'\frac{I_n(k_la)}{k_laI'_n(k_la)}\sin(n\theta)Z_l(z) -\\ &\sum_{n=0}^{\infty}\sum_{l=0}^{\infty}\frac{\epsilon_n ia\omega}{\nu\pi ghA}\int_{-h}^{-d}\int_{0}^{\nu\pi}U(\theta',z')Z_l(z')\cos\left(\frac{n\theta'}{\nu}\right)d\theta' dz'\frac{K_{\frac{n}{\nu}}(k_la)}{k_laK'_{\frac{n}{\nu}}(k_la)}\cos\left(\frac{n\theta}{\nu}\right)Z_l(z)\end{aligned} \tag{2.2.28}$$

Fredholm integral equation for U The previous equation can be rewritten as the integral equation:

$$\int_{-h}^{-d}\int_{0}^{\nu\pi} U(\theta',z')\mathcal{K}(\theta,\theta',z,z')d\theta'dz' = \sum_{n=0}^{\infty}\mathcal{E}_n cos\left(\frac{n\theta}{\nu}\right)Z_0(z) \qquad (2.2.29)$$
$$\text{for} \quad 0 \leq \theta \leq \nu\pi \text{ and } -h \leq z \leq -d$$

with the kernel:

$$\begin{aligned}\mathcal{K}(\theta,\theta',z,z') = \\ \sum_{n=0}^{\infty}\sum_{l=0}^{\infty}\frac{\epsilon_n ia\omega}{2\pi ghA}Z_l(z')Z_l(z)\frac{I_n(k_l a)}{k_l a I_n'(k_l a)}\left[\cos(n\theta')\cos(n\theta)+\sin(n\theta')\sin(n\theta)\right] \\ -\sum_{n=0}^{\infty}\sum_{l=0}^{\infty}\frac{\epsilon_n ia\omega}{\nu\pi ghA}Z_l(z')Z_l(z)\frac{K_{\frac{n}{\nu}}(k_l a)}{k_l a K_{\frac{n}{\nu}}'(k_l a)}\cos\left(\frac{n\theta}{\nu}\right)\cos\left(\frac{n\theta'}{\nu}\right) \qquad (2.2.30)\end{aligned}$$

Expansion of U We expect $U(\theta,z)$ to be singular at the opening $z=-d$. Following Porter and Evans (1995) we expand it as follow:

$$U(\theta,z) = -\frac{igA}{\omega}\sum_{m=0}^{\infty}\sum_{p=0}^{\infty}\alpha_{mp}\mathcal{T}_m(\theta)u_p(z) \qquad (2.2.31)$$

with

$$u_p(z) = \frac{2(-1)^p}{\pi\sqrt{(h-d)^2-(z+h)^2}}T_{2p}\left(\frac{z+h}{h-d}\right) \qquad (2.2.32)$$

$$\mathcal{T}_m(\theta) = T_m^*\left(\frac{\theta}{\nu\pi}\right) \qquad (2.2.33)$$

where T_n is the Chebyshev polynomial of order n and $T_n^*(s)$ is the shifted Chebyshev polynomial (see J.C. Mason (2003), chapter 1, paragraph 1.3). The shifted Chebyshev polynomial expansion in θ is used to speed up the convergence of the serie. Let us described the shifted Chebyshev polynomial and for this let us denote $x=\theta/\nu\pi$. We map the independent variable $x \in [0,1]$ to the independant variable $s \in [-1,1]$ by the relation

$$s = 2x-1$$

Then $s = -1$ corresponds to $\theta = 0$ and $s = 1$ to $\theta = \nu\pi$. The shifted Chebyshev polynomial of degree n in $x \in [0, 1]$ is defined by

$$T_n^*(x) = T_n(s) = T_n(2x - 1)$$

The first polynomials are then

$$T_0^*(x) = 1, \quad T_1^*(x) = 2x - 1, \quad T_2^*(x) = 8x^2 - 8x + 1, ...$$

The shifted polynomial satified the following recurrence relation:

$$T_n^*(x) = 2(2x - 1)T_{n-1}^*(x) - T_{n-2}^*(x)$$

with the initial conditions:

$$T_0^*(x) = 1, \quad T_1^*(x) = 2x - 1$$

We shall make use of the following identity:

$$\int_{-h}^{-d} u_p(z) Z_l(z) dz = \frac{1}{N_l^{1/2}} J_{2p} \{\kappa_l(h - d)\} = F_{pl} \tag{2.2.34}$$

For brievety let us use the following notations for the following integrals:

$$\mathfrak{C}(n, m) = \int_0^{\nu\pi} \mathcal{T}_m(\theta) \cos(n\theta)\, d\theta \tag{2.2.35}$$

$$S(n, m) = \int_0^{\nu\pi} \mathcal{T}_m(\theta) \sin(n\theta)\, d\theta \tag{2.2.36}$$

$$\mathfrak{C}_\nu(n, m) = \int_0^{\nu\pi} \mathcal{T}_m(\theta) \cos\left(\frac{n\theta}{\nu}\right) d\theta \tag{2.2.37}$$

For the numerical computations the previous equations can be easily evaluated as follows. Expanding $\mathcal{T}_m$ as a sum of power of θ, we write:

$$\mathcal{T}_m(\theta) = \sum_{k=0}^{m} \gamma_k \theta^k \tag{2.2.38}$$

The three previous integrals become then:

$$\mathfrak{C}(n,m) = \sum_{k=0}^{m} \gamma_k \int_0^{\nu\pi} \theta^k \cos(n\theta)\, d\theta \tag{2.2.39}$$

$$S(n,m) = \sum_{k=0}^{m} \gamma_k \int_0^{\nu\pi} \theta^k \sin(n\theta)\, d\theta \tag{2.2.40}$$

$$\mathfrak{C}_\nu(n,m) = \sum_{k=0}^{m} \gamma_k \int_0^{\nu\pi} \theta^k \cos\left(\frac{n\theta}{\nu}\right) d\theta \tag{2.2.41}$$

Each integral can now be calculated by making use of the following recurrence relations:

$$\int \theta^k \cos(\theta) d\theta = \theta^k \sin\theta + k\theta^{k-1}\cos\theta - k(k-1)\int \theta^{k-2}\cos(\theta) d\theta \tag{2.2.42}$$

$$\int \theta^k \sin(\theta) d\theta = -\theta^k \cos\theta + k\theta^{k-1}\sin\theta - k(k-1)\int \theta^{k-2}\sin(\theta) d\theta \tag{2.2.43}$$

Replacing $U(\theta, z)$ by its expansion (2.2.31) in equation (2.2.28) leads to:

$$\begin{aligned}
&\frac{h}{a}\sum_{n=0}^{\infty}\mathcal{E}_n cos\left(\frac{n\theta}{\nu}\right) Z_0(z) = \\
&\sum_{m=0}^{\infty}\sum_{p=0}^{\infty}\alpha_{mp}\sum_{n=0}^{\infty}\sum_{l=0}^{\infty}\frac{\epsilon_n}{2\pi}\frac{I_n(k_l a)}{k_l a I_n'(k_l a)} Z_l(z) F_{pl}\left(\cos(n\theta)\,\mathfrak{C}(n,m) + \sin(n\theta)\, S(m,n)\right) \\
&-\sum_{m=0}^{\infty}\sum_{p=0}^{\infty}\alpha_{mp}\sum_{n=0}^{\infty}\sum_{l=0}^{\infty}\frac{\epsilon_n}{\nu\pi}\frac{K_{\frac{n}{\nu}}(k_l a)}{k_l a K_{\frac{n}{\nu}}'(k_l a)}\cos\left(\frac{n\theta}{\nu}\right) Z_l(z) F_{pl}\mathfrak{C}_\nu(n,m)
\end{aligned} \tag{2.2.44}$$

We multiply both side of equation (2.2.44) by $\mathcal{T}_M(\theta)u_P(z)$ and integrate for $0 \leq \theta \leq \nu\pi$ and $-h \leq z \leq -d$. For any M and P we get:

$$\begin{aligned}
&\frac{h}{a}\sum_{n=0}^{\infty}\mathcal{E}_n cos\left(\frac{n\theta}{\nu}\right)Z_0(z) = \\
&\sum_{m=0}^{\infty}\sum_{p=0}^{\infty}\alpha_{mp}\sum_{n=0}^{\infty}\sum_{l=0}^{\infty}\frac{\epsilon_n}{2\pi}\frac{I_n(k_l a)}{k_l a I_n'(k_l a)}Z_l(z)F_{pl}\left(\mathfrak{C}(n,M)\mathfrak{C}(n,m)+S(n,M)S(n,m)\right) \\
&-\sum_{m=0}^{\infty}\sum_{p=0}^{\infty}\alpha_{mp}\sum_{n=0}^{\infty}\sum_{l=0}^{\infty}\frac{\epsilon_n}{\nu\pi}\frac{K_{\frac{n}{\nu}}(k_l a)}{k_l a K_{\frac{n}{\nu}}'(k_l a)}Z_l(z)F_{pl}\mathfrak{C}_\nu(n,m)\mathfrak{C}_\nu(n,M)
\end{aligned} \tag{2.2.45}$$

The coefficients α_{mp} are solutions of a linear infinite system of equations defined by (2.2.45). This system will be solved by truncating the series after the N^{th} term. Once it is solved, we can obtain the coefficients A_{nl},B_{nl} and C_{nl} from respectively (2.2.21),(2.2.23) and (2.2.24). Then the potentials are given by expressions (2.2.11) and (2.2.13).

2.3 Radiation problem

2.3.1 Analysis

The potentials in the water inside and outside the cylinder are governed by Laplace equation and satisfy the no flux condition on all solid surfaces. On the free surface they satisfy :

$$\frac{\partial\phi}{\partial z}-\frac{\omega^2}{g}\phi = \begin{cases} \frac{i\omega}{\rho g}\widehat{p_a} \text{ at } z=0 \text{ for } 0 \leq r < a \\ 0 \text{ at } z=0 \text{ for } r > a \end{cases} \tag{2.3.1}$$

The potential outside must also behave as outgoing waves at infinity. Taking into account the symmetry of the problem with respect to $\theta = \frac{\nu\pi}{2}$, the potential inside can be expanded as the infinite serie of eigenfunctions as follows:

$$\phi_C = -\frac{i\widehat{p_a}}{\rho\omega}\sum_{n=0}^{\infty}\sum_{l=0}^{\infty}D_{nl}\frac{I_n(k_l r)}{k_l a I_n'(k_l a)}\cos\left[n\left(\theta-\frac{\nu\pi}{2}\right)\right]Z_l(z)-\frac{i\widehat{p_a}}{\rho\omega} \tag{2.3.2}$$

where D_{nl} are unknown coefficients. The potential outside can be expressed as:

$$\phi_O = -\frac{i\widehat{p}_a}{\rho\omega}\sum_{n=0}^{\infty}\sum_{l=0}^{\infty} E_{nl}\frac{K_{2n}(k_l r)}{k_l a K'_{2n}(k_l a)}\cos\left(\frac{2n\theta}{\nu}\right)Z_l(z) \tag{2.3.3}$$

where E_{nl} are unknown coefficients. The potentials ϕ_C and ϕ_O satisfy the no flux condition on the bottom, on the walls of the wedge, $r \geq a$, $\theta = 0$ and $\theta = \nu\pi$, as well as the free surface boundary condition given in equation (2.3.1). Note that the radiation problem, the added mass and damping coefficient, do not depend on the angle of incidence.

Continuity of the radial flux At the opening of the cylinder ($r = a$, $\theta \in [0, \nu\pi]$) the radial flux must be continuous:

$$\frac{\partial\phi_C}{\partial r} = \frac{\partial\phi_O}{\partial r} = U(\theta, z),\ 0 \leq \theta \leq \nu\pi\ -h \leq z \leq -d \tag{2.3.4}$$

In addition, the no flux condition must be imposed at $r = a$ on the vertical wall:

$$\frac{\partial\phi_O}{\partial r} = 0,\ 0 \leq \theta \leq \nu\pi\ -d \leq z \leq 0 \tag{2.3.5}$$

$$\frac{\partial\phi_C}{\partial r} = 0,\ [\nu\pi \leq \theta \leq 2\pi\ -h \leq z \leq -d] \text{ and } [0 \leq \theta \leq 2\pi\ -d \leq z \leq 0] \tag{2.3.6}$$

Combining (2.3.7), (2.3.5) and (2.3.6) we finally get:

$$\frac{\partial\phi_O}{\partial r} = \begin{cases} 0 \text{ for } 0 \leq \theta \leq \nu\pi\ -d \leq z \leq 0 \\ U(\theta, z) \text{ for } 0 \leq \theta \leq \nu\pi\ -h \leq z \leq -d \end{cases} \tag{2.3.7}$$

and:

$$\frac{\partial\phi_C}{\partial r} = \begin{cases} 0 & \text{for } 0 \leq \theta \leq 2\pi,\ -d \leq z \leq 0 \\ U(\theta, z) & \text{for } 0 \leq \theta \leq \nu\pi,\ -h \leq z \leq -d \\ 0 & \text{for } \nu\pi \leq \theta \leq 2\pi, -h \leq z \leq -d \end{cases} \tag{2.3.8}$$

The derivatives at $r = a$ are given by:

$$\left.\frac{\partial \phi_C}{\partial r}\right]_{r=a} = -\frac{i\widehat{p_a}}{a\rho\omega}\sum_{n=0}^{\infty}\sum_{l=0}^{\infty} D_{nl}\cos\left[n\left(\theta - \frac{\nu\pi}{2}\right)\right] Z_l(z) \tag{2.3.9}$$

and

$$\left.\frac{\partial \phi_O}{\partial r}\right]_{r=a} = -\frac{i\widehat{p_a}}{a\rho\omega}\sum_{n=0}^{\infty}\sum_{l=0}^{\infty} E_{nl}\cos\left(\frac{2n\theta}{\nu}\right) Z_l(z) \tag{2.3.10}$$

Using equations (2.3.7) and (2.3.10) on the one hand and (2.3.8) and (2.3.9) on the other, and the orthogonality properties, we get:

$$\frac{2\pi}{\epsilon_n} D_{nl} = \frac{ia\rho\omega}{\widehat{p_a}h}\int_{-h}^{-d}\int_{0}^{\nu\pi} U(\theta, z)\cos\left[n\left(\theta - \frac{\nu\pi}{2}\right)\right] Z_l(z) d\theta dz \tag{2.3.11}$$

and

$$\frac{\nu\pi}{\epsilon_n} E_{nl} = \frac{ia\rho\omega}{\widehat{p_a}h}\int_{-h}^{-d}\int_{0}^{\nu\pi} U(\theta, z)\cos\left[\frac{2n\theta}{\nu}\right] Z_l(z) d\theta dz \tag{2.3.12}$$

Note that for $n = 0$ the previous equations gives:

$$E_{0l} = \frac{2}{\nu} D_{0l} \tag{2.3.13}$$

Pressure continuity Continuity of potential at the opening imposes:

$$\phi_O\rfloor_{r=a} = \phi_C\rfloor_{r=a} \text{ for } 0 \leq \theta \leq \nu\pi \text{ and } -h \leq r \leq -d \tag{2.3.14}$$

thus for $0 \leq \theta \leq \nu\pi$ and $-h \leq r \leq -d$,

$$\sum_{n=0}^{\infty}\sum_{l=0}^{\infty} E_{nl}\frac{K_{2n}(k_l a)}{k_l a K'_{2n}(k_l a)}\cos\left(\frac{2n\theta}{\nu}\right) Z_l(z) = \sum_{n=0}^{\infty}\sum_{l=0}^{\infty} D_{nl}\frac{I_n(k_l a)}{k_l a I'_n(k_l a)}\cos\left[n\left(\theta - \frac{\nu\pi}{2}\right)\right] Z_l(z) + 1 \tag{2.3.15}$$

Fredholm integral equation for U We replace in the previous equation D_{nl} and E_{nl} by their expressions in (2.3.11) and (2.3.12). We get an integral equation for

$U(\theta, z)$:

$$\frac{-i\widehat{p_a}h}{\rho\omega a} = \int_0^{\nu\pi}\int_{-h}^{-d} U(\theta', z')\mathcal{K}(\theta, \theta', z, z') = d\theta' dz' \tag{2.3.16}$$

with the kernel:

$$\begin{aligned}\mathcal{K}(\theta, \theta', z, z') = \\ \sum_{n=0}^{\infty}\sum_{l=0}^{\infty} \frac{\epsilon_n}{\nu\pi}\frac{K_{2n}(k_l a)}{k_l a K'_{2n}(k_l a)} \cos\left(\frac{2n\theta}{\nu}\right)\cos\left(\frac{2n\theta'}{\nu}\right) Z_l(z)Z_l(z') \\ -\sum_{n=0}^{\infty}\sum_{l=0}^{\infty} \frac{\epsilon_n}{2\pi}\frac{I_n(k_l a)}{k_l a I'_n(k_l a)} \cos\left[n\left(\theta - \frac{\nu\pi}{2}\right)\right]\cos\left[n\left(\theta' - \frac{\nu\pi}{2}\right)\right] Z_l(z)Z_l(z')\end{aligned} \tag{2.3.17}$$

Expansion of U Taking into account the symmetry of the problem we can expect $U(\theta, z)$ to be symmetrical with respect to $\theta = \nu\pi/2$ and as a consequence we expect $U(0, z) = U(\nu\pi, z)$. Thus it can be expanded as a continuous function in θ. Therefore for this problem the Fourier expansion will converge fast enough and we don't need to use the expansion with Chebyshev polynomials for the independant variable θ:

$$U(\theta, z) = \frac{-i\widehat{p_a}h}{\rho\omega}\sum_{m=0}^{\infty}\sum_{p=0}^{\infty}\alpha_{mp}\cos\left[\frac{2m}{\nu}\left(\theta - \frac{\nu\pi}{2}\right)\right] u_p(z) \tag{2.3.18}$$

We have

$$\int_0^{\nu\pi}\cos\left[\frac{2m}{\nu}\left(\theta - \frac{\nu\pi}{2}\right)\right]\cos\left(\frac{2n\theta}{\nu}\right)d\theta = \delta_{mn}(-1)^m\frac{\nu\pi}{\epsilon_m} \tag{2.3.19}$$

Let us use the following notation for brievety:

$$R_{mn} = \int_0^{\nu\pi}\cos\left[\frac{2m}{\nu}\left(\theta - \frac{\nu\pi}{2}\right)\right]\cos\left[n\left(\theta - \frac{\nu\pi}{2}\right)\right]d\theta \tag{2.3.20}$$

Replacing $U(\theta, z)$ by its expansion in equation (2.3.16) gives:

$$\begin{aligned}\frac{h}{a} = \sum_{m=0}^{\infty}\sum_{p=0}^{\infty}\alpha_{mp}\sum_{n=0}^{\infty}\sum_{l=0}^{\infty}\left\{\frac{\epsilon_n}{\pi}\left[F_{pl}\frac{\delta_{mn}(-1)^m\pi}{\epsilon_m}\frac{K_{2n}(k_l a)}{k_l a K'_{2n}(k_l a)}\cos\left(\frac{2n\theta}{\nu}\right)\right.\right. \\ \left.\left. -\frac{1}{2}F_{pl}R_{mn}\frac{I_n(k_l a)}{k_l a I'_n(k_l a)}\cos n\left(\theta - \frac{\nu\pi}{2}\right)\right] Z_l(z)\right\}\end{aligned} \tag{2.3.21}$$

We multiply both side of the equation by $\cos\left[\frac{2M}{\nu}\left(\theta-\frac{\nu\pi}{2}\right)\right]u_P(z)$ and integrate for $0\leq\theta\leq\nu\pi$ and $-h\leq z\leq 0$. We get for any M and P:

$$\frac{h}{a}\nu\pi\delta_{M0}\delta_{P0}=\sum_{p=0}^{\infty}\alpha_{Mp}\sum_{l=0}^{\infty}F_{pl}F_{Pl}\frac{\nu\pi}{\epsilon_M}\frac{K_{2M}(k_la)}{k_laK'_{2M}(k_la)}$$
$$-\sum_{m=0}^{\infty}\sum_{p=0}^{\infty}\alpha_{mp}\sum_{n=0}^{\infty}\sum_{l=0}^{\infty}\frac{\epsilon_n}{2\pi}F_{pl}F_{Pl}R_{mn}R_{Mn}\frac{I_n(k_la)}{k_laI'_n(k_la)} \quad (2.3.22)$$

Similar to the scattering problem, we have a linear infinite system of equations that will be solved numerically by truncating after the N^{th} term.

2.3.2 Energy conservation

We consider a large vertical cylindrical surface S_∞ enclosing all free surfaces and rigid boundaries and extending from the free surface to the bottom. Let us define the following notations:

- S_C the free surface inside the OWC
- S_O the free surface outside the OWC
- S_b the bottom surface in and outside the OWC at $z=-h$.
- S_w the vertical surface of the cylinder (internal and external surface)

Let us denote for simplicity ϕ the potential solution of the radiation problem: $\phi=\phi_C$ inside the cylinder and $\phi=\phi_O$ outside. By using Green's identity and the Laplace equation , we get

$$2\mathrm{i}\cdot\mathrm{Im}\left(\int\int_S\left(\phi\frac{\partial\phi^*}{\partial n}\right)dS\right)=0 \quad (2.3.23)$$

with

$$S=S_\infty\bigcup S_C\bigcup S_O\bigcup S_b\bigcup S_w \quad (2.3.24)$$

We already know that the integrals for S_O, S_b, and S_w are equal to zero, using the properties of outgoing waves and the boundaries conditions. Thus we get:

$$\mathrm{Im}\int\int_{S_\infty}\left(\phi\frac{\partial\phi^*}{\partial n}\right)dS+\mathrm{Im}\int\int_{S_C}\left(\phi\frac{\partial\phi^*}{\partial n}\right)dS=0 \tag{2.3.25}$$

$$\mathrm{Im}\int\int_{S_\infty}\left(\phi_O\frac{\partial\phi_O^*}{\partial r}\right)dS=-\mathrm{Im}\int_{0\le\theta\le\nu\pi}\int_{|r|\le a}\left(\phi_C\,\frac{\partial\phi_C^*}{\partial z}\right)\Big|_{z=0}dS \tag{2.3.26}$$

Inside the cylinder, on the free surface ($z=0$) we have the condition:

$$\frac{\partial\phi_C}{\partial z}-\frac{\omega^2}{g}\phi_C=\frac{i\omega}{\rho g}\widehat{p_a} \tag{2.3.27}$$

which gives

$$\phi_C=\frac{g}{\omega^2}\frac{\partial\phi_C}{\partial z}-\frac{i}{\rho\omega}\widehat{p_a} \tag{2.3.28}$$

$$\phi_C\frac{\partial\phi_C^*}{\partial z}=\frac{g}{\omega^2}\left|\frac{\partial\phi_C}{\partial z}\right|^2-\frac{\mathrm{i}}{\rho\omega}\widehat{p_a}\frac{\partial\phi_C^*}{\partial z} \tag{2.3.29}$$

Since

$$\left|\frac{\partial\phi_C}{\partial z}\right|^2\in\mathrm{Re} \tag{2.3.30}$$

We obtain:

$$\mathrm{Im}\left(\int\int_{S_\infty}\left(\phi_O\frac{\partial\phi_O^*}{\partial r}\right)rd\theta dz\right)=\mathrm{Im}\left(\int_0^{\nu\pi}\int_0^a\left(\frac{i\widehat{p_a}}{\rho\omega}\,\frac{\partial\phi_C^*}{\partial z}\right)\Big|_{z=0}rdrd\theta\right) \tag{2.3.31}$$

Using the identity: $\mathrm{Im}(iz)=\mathrm{Re}(z)$ we obtain finally:

$$\mathrm{Re}\left(\int\int_{S_\infty}i\left(\phi_O\frac{\partial\phi_O^*}{\partial r}\right)rd\theta dz\right)=-\mathrm{Re}\left(\int_0^{\nu\pi}\int_0^a\left(\frac{\widehat{p_a}}{\rho\omega}\,\frac{\partial\phi_C}{\partial z}\right)\Big|_{z=0}rdrd\theta\right) \tag{2.3.32}$$

Equation (2.3.32) means that the power input by the chamber air inside the cylinder must be equal the power outflux through a vertical cylinder around the column. Using (2.3.3), the left-hand side of (2.3.32) becomes:

$$\mathrm{Re}\left(\mathrm{i}\left(\frac{|\widehat{p_a}|}{\rho\omega}\right)^2hr\nu\pi\sum_{n=0}^{\infty}|E_{n0}|^2\,\frac{K_{2n}(k_0r)K_{2n}'(k_0r)^*}{\epsilon_nk_0a^2\,|K_{2n}'(k_0a)|^2}\right) \tag{2.3.33}$$

which involves only the propagating mode E_{n0}. Making use of the relation:

$$K_{2n}(k_0 r) = \frac{i^{n+1}\pi}{2} H_{2n}(kr) \tag{2.3.34}$$

it becomes:

$$\mathrm{Re}\left(\mathrm{i} \left(\frac{|\widehat{p_a}|}{\rho\omega} \right)^2 hr\nu\pi \sum_{n=0}^{\infty} |E_{n0}|^2 \frac{H_{2n}(kr) H'_{2n}(kr)^*}{\epsilon_n ka^2 \left|H'_{2n}(ka)\right|^2} \right) \tag{2.3.35}$$

On S_∞ kr is very large and the Hankel function can be replaced by its asymptotic form:

$$H_{2n}(kr) \approx \sqrt{\frac{2}{\pi kr}} e^{i(kr - \nu\pi/2 - \pi/4)} \tag{2.3.36}$$

Thus the left-hand side of (2.3.32) is finally reduced to:

$$\left(\frac{|\widehat{p_a}|}{\rho\omega} \right)^2 2h\nu \sum_{n=0}^{\infty} \frac{|E_{n0}|^2}{\epsilon_n \left|kaH'_{2n}(ka)\right|^2} \tag{2.3.37}$$

Using the definition of the damping coefficient, the right-hand side of (2.3.32) becomes

$$\frac{|\widehat{p_a}|^2}{\rho\omega} \mathcal{B} \tag{2.3.38}$$

or with non dimensionalized damping coefficient

$$\left(\frac{|\widehat{p_a}|}{\rho} \right)^2 \frac{h}{\omega\sqrt{g/h}} \widetilde{\mathcal{B}} \tag{2.3.39}$$

Combining equations (2.3.39) and (2.3.37) gives finally

$$\widetilde{\mathcal{B}} = \frac{\sqrt{g/h}}{\omega} 2\nu \sum_{n=0}^{\infty} \frac{|E_{n0}|^2}{\epsilon_n \left|k_0 a K'_{2n}(k_0 a)\right|^2} \tag{2.3.40}$$

This identity can be used to check numerical computations.

2.4 Reciprocal relation of Haskind

In this section we demonstrate a reciprocal relation between the damping coefficient and the scattering coefficient for an OWC at the tip of a wedge of $\nu\pi$. Following Evans (1982), let us consider again a large vertical cylindrical surface S_∞ enclosing all free surfaces and rigid boundaries and extending from the free surface to the bottom. We keep the notations of the previous section. Let us recall that the radiated potential outside the OWC must be outgoing at infinity and thus it satifies:

$$\phi_O \sim \mathcal{A}_0(\theta) \frac{e^{ikr}}{\sqrt{kr}} Z_0(z) \tag{2.4.1}$$

where $\mathcal{A}_0$ is the amplitude of the radiated wave at infinity. The vertical displacement inside the cylinder is given by:

$$\int\int_{S_C} \frac{\partial \phi_C}{\partial z} dS = -(\mathcal{B} - i\mathcal{C})\, \widehat{p_a} \tag{2.4.2}$$

Equation (2.3.32) gives:

$$\mathrm{Re}\left(\int\int_{S_\infty} -i \left(\phi_O \frac{\partial \phi_O^*}{\partial r} \right) r d\theta dz \right) = -\mathrm{Re}\left(\int_0^{\nu\pi} \int_0^a \left(\frac{\widehat{p_a}}{\rho\omega} \frac{\partial \phi_C}{\partial z} \right) \Big|_{z=0} r dr d\theta \right) \tag{2.4.3}$$

And we know from (2.3.38) that the right-hand side of this equality is equal to:

$$\frac{|\widehat{p_a}|^2}{\rho\omega} \mathcal{B} \tag{2.4.4}$$

Using equation 2.4.1 the left-hand-side becomes

$$\begin{aligned} RHS =& \mathrm{Re}\left(\int\int_{S_\infty} -i \left(\phi_O \frac{\partial \phi_O^*}{\partial r} \right) r d\theta dz \right) \\ =& \mathrm{Re}\left(\lim_{r\to\infty} \int_0^{\nu\pi} \int_{-h}^0 \mathcal{A}_0(\theta) \frac{e^{ikr}}{\sqrt{kr}} \mathcal{A}_0^*(\theta) \frac{e^{-ikr}}{\sqrt{kr}} \left(k - \frac{\mathrm{i}}{2r} \right) |Z_0(z)|^2 r d\theta dz \right) \\ =& \mathrm{Re}\left(\lim_{r\to\infty} \int_0^{\nu\pi} h |\mathcal{A}_0(\theta)|^2 \left(1 - \frac{\mathrm{i}}{2kr} \right) d\theta \right) \\ =& h \int_0^{\nu\pi} |\mathcal{A}_0(\theta)|^2 d\theta \end{aligned} \tag{2.4.5}$$

Equaling the two sides gives finally

$$\mathcal{B} = \frac{h\rho\omega}{\widehat{p}_a^2} \int_0^{\nu\pi} |\mathcal{A}_0(\theta)|^2 \, d\theta \tag{2.4.6}$$

Let us focus now on the diffraction problem and consider an incident wave of amplitude A_0 from the direction α. The diffraction potential is the sum of the potential of the incident wave φ^I and the potential of the scattered wave: $\varphi = \varphi^I + \varphi^S$ with φ^S outgoing at infinity. We apply Green's theorem to φ and ϕ and use the boundary conditions. We have:

$$\int\int_{S_C} \left(\varphi \frac{\partial \phi_C}{\partial z} - \phi_C \frac{\partial \varphi}{\partial z}\right) dS = -\int\int_{S_\infty} \left(\varphi \frac{\partial \phi_O}{\partial n} - \phi_O \frac{\partial \varphi}{\partial n}\right) dS \tag{2.4.7}$$

Using equation 2.3.27, we can write the left-hand side as:

$$\begin{aligned} LHS =& \int\int_{S_C} \left(\varphi \frac{\partial \phi_C}{\partial z} - \phi_C \frac{\partial \varphi}{\partial z}\right) dS \\ =& \int\int_{S_C} \left\{ \frac{g}{\omega^2} \frac{\partial \varphi}{\partial z} \left(\frac{i\omega \widehat{p}_a}{\rho g} + \frac{\omega^2}{g} \phi_C \right) - \phi_C \frac{\partial \varphi}{\partial z} \right\} dS \\ =& \frac{i\widehat{p}_a}{\rho\omega} \int\int_{S_C} \frac{\partial \varphi}{\partial z} dS \\ =& \frac{i\widehat{p}_a}{\rho\omega} \widehat{Q}^D(\alpha) \end{aligned} \tag{2.4.8}$$

Both φ and ϕ_O are outgoing at infinity thus $-\int\int_{S_\infty} \left(\varphi^S \frac{\partial \phi_O}{\partial n} - \phi_O \frac{\partial \varphi^S}{\partial n}\right) dS = 0$ and thus the left-hand side can be written as:

$$\begin{aligned} &-\int\int_{S_\infty} \left(\varphi^I \frac{\partial \phi_O}{\partial n} - \phi_O \frac{\partial \varphi^I}{\partial n}\right) dS \\ &\quad = \frac{igA_0}{\omega Z_0(0)} \int\int_{S_\infty} \left(\frac{\partial \phi_O}{\partial r} - \phi_O \frac{\partial}{\partial r}\right) e^{-ik(x\cos(\alpha)+y\sin(\alpha))} Z_0(z) dS \end{aligned} \tag{2.4.9}$$

Replacing ϕ_O by its far-field expression given in 2.4.1 we obtain for the previous expression:

$$\begin{aligned}\frac{ighA_0}{\omega Z_0(0)} \lim_{r\to\infty} \int_0^{\nu\pi} \left[\mathcal{A}_0 \frac{e^{ikr}}{\sqrt{kr}}\left(ik - \frac{1}{2r}\right) + \mathcal{A}_0 \frac{e^{ikr}}{\sqrt{kr}} ik\left(\cos\theta\cos\alpha + \sin\theta\sin\alpha\right)\right] \\ \times e^{-ikr(\cos\theta\cos\alpha+\sin\theta\sin\alpha)} r d\theta \\ = -\frac{ghA_0}{\omega Z_0(0)}\sqrt{kr}\int_0^{\nu\pi} \mathcal{A}_0(\theta)(1+\cos(\theta-\alpha)) e^{ikr(1-\cos(\theta-\alpha))} d\theta\end{aligned} \tag{2.4.10}$$

From the method of stationnary phase it follows that the right-hand side of equation (2.4.7) is finally equal to:

$$-\frac{ghA_0\sqrt{kr}}{\omega Z_0(0)} 2\mathcal{A}_0(\alpha)\sqrt{\frac{2\pi}{kr}} e^{i\pi/4} = -\frac{ghA_0}{\omega Z_0(0)} 2\sqrt{2\pi} e^{i\pi/4}\mathcal{A}_0(\alpha) \tag{2.4.11}$$

Thus equaling (2.4.8) and (2.4.11) we obtain:

$$\mathcal{A}_0(\alpha) = -\frac{iZ_0(0)\widehat{p_a} e^{-i\pi/4}}{2\sqrt{2\pi}\rho g h A_0}\widehat{Q}^D(\alpha) \tag{2.4.12}$$

which is a relation between the radiation and the scattering problems. We can now replace in (2.4.6) the expression we got previously in equation (2.4.12). This gives :

$$\mathcal{B} = \frac{\omega Z_0(0)^2}{8\pi\rho g^2 h A_0^2}\int_0^{\nu\pi} \left|\widehat{Q}^D(\theta)\right|^2 d\theta \tag{2.4.13}$$

Since $Z_0(0)^2 = \frac{kgh}{C_g\omega}$, we obtain the final relation:

$$\mathcal{B} = \frac{k}{8\pi C_g \rho g A_0^2}\int_0^{\nu\pi} \left|\widehat{Q}^D(\theta)\right|^2 d\theta \tag{2.4.14}$$

and with (2.1.9)

$$\mathcal{B} = \frac{k}{8\pi C_g \rho g^2}\int_0^{\nu\pi} \left|\Gamma(\theta)\right|^2 d\theta \tag{2.4.15}$$

This can be rewritten with dimensionless variables as

$$\widetilde{\mathcal{B}} = \frac{kh^2\sqrt{g/h}}{8\pi C_g}\int_0^{\nu\pi}\left|\widetilde{\Gamma}(\theta)\right|^2 d\theta \tag{2.4.16}$$

This expression is the generalisation of the formula given by Evans (1982) for the case of $\nu = 2$ and by Martin-Rivas and Mei (2009) and Evans (1988) for the case $\nu = 1$.

2.5 Energy extraction

Recall from 2.1.15 that the extraction efficiency is given by

$$kL = \frac{khg}{C_g\sqrt{g/h}}\frac{\chi\left|\widetilde{\Gamma}\right|^2}{\left(\chi+\widetilde{\mathcal{B}}\right)^2+\left(\widetilde{\mathcal{C}}-\beta\right)^2} \tag{2.5.1}$$

and let us focus on method to optimize the power output.

2.5.1 Optimization for a given frequency

A natural optimization method is to differentiate the previous expression with respect to both β (size of the cylinder) and χ (turbine characteristics) and to set these derivatives equal to zero. This leads to the well-known criteria:

$$\beta(\omega) = \widetilde{\mathcal{C}}(\omega) \quad \text{and} \quad \chi(\omega) = \widetilde{\mathcal{B}}(\omega) \tag{2.5.2}$$

Under these criteria, (2.5.1) becomes

$$kL_{\max} = \frac{khg}{C_g\sqrt{g/h}}\frac{\left|\widetilde{\Gamma}(\alpha)\right|^2}{4\widetilde{\mathcal{B}}} \tag{2.5.3}$$

Replacing $\widetilde{\mathcal{B}}$ by its expression in (2.4.16) we obtain that the maximum capture length is equal to

$$kL_{\max}(\alpha) = \frac{2\pi \left|\widetilde{\Gamma}(\alpha)\right|^2}{\int_0^{\nu\pi} \left|\widetilde{\Gamma}(\theta)\right|^2 d\theta} \tag{2.5.4}$$

However in practice it is impossible to use the strategy for all ω. Indeed, once the OWC is built, the value of β/ω is fixed (see equation (2.1.16)). However the value of χ may still be controled in real time through the rotationnal speed of the turbine blades. An idealized strategy for the OWC is thus to optimize the power output for all frequencies. This strategy will be studied in the next section and used further in our pratical cases.

2.5.2 Optimization for all frequencies

Let us find now the best extraction rate for maximum extracted energy at all frequecies. The coefficient β is now a known function of the frequency. By differentiating (2.5.1) with respect to the extraction coefficient χ and setting the derivative equal to zero leads to the following criterion:

$$\chi_{opt}(\omega) = \sqrt{\widetilde{\mathcal{B}}^2 + \left(\widetilde{\mathcal{C}} - \beta\right)^2} \tag{2.5.5}$$

Pluging this result into (2.5.1) and making use of the reciprocal relation (2.4.16), we obtain the expression of the optimum capture length:

$$kL_{\text{opt}} = \frac{8\pi\widetilde{\mathcal{B}}\sqrt{\widetilde{\mathcal{B}}^2 + \left(\widetilde{\mathcal{C}} - \beta\right)^2}\left|\widetilde{\Gamma}\right|^2}{\left(\left(\sqrt{\widetilde{\mathcal{B}}^2 + \left(\widetilde{\mathcal{C}} - \beta\right)^2} + \widetilde{\mathcal{B}}\right)^2 + \left(\widetilde{\mathcal{C}} - \beta\right)^2\right)\int_0^{\nu\pi}\left|\widetilde{\Gamma}(\alpha')\right|^2 d\alpha'} \tag{2.5.6}$$

Note that

$$kL_{\text{opt}}(\alpha) = kL_{\max}(\alpha) = \frac{2\pi\left|\widetilde{\Gamma}(\alpha)\right|^2}{\int_0^{\nu\pi}\left|\widetilde{\Gamma}(\alpha')\right|^2 d\alpha'} \quad \text{if and only if } \beta(\omega) = \widetilde{\mathcal{C}}(\omega) \tag{2.5.7}$$

Thus when $\beta(\omega) = \widetilde{\mathcal{C}}(\omega)$, the angular average, i.e. average over all angles of incidence, of the capture length is equal to

$$\overline{kL_{\text{opt}}} = \frac{1}{\nu\pi}\int_0^{\nu\pi} kL_{\text{opt}}(\alpha)\, d\alpha = \frac{2}{\nu} \tag{2.5.8}$$

The angular average $\overline{kL_{\text{opt}}}$ is a decreasing function of ν represented on figure (2-2). In particular, it is equal to 1 for a thin breakwater ($\nu = 2$) as already found by Martin-Rivas and Mei (2008) and to 2 for a straight coastline ($\nu = 1$) as described by Martin-Rivas and Mei (2009). Let us note that at the limit when ν goes to zero,

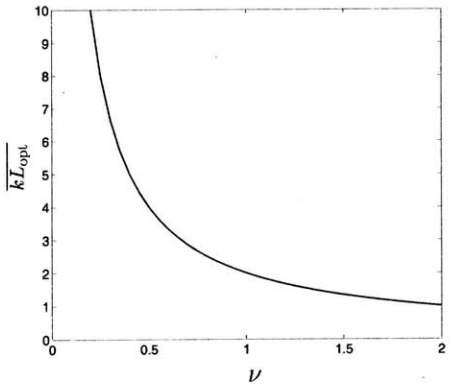

Figure 2-2: Evolution of the angular average of the capture length with ν

$\overline{kL_{\text{opt}}}$ goes to infinity. Indeed (2.5.3) shows that kL_{opt} is proportial to the inverse of $\widetilde{\mathcal{B}}$. As $\nu \to 0$, numerical simulations (see figure 2-3) show that the damping coefficient diminishes with the angle $(2-\nu)\pi$. Also even for a small opening angle, using optical geometry analogy (see figure 2-4), all the incident wave energy is channeled to focus at the OWC. This explains why the averaged capture width goes to infinity.

2.5.3 A more practical optimization

The previous optimization assumes that the value of χ can be controlled in real-time so that for any frequency $\chi = \chi_{opt}$ where χ_{opt} has been defined in equation (2.5.5). However this may be difficult in reality, especially if the range of value of $\chi_{opt}(\omega)$ is large. Thus a more practical optimization can be achieved by considering that χ is a simple function taking only two values. Let us now turn to two specific cases for

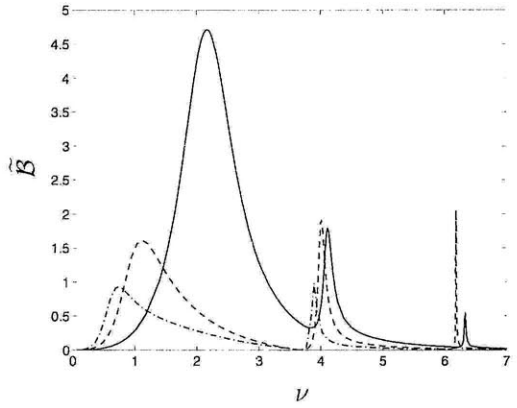

Figure 2-3: Damping coefficient as function of kh for ν equal to 3/2 (plain), 1/2 (dotted) and 1/4 (dashed-dotted)

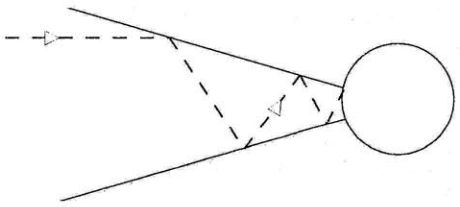

Figure 2-4: Pattern of an incident wave focused toward the OWC

further details. The method on how to choose the two values for χ will be explained then. We now describe explicit results for two special cases: $\nu = 3/2$ (convex corner) and $\nu = 1/2$ (concave corner).

Chapter 3

OWC at the convex corner of right angle coast

In this chapter we consider the specific case where $\nu = 3/2$ and thus the angle of the wedge is comprised between $\theta = 3\pi/2$ and $\theta = 2\pi$ as shown in figure 3-1. We only need to replace ν by $3/2$ in the previous chapter to obtain the equations for this specific case. We will only summarize the results here.

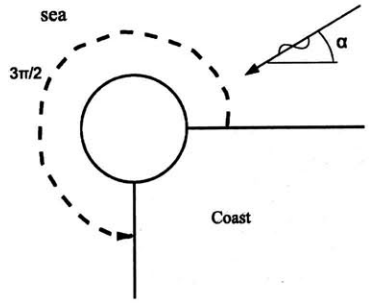

Figure 3-1: OWC at the tip of a wedge of angle $3\pi/2$, top view

3.1 Diffraction problem

We consider an incident wave from infinity at the angle $\theta = \alpha$ with respect to the wedge. The potential outside is given by equations (2.2.9), (2.2.10) and (2.2.11):

$$\varphi_{ext} = \varphi_1 + \varphi_2 \tag{3.1.1}$$

with:

$$\varphi_1 = -\frac{igA}{\omega}\sum_{n=0}^{\infty}\frac{4\epsilon_n}{3}\frac{icos(\frac{2n\alpha}{3})e^{-1\frac{n\pi}{3}}Y'_{\frac{2n}{3}}(ka)}{3H'_{\frac{2n}{3}}(ka)}\left(J_{\frac{2n}{3}}(kr) - \frac{J'_{\frac{2n}{3}}(ka)}{Y'_{\frac{2n}{3}}(ka)}Y_{\frac{2n}{3}}(kr)\right)cos\left(\frac{2n\theta}{3}\right)\frac{Z_0(z)}{Z_0(0)} \tag{3.1.2}$$

$$\epsilon_0 = 1 \text{and } \epsilon_n = 2 \text{for } n \geq 1$$

. and:

$$\varphi_2 = -\frac{igA}{\omega}\sum_{n=0}^{\infty}\sum_{l=0}^{\infty}A_{nl}\frac{K_{\frac{2n}{3}}(k_l r)}{k_l a K'_{\frac{2n}{3}}(k_l a)}\cos\left(\frac{2n\theta}{3}\right)Z_l(z) \tag{3.1.3}$$

The potential inside is given by (2.2.13)

$$\varphi_C = -\frac{igA}{\omega}\sum_{n=0}^{\infty}\sum_{l=0}^{\infty}\left(B_{nl}\cos(n\theta) + C_{nl}\sin(n\theta)\right)\frac{I_n(k_l r)}{k_l a I'_n(k_l a)}Z_l(z) \tag{3.1.4}$$

Coefficients A_{nl}, B_{nl} and C_{nl} are given respectively by (2.2.21), (2.2.23) and (2.2.24):

$$\frac{3\pi}{2\epsilon_n}A_{nl} = \frac{ia\omega}{ghA}\int_{-h}^{-d}\int_{0}^{3\pi/2}U(\theta,z)Z_l(z)\cos\left(\frac{2n\theta}{3}\right)d\theta dz \tag{3.1.5}$$

$$\frac{2\pi}{\epsilon_n}B_{nl} = \frac{ia\omega}{ghA}\int_{-h}^{-d}\int_{0}^{3\pi/2}U(\theta,z)Z_l(z)\cos(n\theta)d\theta dz \tag{3.1.6}$$

$$\frac{2\pi}{\epsilon_n}C_{nl} = \frac{ia\omega}{ghA}\int_{-h}^{-d}\int_{0}^{3\pi/2}U(\theta,z)Z_l(z)\sin(n\theta)d\theta dz \tag{3.1.7}$$

where $U(\theta, z)$ is defined in equation (2.2.31)

$$U(\theta, z) = -\frac{igA}{\omega} \sum_{m=0}^{\infty} \sum_{p=0}^{\infty} \alpha_{mp} \mathcal{T}_m(\theta) u_p(z) \tag{3.1.8}$$

where

$$u_p(z) = \frac{2(-1)^p}{\pi \sqrt{(h-d)^2 - (z+h)^2}} T_{2p}\left(\frac{z+h}{h-d}\right) \tag{3.1.9}$$

$$\mathcal{T}_m(\theta) \equiv T_m^*\left(\frac{2\theta}{3\pi}\right) \tag{3.1.10}$$

Coefficients α_{mp} are solution of the system defined by equation (2.2.45):

$$\begin{aligned}
&\frac{h}{a} \sum_{n=0}^{\infty} \mathcal{E}_n cos\left(\frac{2n\theta}{3}\right) Z_0(z) = \\
&\sum_{m=0}^{\infty} \sum_{p=0}^{\infty} \alpha_{mp} \sum_{n=0}^{\infty} \sum_{l=0}^{\infty} \frac{\epsilon_n}{2\pi} \frac{I_n(k_l a)}{k_l a I_n'(k_l a)} F_{Pl} F_{pl} \left(\mathfrak{C}(n, M)\mathfrak{C}(n, m) + S(n, M)S(n, m)\right) \\
&- \sum_{m=0}^{\infty} \sum_{p=0}^{\infty} \alpha_{mp} \sum_{n=0}^{\infty} \sum_{l=0}^{\infty} \frac{2\epsilon_n}{3\pi} \frac{K_{\frac{2n}{3}}(k_l a)}{k_l a K'_{\frac{2n}{3}}(k_l a)} F_{Pl}(z) F_{pl} \mathfrak{C}_{3/2}(n, m) \mathfrak{C}_{3/2}(n, M)
\end{aligned} \tag{3.1.11}$$

with the notations given by (2.2.35), (2.2.36) and (2.2.37):

$$\mathfrak{C}(n, m) = \int_0^{3\pi/2} \mathcal{T}_m(\theta) \cos(n\theta)\, d\theta \tag{3.1.12}$$

$$S(n, m) = \int_0^{3\pi/2} \mathcal{T}_m(\theta) \sin(n\theta)\, d\theta \tag{3.1.13}$$

$$\mathfrak{C}_{3/2}(n, m) = \int_0^{3\pi/2} \mathcal{T}_m(\theta) \cos\left(\frac{2n\theta}{3}\right) d\theta \tag{3.1.14}$$

3.2 Radiation problem

The potential inside the cylinder is given by equation (2.3.2):

$$\phi_C = -\frac{i\widehat{p_a}}{\rho\omega} \sum_{n=0}^{\infty} \sum_{l=0}^{\infty} D_{nl} \frac{I_n(k_l r)}{k_l a I_n'(k_l a)} \cos\left[n\left(\theta - \frac{3\pi}{4}\right)\right] Z_l(z) - \frac{i\widehat{p_a}}{\rho\omega} \tag{3.2.1}$$

The potential outside is given by equation (2.3.3):

$$\phi_O = -\frac{i\widehat{p_a}}{\rho\omega}\sum_{n=0}^{\infty}\sum_{l=0}^{\infty} E_{nl}\frac{K_{2n}(k_l r)}{k_l a K'_{2n}(k_l a)}\cos\left(\frac{4n\theta}{3}\right) Z_l(z) \tag{3.2.2}$$

Coefficients D_{nl} and E_{nl} are can be calculated with equations (2.3.11) and (2.3.12):

$$\frac{2\pi}{\epsilon_n}D_{nl} = \frac{ia\rho\omega}{\widehat{p_a}h}\int_{-h}^{-d}\int_{3\pi/2}^{0} U(\theta,z)\cos\left[n\left(\theta-\frac{3\pi}{4}\right)\right] Z_l(z)d\theta dz \tag{3.2.3}$$

$$\frac{3\pi}{2\epsilon_n}E_{nl} = \frac{ia\rho\omega}{\widehat{p_a}h}\int_{-h}^{-d}\int_{3\pi/2}^{0} U(\theta,z)\cos\left[\frac{4n\theta}{3}\right] Z_l(z)d\theta dz \tag{3.2.4}$$

The expansion of $U(\theta, z)$ is given by (2.3.18):

$$U(\theta,z) = \frac{-i\widehat{p_a}h}{\rho\omega}\sum_{m=0}^{\infty}\sum_{p=0}^{\infty}\alpha_{mp}\cos\left[\frac{4m}{3}\left(\theta-\frac{3\pi}{4}\right)\right] u_p(z) \tag{3.2.5}$$

Coefficients α_{mp} are calculated by solving the linear system given by (2.3.22):

$$\begin{aligned}\frac{h}{a}3\pi\delta_{M0}\delta_{P0} = &\sum_{p=0}^{\infty}\alpha_{Mp}\sum_{l=0}^{\infty}F_{pl}F_{Pl}\frac{3\pi}{\epsilon_M}\frac{K_{2M}(k_l a)}{k_l a K'_{2M}(k_l a)} \\ &-\sum_{m=0}^{\infty}\sum_{p=0}^{\infty}\alpha_{mp}\sum_{n=0}^{\infty}\sum_{l=0}^{\infty}\frac{\epsilon_n}{\pi}F_{pl}F_{Pl}R_{mn}R_{Mn}\frac{I_n(k_l a)}{k_l a I'_n(k_l a)}\end{aligned} \tag{3.2.6}$$

where

$$R_{mn} = \int_0^{3\pi/2}\cos\left[\frac{4m}{3}\left(\theta-\frac{3\pi}{4}\right)\right]\cos\left[n\left(\theta-\frac{3\pi}{4}\right)\right]d\theta \tag{3.2.7}$$

3.3 Numerical results

We present in this section the results obtained with the program for the diffraction problem and the radiation problem separately. The results of two programs will be combined further to study the energy extraction rate. All the results are computed with non-dimensionalized variables.

3.3.1 Numerical results for the diffraction problem

It has been shown by Martin-Rivas and Mei (2008) that for an axi-symmetric structure in the open sea (corresponding to $\nu = 2$) the vertical flux rate inside the cylinder is independant of the angle of incidence α. This is no longer the case if $\nu \neq 2$ and the scattered wave must depend strongly of the angle of incidence.

Figure 3-2a presents the square of the absolute value of the scattering coefficient $\widetilde{\Gamma}$ at three different frequencies, kh = 2.21, 4.12, 6.34 as a function of α. The inputs are h/a =2 and d/h = 0.2. Figure 3-2b presents the same coefficient for a/h=1/4 and kh=2.909. Due to the symmetry of the problem with respect to $\theta = 3\pi/4$, the figures only present the results for a range of α between 0 and $3\pi/4$. We see that for the two

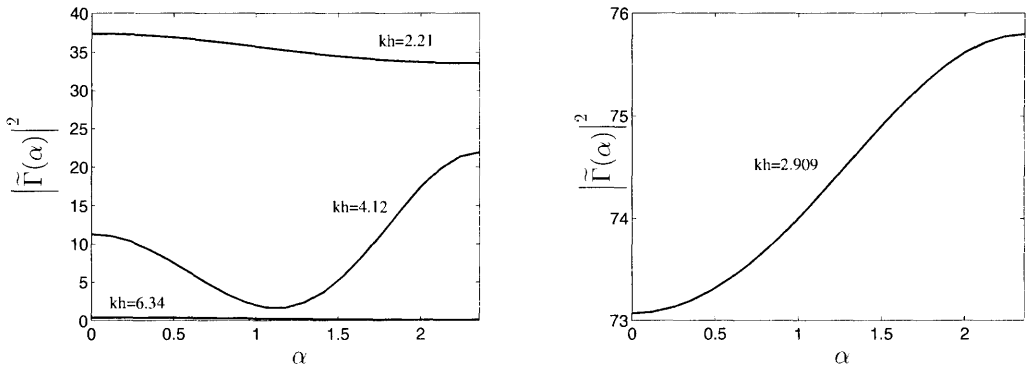

(a) a/h=1/2 (b) a/h=1/4

Figure 3-2: Scattering coefficient function of α. Left: a/h=1/2 and right: a/h=1/4. d/h=0.2

configurations the incidence angle has a strong influence on $\left|\widetilde{\Gamma}(\alpha)\right|^2$. This influence is more or less strong depending on the frequency. Figure 3-3 presents the relative difference between the scattering coefficient at the angle α and at the angle 0. We see that for $a/h = 1/2$ and $kh = 2.21$ the value of $\left|\widetilde{\Gamma}(\alpha)\right|^2$ remains almost constant as α increases whereas for $kh = 4.12$ the relative difference decreases of 85% and then increases up to 95%.

Figure 3-4 presents the variation of $\left|\widetilde{\Gamma}(kh)\right|^2$ as a function of kh for a fixed incidence angle $\alpha = \pi/4$ and $a/h = 1/2,\ 1/4$. In the two cases, the scattering coefficient presents one broad maximum. Its intensity decreases and its frequency increases as

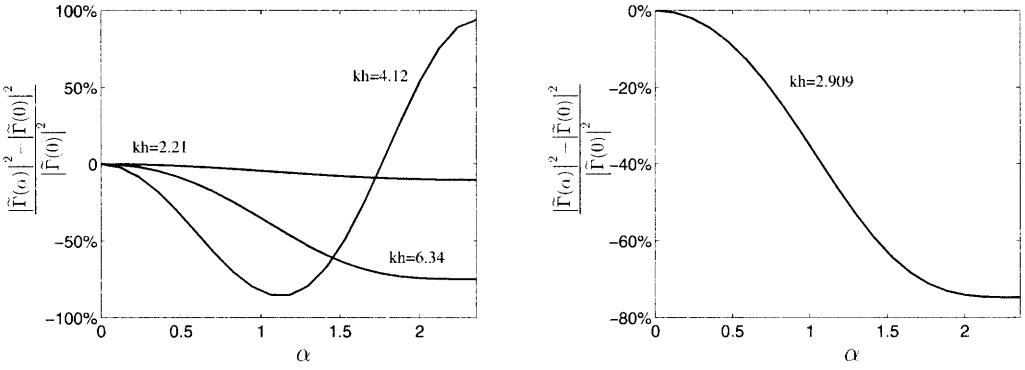

(a) a/h=1/2 (b) a/h=1/4

Figure 3-3: Relative difference of the scattering coefficient function of α. Left: a/h=1/2 and right: a/h=1/4. d/h=0.2

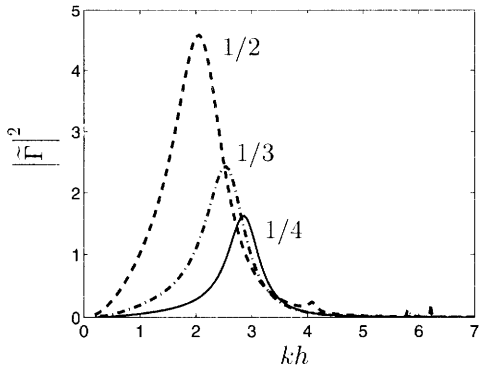

Figure 3-4: Diffraction-induced vertical flux coefficient as a function of kh. Plain: a/h=1/4, dahs-dots: 1/2 and dash: a/h=1/4. d/h=0.2 and $\alpha = \pi/4$

a/h decreases.

3.3.2 Numerical results for the radiation problem

Two important quantities for this problem are the damping coefficient $\mathcal{B}$ and the added mass $\mathcal{C}$. They will further be usefull to calculate the energy extraction rate. We recall that these coefficients are given by

$$Q^R = -(\mathcal{B} - i\mathcal{C})\,\widehat{p_a} = \int\int_S \left.\frac{\partial\phi}{\partial z}\right|_{z=0} dS \tag{3.3.1}$$

Replacing the potential by its expression in (3.2.1) and using the dimensionless variables defined in (2.1.14) gives

$$\tilde{\mathcal{B}} = \frac{1}{\sqrt{kh\tanh(kh)}}\,\mathcal{R}\left(\int\int_S \sum_l \frac{iD_l}{h}\frac{I_0(k_l r)}{k_l a I_0'(k_l r)} Z_l'(0) dS\right) \tag{3.3.2}$$

$$\tilde{\mathcal{C}} = -\frac{1}{\sqrt{kh\tanh(kh)}}\,\mathcal{I}\left(\int\int_S \sum_l \frac{iD_l}{h}\frac{I_0(k_l r)}{k_l a I_0'(k_l r)} Z_l'(0) dS\right) \tag{3.3.3}$$

where we have used the relation $\sqrt{g/h}\big/\omega = 1\big/\sqrt{kh\tanh(kh)}$. The previous integrales have been discretized with a integration step of equals to $\delta r = 0.01$ in order to perform the integration numerically.

Variation of $\tilde{\mathcal{B}}$ and $\tilde{\mathcal{C}}$ with kh for a large OWC

We first fix $a/h = 1/2$ and $d/h = 0.2$. Figure 3-5 presents the variation of $\tilde{\mathcal{B}}$ and $\tilde{\mathcal{C}}$ as kh increases.

The damping coefficient presents three peaks of resonance at kh equals to 2.18, 4.12 and 6.34. The intensity of the first peak (equal to 4.72) is much larger and broader than the second (1.78) and third one (0.54). The added mass $\tilde{\mathcal{C}}$ presents also peaks at the same frequence as those of $\tilde{\mathcal{B}}$ and changes sign around $kh = 2.15$. This is

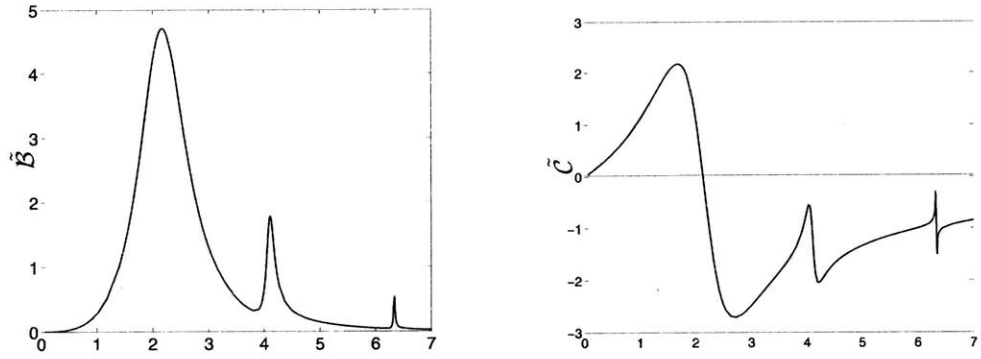

(a) Damping coefficient $\tilde{\mathcal{B}}$ (b) Added mass $\tilde{\mathcal{C}}$

Figure 3-5: Variation of the damping coefficient and the added mass as kh increases for $a/h = 1/2$ and $d/h = 0.2$

an important property of OWC already known and dicussed by Smith (1958), Evans and Porter (1997) and Evans and Porter (1995). Here $\tilde{\mathcal{C}}$ only changes one time of sign and has a shape similar to two N juxtaposed. It is now interesting to understand which modes are responsible for the peaks we observed before. For this purpose, let us focus on the free surface elevation inside the cylinder for frequences near to each peak's frequency.

First peak of resonance

Figure 3-6 presents for different instants a 3D view of the free surface oscillation inside the cylinder for kh near the first peak of $\tilde{\mathcal{B}}$. The surface oscillates and is very flat with a slight tilt (see for example figure 3-6d). These oscillations of the surface are similar to Helmholtz mode oscillation. The free surface inside the cylinder has a piston-like motion. However pure Helmholtz mode cannot exist because of the asymmetry of the opening. Another mode must be excited, and is responsible for the slight slope. This can be verified in the following way: from equation (3.2.1), we know that the coefficient associated with each cosine is given by:

$$c_n = \sum_{l=0}^{\infty} D_{nl} \frac{I_n(k_l r)}{k_l a I_n'(k_l a)} Z_l(0) \tag{3.3.4}$$

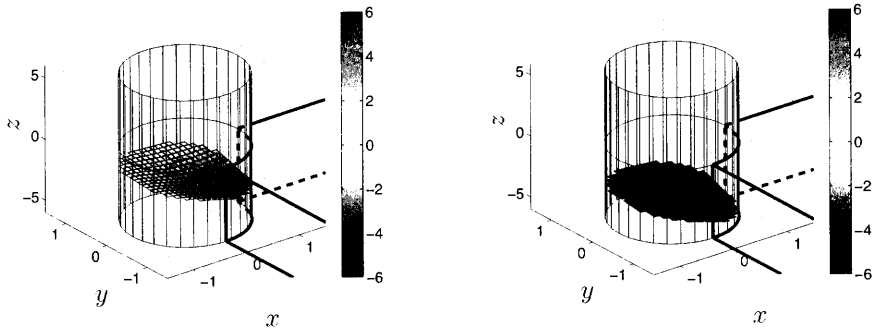

(a) $t = 0.6\pi/2\omega$ (b) $t = 1.2\pi/2\omega$

(c) $t = 2.5\pi/2\omega$ (d) $t = 3\pi/2\omega$

Figure 3-6: 3D plot of the free surface elevation inside the cylinder, η/A_0 for $kh = 2.21$. $a/h = 1/2$, $d/h = 0.2$. Radiation problem

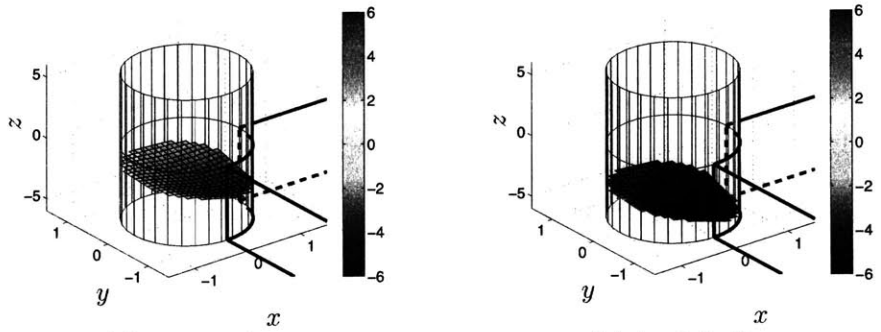

(a) $t = 0.6\pi/2\omega$ (b) $t = 1.2\pi/2\omega$

(c) $t = 2.5\pi/2\omega$ (d) $t = 3\pi/2\omega$

Figure 3-6: 3D plot of the free surface elevation inside the cylinder, η/A_0 for $kh = 2.21$. $a/h = 1/2$, $d/h = 0.2$. Radiation problem

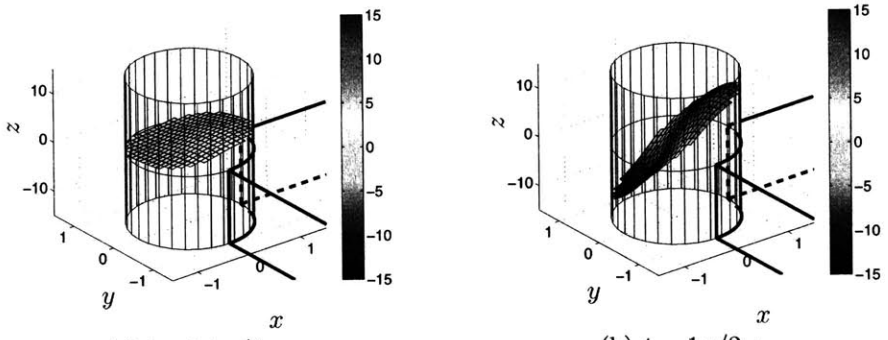

(a) $t = 0.1\pi/2\omega$ (b) $t = 1\pi/2\omega$

(c) $t = 2.1\pi/2\omega$ (d) $t = 3\pi/2\omega$

Figure 3-8: 3D plot of the free surface elevation inside the cylinder for $kh = 4.12$. $a/h = 1/2$, $d/h = 0.2$. Radiation problem

m	0	1	2	3
j'_{m1}	0	1.84118	3.05424	4.20119

Table 3.1: Value of j'_{m1}, eigenvalues of a close circular basin

Third peak of resonance

Figure 3-9 presents for different time a 3D view of the free surface oscillation inside the OWC for $kh = 6.34$. We see that these oscillations are very different from the

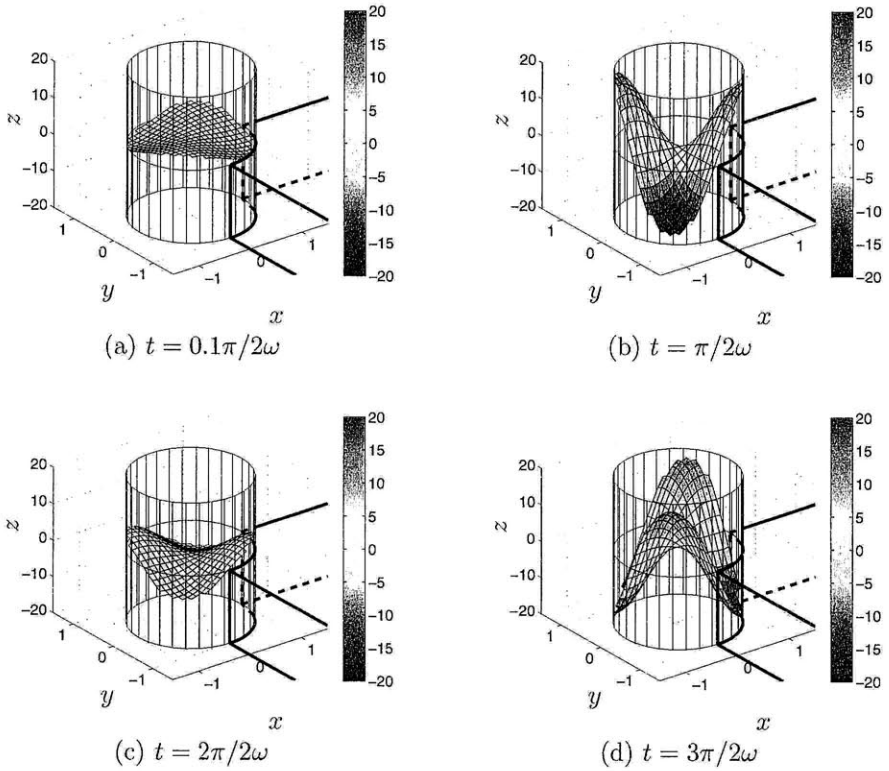

(a) $t = 0.1\pi/2\omega$ (b) $t = \pi/2\omega$

(c) $t = 2\pi/2\omega$ (d) $t = 3\pi/2\omega$

Figure 3-9: 3D plot of the free surface elevation inside the cylinder for $kh = 6.34$. $a/h = 1/2$, $d/h = 0.2$. Radiation problem

two previous situations. The free surface has sometimes the shape of a simple saddle whose curvature changes sign with time (figure 3-9b and 3-9d). The amplitude of the oscillation is comparable to that of the second peak: between -20 and 20. Figure 3-7c presents the absolute value of the coefficients of the first four modes for $r/a = 0.5$. Clearly the coefficient c_2 corresponding to $\cos(2\theta)$ dominates. In addition, for this peak $ka = 3.17$ is close to $j'_{21} = 3.05424$ that corresponds to the natural mode $\alpha J_1(k_{11}r)\cos(2\theta) + \beta J_1(k_{11}r)\sin(2\theta)$.

Figure 3-10 presents the free surface elevation for the diffraction problem at the same frequencies. We see that the pattern of the surface is identical to the one observed previously.

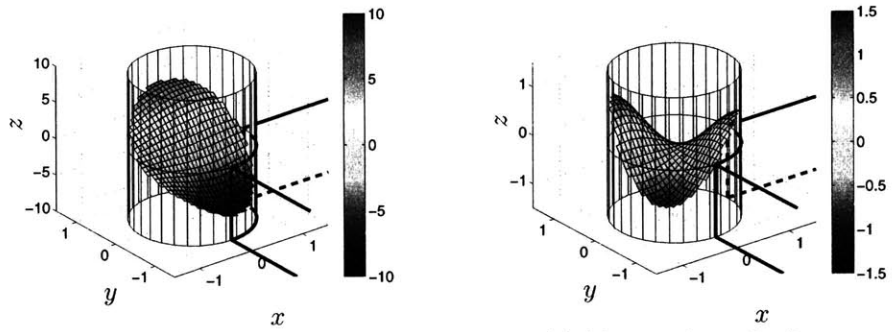

(a) $kh = 4.12, t = 2\pi/2\omega$ (b) $kh = 6.34, t = 2\pi/2\omega$

Figure 3-10: 3D plot of the free surface elevation inside the cylinder for $kh = 6.34$. $a/h = 1/2$, $d/h = 0.2$, $\alpha = 3\pi/4$. Diffraction problem

As we can see from the study of each peak, the amplitude of the free surface inside the cylinder is not large in the three cases. This is because the opening of the cylinder is large ($d/h = 0.2$). If we reduce the dimension of the opening ($d/h \to 1$), the results are no longer the same. It can be expected for this case that the first mode corresponds to the Helmholtz mode. The free surface inside the cylinder acts like a piston and the amplitude of its elevation is very large. This mode is predominent and the amplitudes of the other mode are extremely small. In order to veridy these assumptions, figure 3-11 presents the damping coefficient and the added mass for $d/h = 0.7$. There is

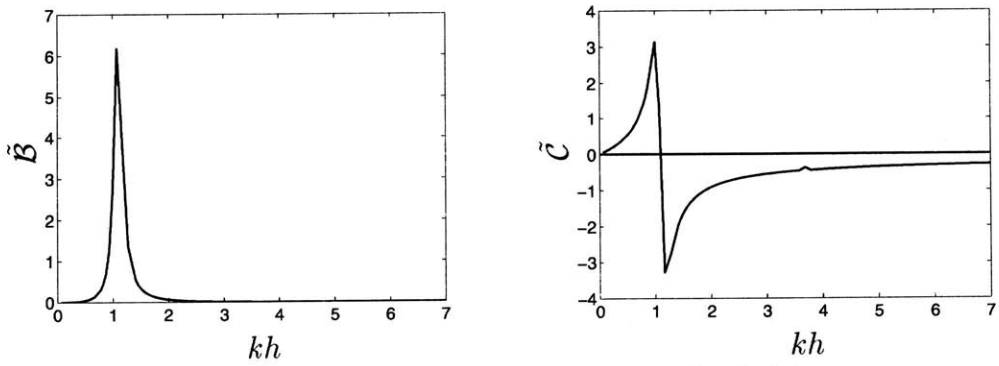

(a) Damping coefficient (b) Added mass

Figure 3-11: Variation of the damping coefficient and the added mass as kh increases. $a/h = 1/2$ and $d/h = 0.7$

only one large peak for $kh = 1.07$. Figure 3-12 presents the variation of the free

surface elevation inside the cylinder at different times for $kh = 1.07$. We see that the free surface acts like a piston, thus the peak we observe corresponds to Helmholtz mode. Let us note that a second and extremely small peak is visible on figure 3-11b

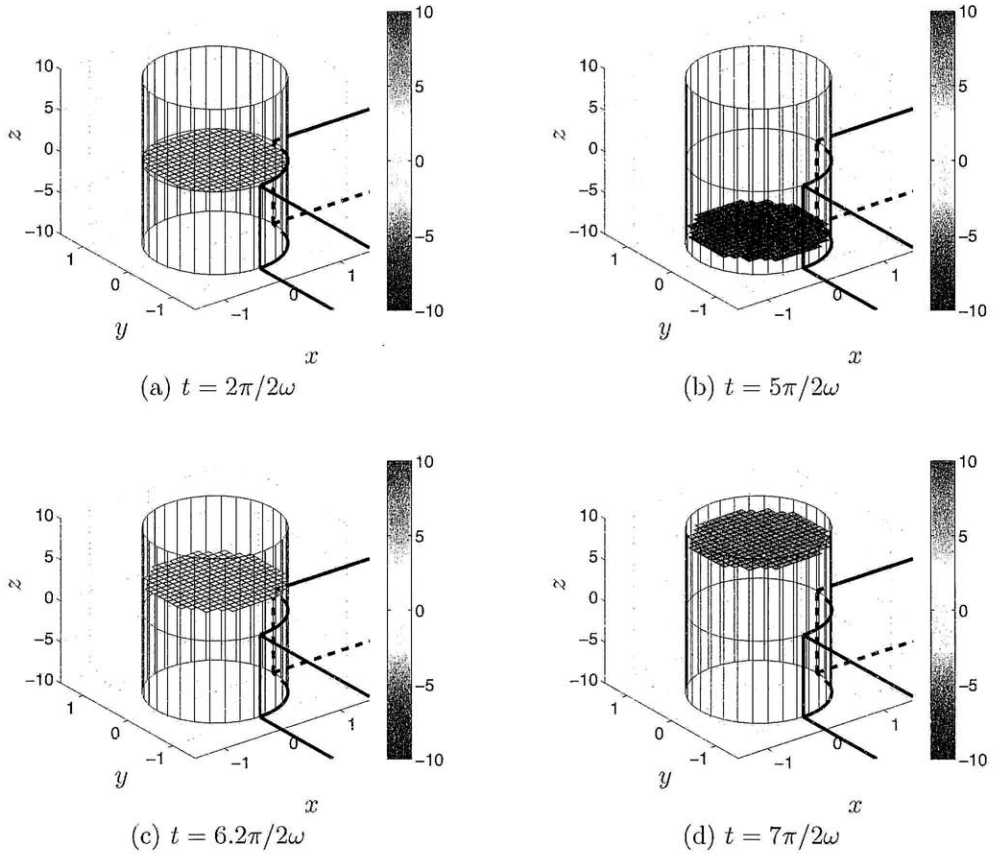

(a) $t = 2\pi/2\omega$ (b) $t = 5\pi/2\omega$

(c) $t = 6.2\pi/2\omega$ (d) $t = 7\pi/2\omega$

Figure 3-12: 3D plot of the free surface elevation inside the cylinder for $kh = 2.21$. $a/h = 1/2$, $d/h = 0.7$

for $kh = 3.689$, that is $ka = 1.845$. This frequency is now very close to the eigenvalue $j'_{11} = 1.84118$. Thus, as it can be expected, as $d/h \to 1$ the frequency of each peaks tends toward the frequency of a natural mode of a close circular basin.

Variation of $\tilde{\mathcal{B}}$ and $\tilde{\mathcal{C}}$ with a/h

.

Figure 3-13 presents the dependence of $\tilde{\mathcal{B}}$ and $\tilde{\mathcal{C}}$ on kh for three different values of the ratio a/h: 1/4, 1/3, and 1/2.

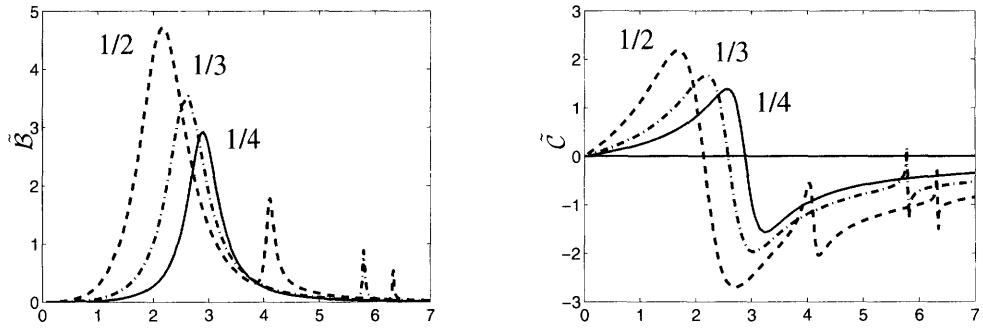

(a) Damping coefficient (b) Added mass

Figure 3-13: Variation of the damping coefficient and the added mass as kh increases. Plain: $a/h = 1/4$, dash-dot: $a/h = 1/3$, dash: $a/h = 1/2$. In every cases, $d/h = 0.2$.

Let us comment on the variation of $\tilde{\mathcal{B}}$. As a/h decreases, the frequency of each peaks of resonance increases: for a/h respectively equal to 1/4, 1/3, and 1/2, the first peak of resonance happens for kh respectively equal to 2.2, 2.6, and 2.9. Physically, as a/h decreases, the fluid inside the OWC tends to behave like a piston. In the limit, a hydrostatic approximation predicts resonance at $kd = \tanh(kh) = 1$, which corresponds to $kh \approx 5$. This trend is confirmed by our computations. For $a/h = 1/4$ the curve of $\tilde{\mathcal{B}}$ shows only one peak of resonance at $kh = 2.9$. For $a/h = 1/3$, the curve shows two peaks of resonance (at $kh = 2.6$ and 5.8) and for $a/h = 1/2$ the curves shows the three peaks that have been studied in a previous section. For a fixed depth h, the peaks of resonance are narrower for a small radius a and the intensity of the peaks increases if the radius increases.

Variation of $\tilde{\mathcal{B}}$ and $\tilde{\mathcal{C}}$ with d/h

.

Let us now consider a fixed radius a/h=1/4 and examine the influence of d/h. Figure 3-14 presents the variation of $\tilde{\mathcal{B}}$ and $\tilde{\mathcal{C}}$ for d/h equal to 0.1, 0.2 and 0.3. As d/h decreases (which corresponds to a larger opening) the curves are flatter. The peaks are lower and broader and their intensity is higher. Thus for $d/h = 0.1$, the peak of resonance of $\tilde{\mathcal{B}}$ happens for $kh = 4.18$ and is equal to 1.85 whereas for d/h=0.3 it happens for $kh = 2.22$ and is equal to 3.8.

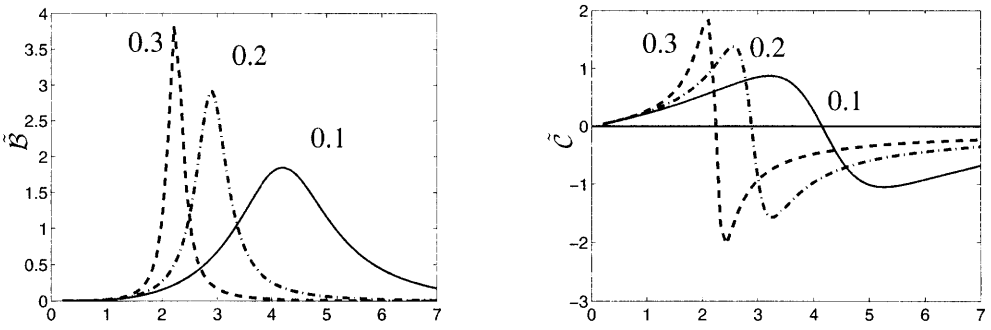

(a) Damping coefficient (b) Added mass

Figure 3-14: Variation of the damping coefficient and the added mass as kh increases for different values of d. Plain: $d/h = 0.1$, dash-dot: $d/h = 0.2$, dash: $d/h = 0.3$. In every cases, $a/h = 1/4$

Figure 3-15 presents the same curves for $a/h = 1/2$. The damping coefficient presents several peaks of resonance but the previous observations are still valid for this case.

For most of the simulations, we will take d/h=0.2.

Comparison between a thin beakwater and a straight coastline

The case of an OWC at the tip of a thin breakwater has been study by Martin-Rivas and Mei (2008) and the case of an OWC along a straight coast by Martin-Rivas and Mei (2009). Their results, as well as the results of this nd the following chapter are combined in the section 4.3 of the following chapter for comparison.

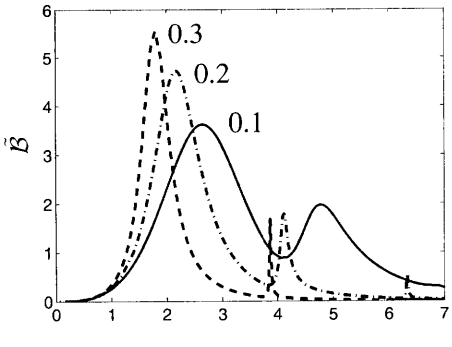

(a) Damping coefficient

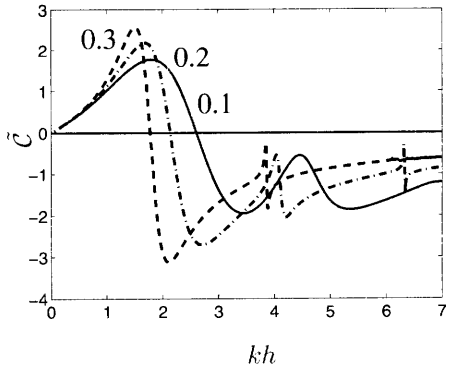

(b) Added mass

Figure 3-15: Variation of the damping coefficient and the added mass as kh increases for different values of d. Plain: $d/h = 0.1$, dash-dot: $d/h = 0.2$, dash: $d/h = 0.3$. In every cases, $a/h = 1/2$

3.4 Energy extraction

By combining the diffraction and radiation problems, we can now study the power that one may extract from this device. Let us recall from equation (2.5.1) that the capture length is given by

$$kL = \frac{khg}{C_g\sqrt{g/h}} \frac{\chi \left|\widetilde{\Gamma}\right|^2}{\left(\chi + \widetilde{\mathcal{B}}\right)^2 + \left(\widetilde{\mathcal{C}} - \beta\right)^2} \tag{3.4.1}$$

where χ is the turbine characteristic and β the size of the chamber/turbine.

3.4.1 Optimization for all frequencies

This strategy has been developped in section 2.5.2. Let us recall that it assumes that it is possible to adapt in real-time the value of χ to extract the maximum power. From equation (2.5.6) we have:

$$kL_{\text{opt}} = \frac{8\pi\widetilde{B}\sqrt{\widetilde{B}^2 + \left(\widetilde{C} - \beta\right)^2}\left|\widetilde{\Gamma}\right|^2}{\left(\left(\sqrt{\widetilde{B}^2 + \left(\widetilde{C} - \beta\right)^2} + \widetilde{B}\right)^2 + \left(\widetilde{C} - \beta\right)^2\right)\int_0^{\nu\pi}\left|\widetilde{\Gamma}(\alpha')\right|^2 d\alpha'} \tag{3.4.2}$$

and the maximum efficiency is given by

$$kL_{opt}(\alpha) = \frac{2\pi \left|\widetilde{\Gamma}(\alpha)\right|^2}{\int_0^{3\pi/2} \left|\widetilde{\Gamma}(\alpha)\right|^2 d\alpha} \quad \text{if and only if} \quad \beta(kh) = \widetilde{C}(kh) \tag{3.4.3}$$

The result are presented with numerical values similar to those of the pilot station in Pico Island, Azores, Portugal (Falcão (2000)). The inputs are: $D = 2a$, $N =$ 2000rpm, $K = 0.45$ (for one turbine), $V_0 = \pi a^2 h$, $h = 10$m, $\rho_w/\rho_a = 1000$, $g = 9.81$ $m.s^{-2}$ and c_a=340 $m.s^{-1}$.

Influence of the radius a/h

Let us fix $\alpha = \pi/2$ and examine the variation of the capture length and the turbine parameter for 3 values of the ratio a/h. The results are presented on figures 3-16a and 3-16b. The shape of the curves and their amplitude depend strongly of the value

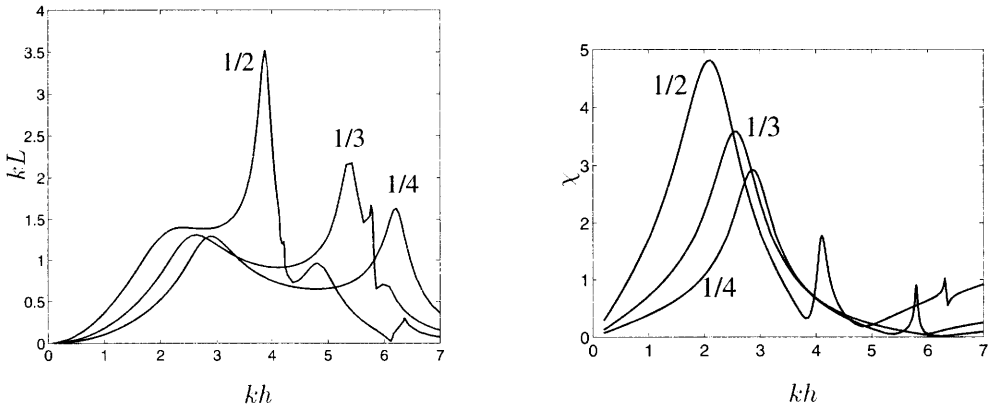

(a) Capture length (b) Turbine parameter

Figure 3-16: Capture length function of kh for $a/h = 1/2$, $1/3$ and $=1/4$. For each case $\alpha = 0$, $d/h = 0.2$ and $V_0 = \pi a^2 h$

of a/h. When a/h decreases, the curve of the capture length becomes flatter and the peak of resonance has a smaller value. For a/h=1/4, the capture length has only two maxima whereas it has 4 maxima for the two other cases. The frequence of the peak of resonance increases when a/h is smaller. The variation of the turbine parameter is smoother as a/h decreases.

We know from the theory (see equation (3.4.3)) that maxima of the capture length correpond to point of intersection of the curve of β and $\widetilde{\mathcal{C}}$. This can be verified on figure 3-17.

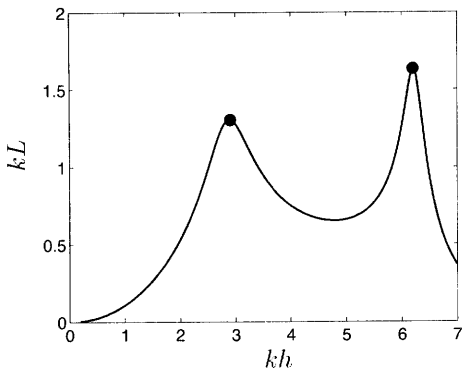

(a) Capture length

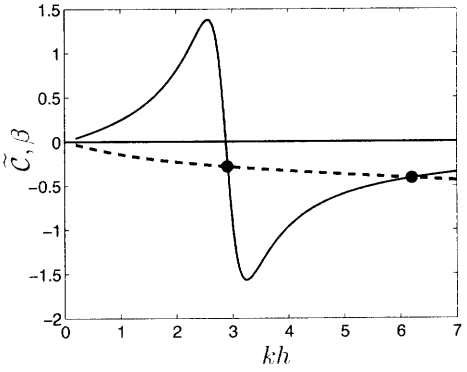

(b) Added mass and β coefficient

Figure 3-17: Left: Capture length function of kh. Right: $\widetilde{\mathcal{C}}$ (plain) and β (dotted) function of kh. $a/h = 1/4$, $d/h = 0.2$, $\alpha = 0$ and $V_0 = \pi a^2 h$

Finally let us recall that $\beta = -\frac{\omega V_o \rho_w \sqrt{g/h}}{C_a^2 \rho_a h} \propto \omega \propto \sqrt{kh \tanh(kh)}$. Thus for $kh \geq 2$, $\beta \propto \sqrt{kh}$.

Figure 3-18 presents the same curves for $\alpha = \pi/2$.

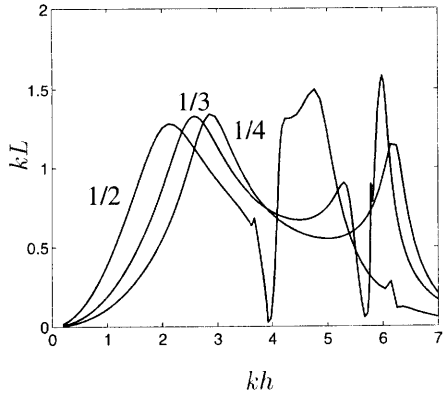

(a) Capture length

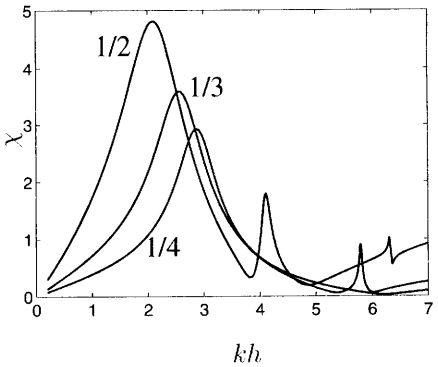

(b) Turbine parameter

Figure 3-18: Capture length function of kh for $a/h = 1/2$, $1/3$ and $=1/4$. For each case $\alpha = \pi/2$, $d/h = 0.2$ and $V_0 = \pi a^2 h$

Infuence of the incidence angle on the energy extraction rate

As we have seen previously, the scattering coefficient depends strongly on the incidence angle α. Thus one can predict that the capture length kL will also depends on it. Figure 3-19a presents the variation of kL with kh for different incidence angles and $a/h = 1/4$. Figure 3-19b presents the same variation for $a/h = 1/2$.

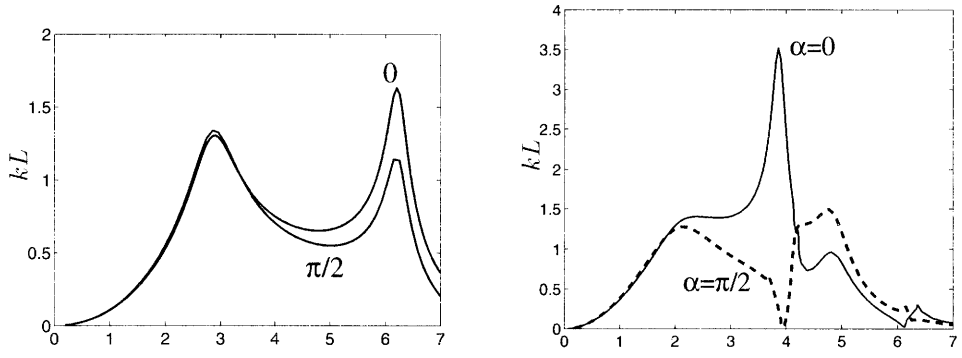

(a) $a/h = 1/4$ (b) $a/h = 1/2$

Figure 3-19: Capture length function of kh for different incidence angle α: $\alpha = 0$, $\alpha = \pi/2$. $V_0 = \pi a^2 h$

We see that indeed the incidence angle has a strong influence on the shape of the curve as well as its amplitude. The capure length remains mostly under 2.

For some angle of incidence and some frequencies (in particular $kh = 3.93$ (ka=1.96) for $\alpha = \pi/2$ and a/h=1/2), the capture length is equal to zero: no power is extracted from the incident wave. This frequency is closed to the first zero of $J_1'(ka)$ ($J_1'(ka = 1.84) = 0$). From section 2.5.2 that the angular average, i.e. average over all angles of incidence, of the capture length is equal to

$$\overline{kL_{\text{opt}}} = \frac{1}{3\pi/2} \int_0^{3\pi/2} kL_{\text{opt}}(\alpha)\, d\alpha = \frac{4}{3} \tag{3.4.4}$$

Influence of the size of the chamber.

In general, to increase the energy extraction rate, a strategy is to introduce control in the power-takeoff system and to have a extraction rate complex where the real part corresponds to elasticity. For the OWC, air compressibility provides such elasticity. Let us recal that air compressibility is related to the parameter β through $\beta = -\frac{\omega V_o \rho_w \sqrt{g/h}}{C_a^2 \rho_a h}$, and depends thus of the volume of the chamber V_0. Since the energy extraction depends of the relativ behavior of the curve of β and $\widetilde{\mathcal{C}}$, we will examine in this paragraph the influence of the volume of the chamber on the efficiency of the device.

Figure 3-20 presents the results for $a/h = 1/4$ and $\alpha = \pi/2$. The first case ($V_0 = 0$ on figure 3-20a) corresponds to incompressible air. In this case the curve of β merges with the x-axis and intersects the curve of $\widetilde{\mathcal{C}}$ at one point at $kh \approx 3$. At this frequency the curve of kL has a maximum. As the volume V_0 increases the curve of β is shifted downwards and the number of points of intersection between the curves of β and $\widetilde{\mathcal{C}}$ increases up to 2 points (see figure 3-20c). Each point of intersection corresponds to a maximum of the capture length kL. As V_0 continues to increase and reaches $5\pi a^2 h$, the two points of intersection of β and $\widetilde{\mathcal{C}}$ converge toward a single point of intersection corresponding to the minimum of $\widetilde{\mathcal{C}}$ at $kh \approx 3.2$ and as a result the two maxima of kL merge into a single one (see figure 3-20e). As the volume of the chamber exceeds 5 (see figure 3-20f) the curves of β and $\widetilde{\mathcal{C}}$ do not intersect anymore and the capture length shows one local maxima, which intensity decreases as the volume of the chamber increases. This corresponds to a situation of poor energy efficiency.

Figure 3-21 presents the same study for $\alpha = 0$. The same discussion can be done for $a/h = 1/3$ and is presented in figure 3-22 for $\alpha = 0$ and in figure 3-23 for $\alpha = \pi/2$..

For incompressible air the curves of β merges with the x-axis and intersects the curve of $\widetilde{\mathcal{C}}$ at one point at $kh \approx 2.5$. At this frequency the curve of kL has a maximum. A second maximum is visible around $kh \approx 5.7$. As the volume V_0 increases the curve of β is shifted downwards and the number of points of intersection between the curves

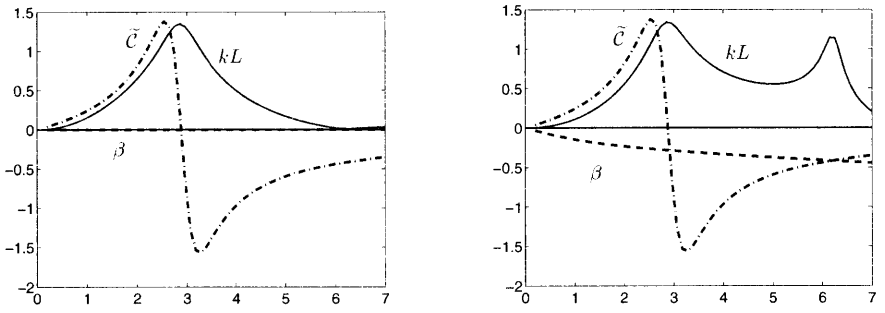

(a) V_0 =0 (b) $V_0 = \pi a^2 h$

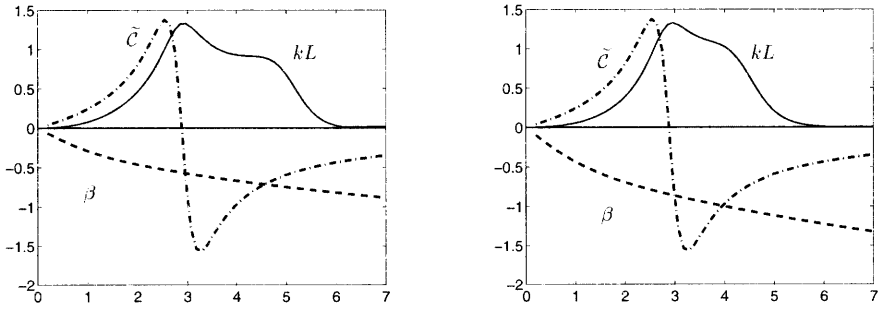

(c) V_0 =$2\pi a^2 h$ (d) V_0 =$3\pi a^2 h$

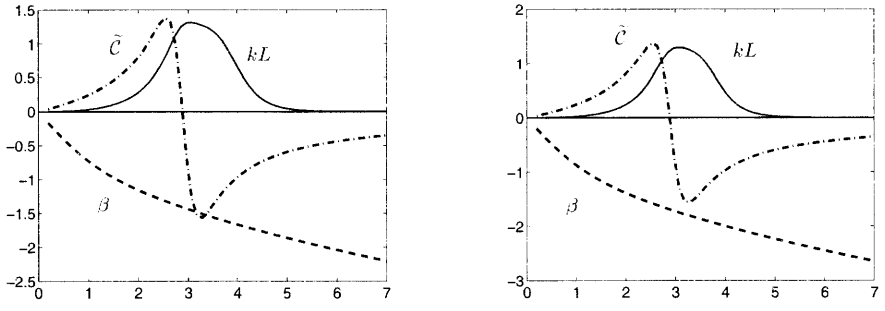

(e) V_0 =$5\pi a^2 h$ (f) V_0 =$6\pi a^2 h$

Figure 3-20: Capture length (dashed), added mass (plain) and β coefficient (dashed-dotted) against the normalized frequency kh for different pneumatic chamber volume V_0. $a/h = 1/4$, $d/h = 0.2$, $\alpha = \pi/2$, $h = 10$m.

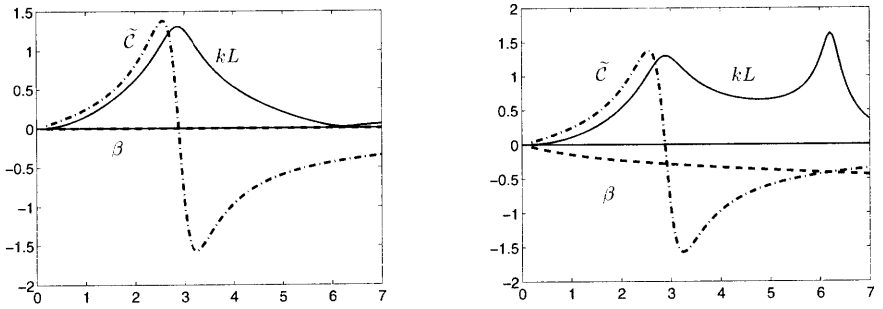

(a) V_0 =0 (b) $V_0 = \pi a^2 h$

(c) $V_0 = 3\pi a^2 h$ (d) $V_0 = 6\pi a^2 h$

Figure 3-21: Capture length (dashed), added mass (plain) and β coefficient (dashed-dotted) against the normalized frequency kh for different pneumatic chamber volume V_0. $a/h = 1/4$, $d/h = 0.2$, $\alpha = 0$, $h = 10$m.

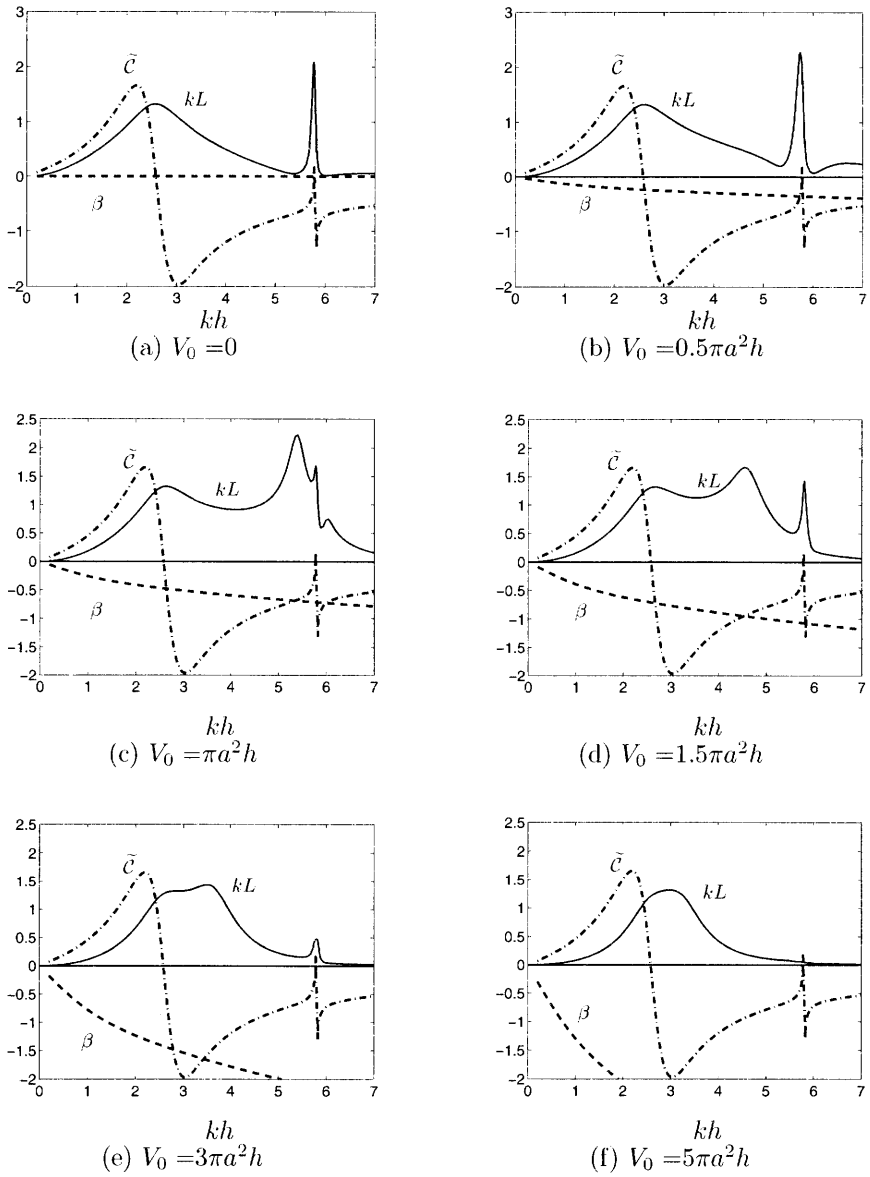

(a) $V_0 = 0$ (b) $V_0 = 0.5\pi a^2 h$

(c) $V_0 = \pi a^2 h$ (d) $V_0 = 1.5\pi a^2 h$

(e) $V_0 = 3\pi a^2 h$ (f) $V_0 = 5\pi a^2 h$

Figure 3-22: Capture length (dashed), added mass (plain) and β coefficient (dashed-dotted) against the normalized frequency kh for different pneumatic chamber volume V_0. $a/h = 1/3$, $d/h = 0.2$, $\alpha = 0$, $h = 10$m.

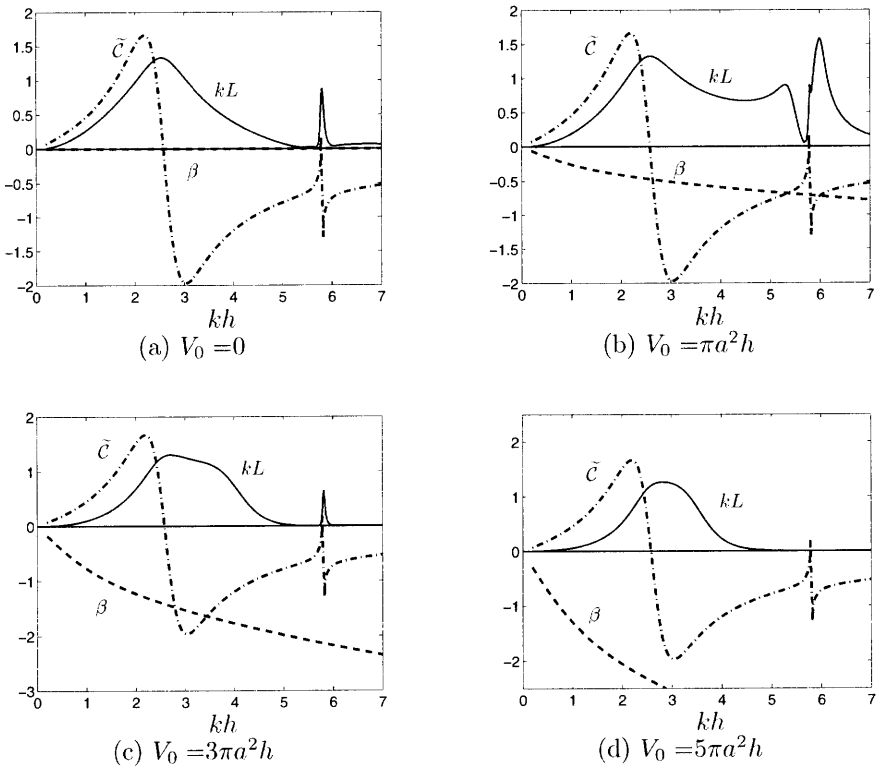

(a) $V_0 = 0$ (b) $V_0 = \pi a^2 h$

(c) $V_0 = 3\pi a^2 h$ (d) $V_0 = 5\pi a^2 h$

Figure 3-23: Capture length (dashed), added mass (plain) and β coefficient (dashed-dotted) against the normalized frequency kh for different pneumatic chamber volume V_0. $a/h = 1/3$, $d/h = 0.2$, $\alpha = \pi/2$, $h = 10$m.

of β and $\widetilde{\mathcal{C}}$ increases up to 4 points (see figure 3-22c). Each point of intersection corresponds to a maximum of the capture length kL. As V_0 continues to increase and reaches $1.5\pi a^2 h$, the last two points of intersection of β and $\widetilde{\mathcal{C}}$ converge toward a single point corresponding to the minimum of $\widetilde{\mathcal{C}}$ at $kh = 5.8$. As a result the two last maxima of kL merge into a single one (see figure 3-22d). Similarly as V_0 increases up to $4\pi a^2 h$ the fist two points of intersection converge toward the minimum of $\widetilde{\mathcal{C}}$ at $kh = 3.1$ and thus the two first maxima of kL merge into one maxima. In the same time the value of the last maximum decreases with the increase of V_0. As the volume of the chamber exceeds 4 (see figure 3-22f) the curves of β and $\widetilde{\mathcal{C}}$ do not intersect anymore and the capture length presents two local maxima, which intensity decreases as the volume of the chamber increases. This corresponds to a situation of poor energy efficiency.

3.4.2 Comparison between a thin breakwater and a straight coastline

The present case will be compared in the next chapter with the case of a thin breakwater, studied by Martin-Rivas and Mei (2008), the straight coastline, studied by Martin-Rivas and Mei (2009) and the convex corner, studied in the next chapter.

3.4.3 A more practical optimization

In this section we shall develop a simpler and more practical way of optimizing the energy extraction rate than the previous method. Indeed the previous optimization assumes that the value of χ can be controlled and adapted for all ω which in practice may be difficult. Figure 3-16b shows indeed that the range of variation χ is large.

In this new strategy the turbine parameter χ will only have two values χ_1 and χ_2. From the curve of the capture length kL obtained from the previous optimization method we choose to focus on two maxima of kL. The frequency of each maxima (kh_1 and kh_2) corresponds to a given value of χ_{opt}. These two values of χ_{opt} are the one we consider for our new strategy. Let us note that each of these two value is

equal to the damping coefficient at the resonance frequency kh_1 or kh_2. Indeed, at the two maxima frequencies we have $\beta = \widetilde{\mathcal{C}}$ and thus $\chi_{opt}(\omega) = \sqrt{\widetilde{\mathcal{B}}^2 + \left(\widetilde{\mathcal{C}} - \beta\right)^2} = \widetilde{\mathcal{B}}$. From now on χ is a step function χ_s only taking two values and the capture length is then calculated using formula (3.4.1). With this strategy the new curve of the capture length, kL_s, is calculated. We will denote by $(kh)^*$ the frequency at wich the turbine parameter changes of value. It is chosen in order to optimize kL_s as it will be described later.

Let us illustrate this method for two different configurations: $a/h = 1/2$ and $a/h = 1/4$.

We first fix a/h=1/4, d/h=0.2 and the angle of incidence is equal to $\pi/2$. The curve of kL and χ_{opt} from the previous optimization are presented on figure 3-24 in plain line. The two crosses on the curve of kL indicate the maxima we choose.

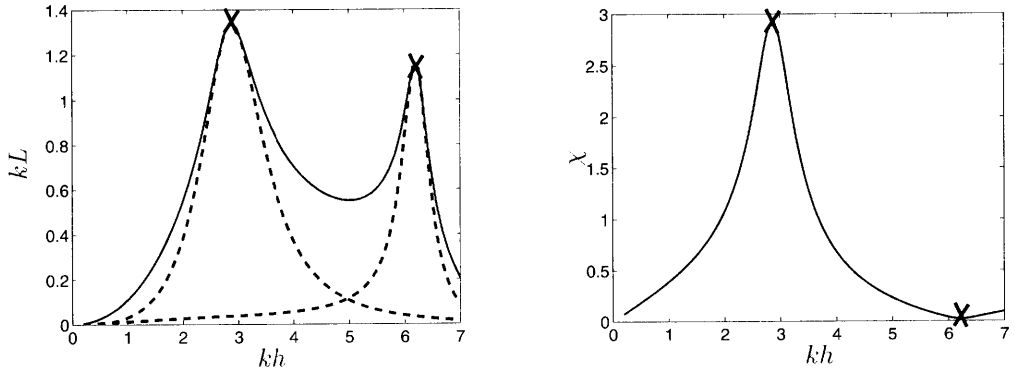

(a) Capture length (b) Turbine parameter χ

Figure 3-24: Optimization for all frequencies. a/h=1/4, d/h=0.2, $\alpha=\pi/2$ and $V_0 = \pi a^2 h$.

The two crosses on figure 3-24b indicates the corresponding points on the curve of χ_{opt}. Here we take thus $\chi_1 = 2.912$ and $\chi_2 = 0.02$. For each of these two values, the corresponding capture length has been plot in dashed line on figure 3-24a. They intersect in one point for $kh = 4.93$ and thus we choose $(kh)^* = 4.93$.

The new curves kL_s and χ_s are now presented on figure 3-25. The curve of kL has been superposed in dash line for comparison. The curves of kL and kL_s agree at $kh = 2.91$ and $kh = 6.20$. We see that the simpler scheme can achieve almost as high as an efficiency than the idealized optimization except for frequencies between

$kh = 4$ and $kh = 6$. For comparison, figure 3-26 presents the optimization with

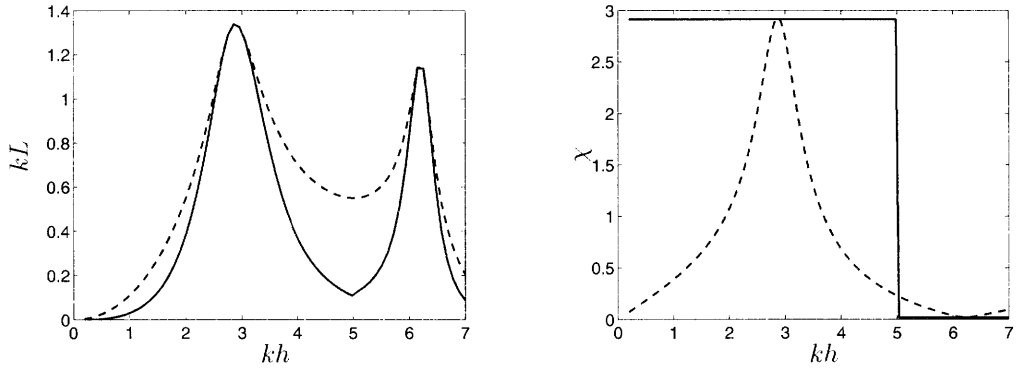

(a) Capture length (b) Turbine parameter χ_s

Figure 3-25: Practical optimization results for a/h=1/4, d/h=0.2, $\alpha=\pi/2$ and $V_0 = \pi a^2 h$. Left: Capture length. Right: Turbine parameter. Plain: practical optimization, dashed: optimization for all frequencies

only one value for the turbine ($\chi_1 = 2.912$).We see that we miss the second peak of resonance in this case.

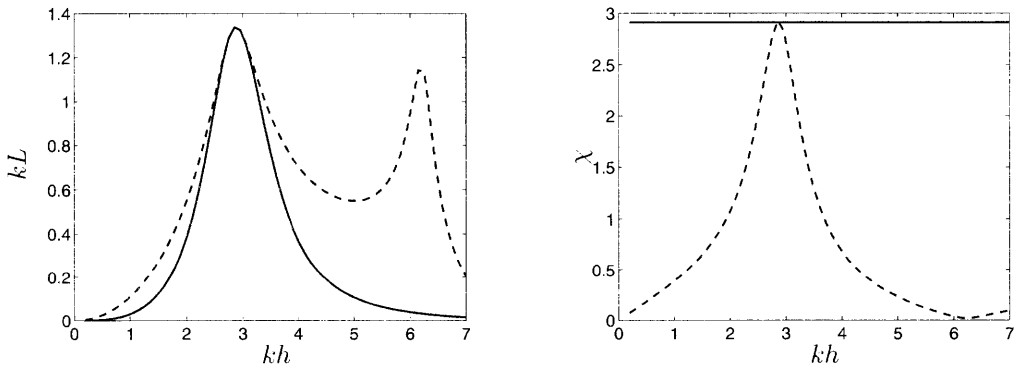

(a) Capture length (b) Turbine parameter χ_s

Figure 3-26: Practical optimization results for a/h=1/4, d/h=0.2, $\alpha=\pi/2$ and $V_0 = \pi a^2 h$ and one value of χ. Left: Capture length. Right: Turbine parameter. Plain: practical optimization, dashed: optimization for all frequencies

It may be surprising at the first glance that the small value of χ_2 corresponds to such a maxima of the capture length. However, let us recall that the analytical expression of the optimum of the capture length is given by equation 2.5.3:

$$kL_{\max} = \frac{khg}{C_g\sqrt{g/h}} \frac{\left|\widetilde{\Gamma}(kh,\alpha)\right|^2}{4\chi} \tag{3.4.5}$$

The curves of $\left|\widetilde{\Gamma}(kh)\right|^2$ and χ are given in figure 3-27. At the frequency of the first

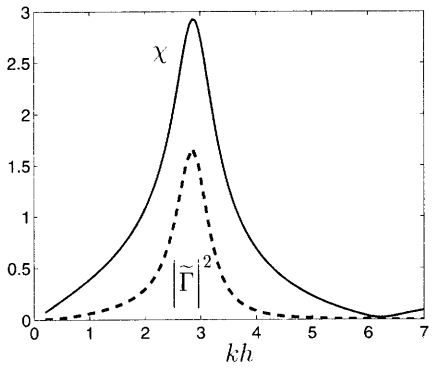

Figure 3-27: Diffraction coefficient (dashed) and turbine coefficient (plain) function of kh for $a/h = 1/4$, $d/h = 0.2$ and $\alpha = \pi/2$.

peak of resonance of the capture length ($kh = 2.91$) both the diffraction coefficient and the turbine parameter presents a maxima and they are of the same order. As a consequence their ratio is of order 1. For the frequency of the second maxima of kL ($kh = 6.20$), both the diffraction coefficient and the turbine parameter are extremely small and thus their ratio is again of order unity. Thus the value of the maximum of the capture length will be roughly of the same order than the first maximum.

Figure 3-28 presents the results for the same configuration and the angle of incidence $\alpha = 0$. We have $\chi_1 = 2.926$, $\chi_2 = 0.02$ and $(kh)^* = 4.98$.We see that the

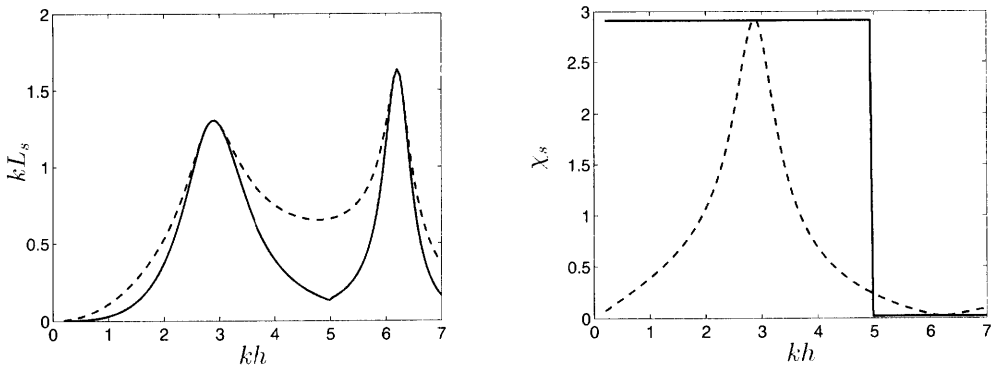

(a) Capture length (b) Turbine parameter χ_s

Figure 3-28: Practical optimization results for a/h=1/4, d/h=0.2, α=0 and $V_0 = \pi a^2 h$. Left: Capture length. Right: Turbine parameter. Plain: practical optimization, dashed: optimization for all frequencies

observation are similar to previously.

We now fix a/h=1/2, d/h=0.2 and the angle of incidence is equal to $\pi/2$. For this configuration $\chi_1 = 4.812$, $\chi_2 = 0.202$ and $(kh)^* = 3.97$. The new curves kL_s and χ_s are presented on figure 3-29. The curve of kL has been superposed in dash line on

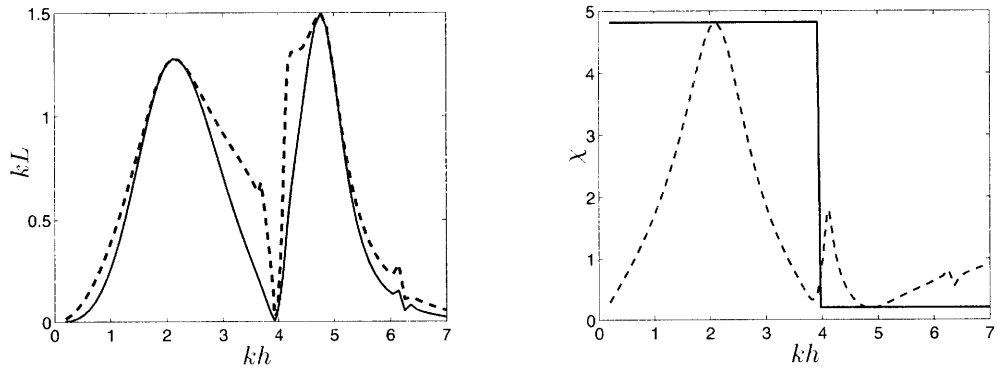

(a) Capture length (b) Turbine parameter

Figure 3-29: Practical optimization results for a/h=1/2, d/h=0.2, $\alpha=\pi/2$ and $V_0 = \pi a^2 h$. Left: Capture length. Right: Turbine parameter. Plain: practical optimization, dashed: optimization for all frequencies

figure 3-29a for comparison. As predicted the two curves coincide at the two maxima at $kh = 2.11$ and 4.77. Broadly speaking, the curve of kL_s is a good approximation of the curve of kL. It is always under it and is close to it for kh below 2.11 and above 4.77.

The strategy developed here is thus very encouraging since only two values of χ are required to obtained a curve closed to the previous optimization method, with two braod large peaks of resonance.

Figure 3-30 presents the optimization for $\alpha = 0$. Here $\chi_1 = 4.81$, $\chi_2 = 0.34$ and $(kh)^* = 3.28$.

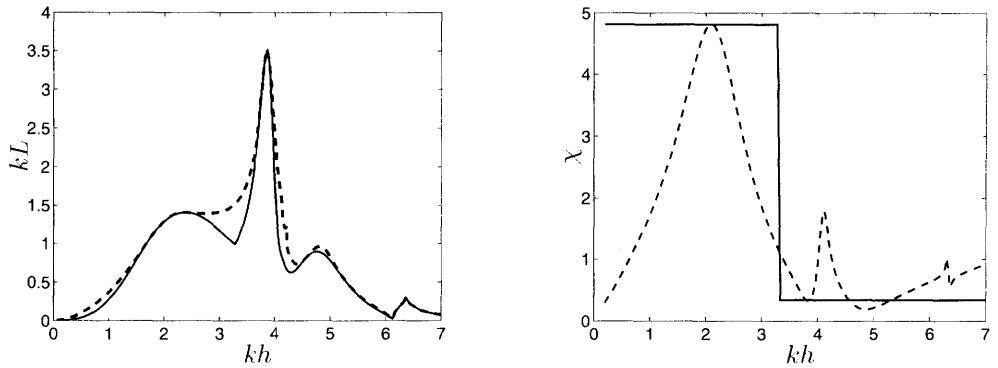

(a) Capture length (b) Turbine parameter

Figure 3-30: Practical optimization results for a/h=1/2, d/h=0.2, $\alpha = 0$ and $V_0 = \pi a^2 h$. Left: Capture length. Right: Turbine parameter. Plain: practical optimization, dashed: optimization for all frequencies

Chapter 4

OWC at the concave corner of right angle coast

Let us now consider the case where $\nu = 1/2$. The up view is presented on figure 4-1. Let us first briefely recall the equations for this case.

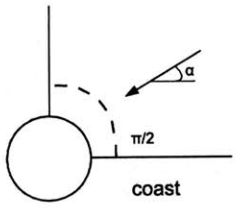

Figure 4-1: Scheme of the OWC at the end of a wedge of angle $3\pi/2$

4.1 Diffraction problem

For a plane incident wave arriving with an angle $\theta = \alpha$, the diffraction potential is given by:

$$\varphi_{ext} = \varphi_1 + \varphi_2 \tag{4.1.1}$$

with:

$$\varphi_1 = -\frac{igA}{\omega}\sum_{n=0}^{\infty}\frac{\epsilon_n}{\pi}\frac{4\pi i\cos(2n\alpha)e^{-in\pi}Y'_{2n}(ka)}{H'_{2n}(ka)}\left(J_{2n}(kr)\right.$$
$$\left.-\frac{J'_{2n}(ka)}{Y'_{2n}(ka)}Y_{2n}(kr)\right)cos\left(2n\theta\right)\frac{Z_0(z)}{Z_0(0)} \quad (4.1.2)$$

and:

$$\varphi_2 = -\frac{igA}{\omega}\sum_{n=0}^{\infty}\sum_{l=0}^{\infty}A_{nl}\frac{K_{2n}(k_l r)}{k_l a K'_{2n}(k_l a)}\cos\left(2n\theta\right)Z_l(z) \quad (4.1.3)$$

The potential inside is given by

$$\varphi_C = -\frac{igA}{\omega}\sum_{n=0}^{\infty}\sum_{l=0}^{\infty}\left(B_{nl}\cos(n\theta)+C_{nl}\sin(n\theta)\right)\frac{I_n(k_l r)}{k_l a I'_n(k_l a)}Z_l(z) \quad (4.1.4)$$

Coefficients A_{nl}, B_{nl} and C_{nl} are given respectively by

$$\frac{\pi}{2\epsilon_n}A_{nl} = \frac{ia\omega}{ghA}\int_{-h}^{-d}\int_0^{\pi/2}U(\theta,z)Z_l(z)\cos\left(2n\theta\right)d\theta dz \quad (4.1.5)$$

$$\frac{2\pi}{\epsilon_n}B_{nl} = \frac{ia\omega}{ghA}\int_{-h}^{-d}\int_0^{\pi/2}U(\theta,z)Z_l(z)\cos(n\theta)d\theta dz \quad (4.1.6)$$

$$\frac{2\pi}{\epsilon_n}C_{nl} = \frac{ia\omega}{ghA}\int_{-h}^{-d}\int_0^{\pi/2}U(\theta,z)Z_l(z)\sin(n\theta)d\theta dz \quad (4.1.7)$$

where $U(\theta,z)$ is expanded as follow:

$$U(\theta,z) = -\frac{igA}{\omega}\sum_{m=0}^{\infty}\sum_{p=0}^{\infty}\alpha_{mp}\mathcal{T}_m(\theta)u_p(z) \quad (4.1.8)$$

$$\mathcal{T}_m(\theta) = T_m^*\left(\frac{2\theta}{\pi}\right) \quad (4.1.9)$$

Coefficients α_{mp} are solution of the systeme defined by equation (2.2.45):

$$\begin{aligned}
&\frac{h}{a}\sum_{n=0}^{\infty}\mathcal{E}_n cos\,(2n\theta)\,Z_0(z) = \\
&\sum_{m=0}^{\infty}\sum_{p=0}^{\infty}\alpha_{mp}\sum_{n=0}^{\infty}\sum_{l=0}^{\infty}\frac{\epsilon_n}{2\pi}\frac{I_n(k_l a)}{k_l a I_n'(k_l a)}F_{Pl}F_{pl}\left(\mathfrak{C}(n,M)\mathfrak{C}(n,m)+S(n,M)S(n,m)\right) \\
&-\sum_{m=0}^{\infty}\sum_{p=0}^{\infty}\alpha_{mp}\sum_{n=0}^{\infty}\sum_{l=0}^{\infty}\frac{2\epsilon_n}{\pi}\frac{K_{2\nu}(k_l a)}{k_l a K'_{\frac{2n}{3}}(k_l a)}F_{Pl}F_{pl}\mathfrak{C}_{1/2}(n,m)\mathfrak{C}_{1/2}(n,M)
\end{aligned} \tag{4.1.10}$$

with the notations:

$$\mathfrak{C}(n,m) = \int_0^{\pi/2}\mathcal{T}_m(\theta)\cos(n\theta)\,d\theta \tag{4.1.11}$$

$$S(n,m) = \int_0^{\pi/2}\mathcal{T}_m(\theta)\sin(n\theta)\,d\theta \tag{4.1.12}$$

$$\mathfrak{C}_{1/2}(n,m) = \int_0^{\pi/2}\mathcal{T}_m(\theta)\cos(2n\theta)\,d\theta \tag{4.1.13}$$

4.2 Radiation problem

The potential inside the cylinder is given by

$$\phi_C = -\frac{i\widehat{p_a}}{\rho\omega}\sum_{n=0}^{\infty}\sum_{l=0}^{\infty}D_{nl}\frac{I_n(k_l r)}{k_l a I_n'(k_l a)}\cos\left[n\left(\theta-\frac{\pi}{4}\right)\right]Z_l(z) - \frac{i\widehat{p_a}}{\rho\omega} \tag{4.2.1}$$

The potential outside is given by:

$$\phi_O = -\frac{i\widehat{p_a}}{\rho\omega}\sum_{n=0}^{\infty}\sum_{l=0}^{\infty}E_{nl}\frac{K_{2n}(k_l r)}{k_l a K'_{2n}(k_l a)}\cos(4n\theta)\,Z_l(z) \tag{4.2.2}$$

Coefficients D_{nl} and E_{nl} are given by

$$\frac{2\pi}{\epsilon_n}D_{nl} = \frac{ia\rho\omega}{\widehat{p_a}h}\int_{-h}^{-d}\int_{\pi/2}^{0}U(\theta,z)\cos\left[n\left(\theta-\frac{\pi}{4}\right)\right]Z_l(z)d\theta dz \tag{4.2.3}$$

$$\frac{3\pi}{2\epsilon_n} E_{nl} = \frac{ia\rho\omega}{\widehat{p_a} h} \int_{-h}^{-d} \int_{\pi/2}^{0} U(\theta, z) \cos\left[4n\theta\right] Z_l(z) d\theta dz \tag{4.2.4}$$

The expansion of $U(\theta, z)$ is given by:

$$U(\theta, z) = \frac{-i\widehat{p_a} h}{\rho\omega} \sum_{m=0}^{\infty} \sum_{p=0}^{\infty} \alpha_{mp} \cos\left[4m\left(\theta - \frac{\pi}{4}\right)\right] u_p(z) \tag{4.2.5}$$

Coefficients α_{mp} are calculated by solving the linear system :

$$\begin{aligned} \frac{h}{a}\pi\delta_{M0}\delta_{P0} = & \sum_{p=0}^{\infty} \alpha_{Mp} \sum_{l=0}^{\infty} F_{pl} F_{Pl} \frac{\pi}{\epsilon_M} \frac{K_{2M}(k_l a)}{k_l a K'_{2M}(k_l a)} \\ & - \sum_{m=0}^{\infty} \sum_{p=0}^{\infty} \alpha_{mp} \sum_{n=0}^{\infty} \sum_{l=0}^{\infty} \frac{\epsilon_n}{\pi} F_{pl} F_{Pl} R_{mn} R_{Mn} \frac{I_n(k_l a)}{k_l a I'_n(k_l a)} \end{aligned} \tag{4.2.6}$$

4.3 Numerical results for each problem

Variation of the scattering coefficient with the incidence angle and kh.

Figure 4-2 presents the variation of the scattering coefficient with α for given frequencies and $a/h = 1/2$, $a/h = 1/4$. For reason of symmetry, the results are only presented for $\alpha \in [0, \pi/4]$. We see that the scattering coefficient is constant and seems to not depend of the angle of incidence.

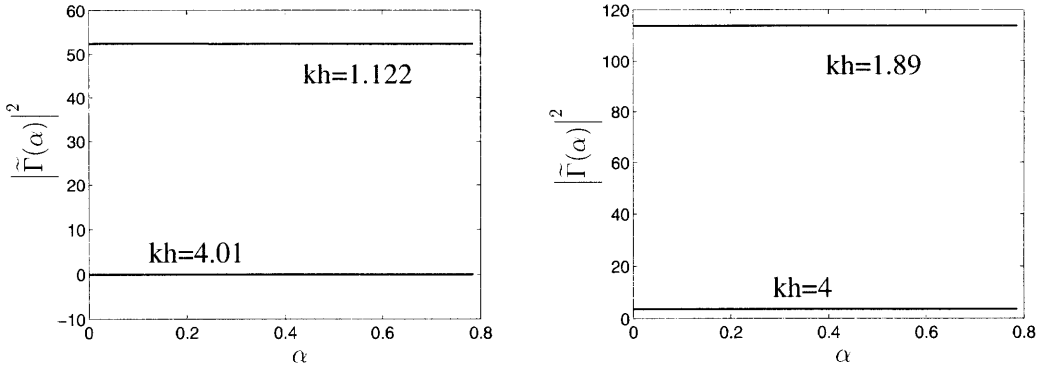

(a) a/h=1/2 (b) a/h=1/4

Figure 4-2: Scattering coefficient function of α. Left: a/h=1/2 and right: a/h=1/4. d/h=0.2

Figure 4-3 presents in percent the variation of the relative difference between

$\left|\widetilde{\Gamma}(\alpha)\right|^2$ and $\left|\widetilde{\Gamma}(0)\right|^2$ with respect to α for $a/h = 1/2$ and $a/h = 1/4$ and for the same frequencies.

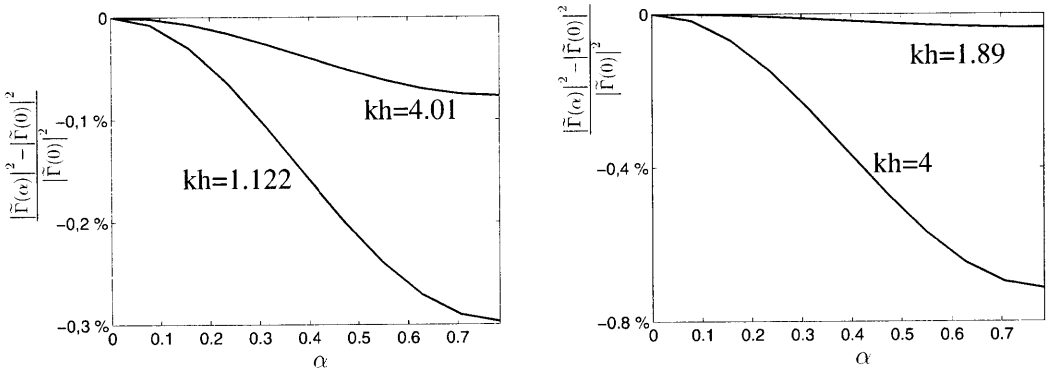

(a) a/h=1/2 (b) a/h=1/4

Figure 4-3: Relative difference of the scattering coefficient function of α. Left: a/h=1/2 and right: a/h=1/4. d/h=0.2

As it can be observed, the value of the scattering coefficient depends indeed on the incidence angle, however this dependence is very weak, less than 1% in all the cases presented.

Figure 4-4 presents the variation of $\left|\widetilde{\Gamma}\right|^2$ as a function of kh for a/h=1/2 and 1/4. The scattering coefficient has in the two cases one large maxima. The value of the maxima decreases and its frequency increases as a/h decreases. For $a/h = 1/2$ its presents also two additionnal small local maxima at higher frequency.

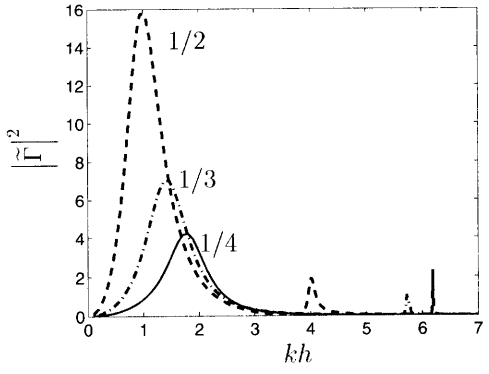

Figure 4-4: Diffraction-induced vertical flux coefficient as a function of kh. Plain: a/h=1/4, dash-dots: 1/3 and dash: a/h=1/2. d/h=0.2 and $\alpha = \pi/4$

Comparison of $\widetilde{\mathcal{B}}$ and $\widetilde{\mathcal{C}}$ with other coastal geometries

The case of a thin breakwater has been studied by Martin-Rivas and Mei (2008) and the straight coastline by Martin-Rivas and Mei (2009). Figure 4-5 presents the variation of $\widetilde{\mathcal{B}}$ and $\widetilde{\mathcal{C}}$ with respect to kh for $a/h = 1/4$ for the thin breakwater, the convex corner, the straight coastline and the concave corner. As ν decreases, the magnitude of $\widetilde{\mathcal{B}}$ and $\widetilde{\mathcal{C}}$ decreases. In each case the damping coefficient presents one peak of resonance. The peak of resonance of the concave corner, previously identified as Helmholtz mode, is around 75% smaller than the peak of the thin breakwater. Let us also note than for the straight coastline it is 50% smaller than for thin breakwater and that for the convex corner of right angle it is 25% smaller.

The curve of the added mass is flatter and its amplitude smaller as ν goes to zero. We can finally note that the added mass changes sign only once for each configuration and has the shape of a single N.

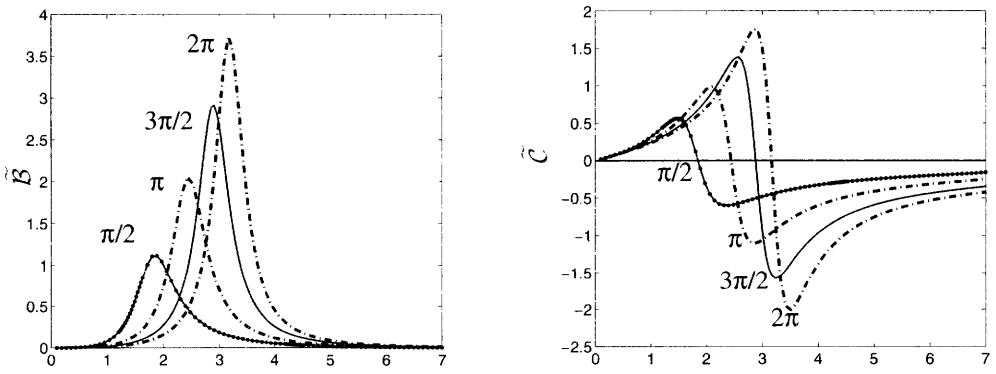

(a) Damping coefficient (b) Added mass

Figure 4-5: Damping coefficient and added mass function of kh for different value of ν. Plain with points markers: $\pi/2$, dashed: π, plain: $3\pi/2$, dash-dot: 2π. $a/h = 1/4$, $d/h = 0.2$

Figure 4-6 presents now the same comparison for $a/h = 1/2$. The damping coefficient for the concave corner presents now three peaks of resonance at kh equal to 1.122, 4.01 and 6.186. Again their magnitude is smaller than the other cases. The frequency of the first peak of resonance decrases strongly as ν decreases, whereas the frequency of the second and third peak remains almost constant, with only a light

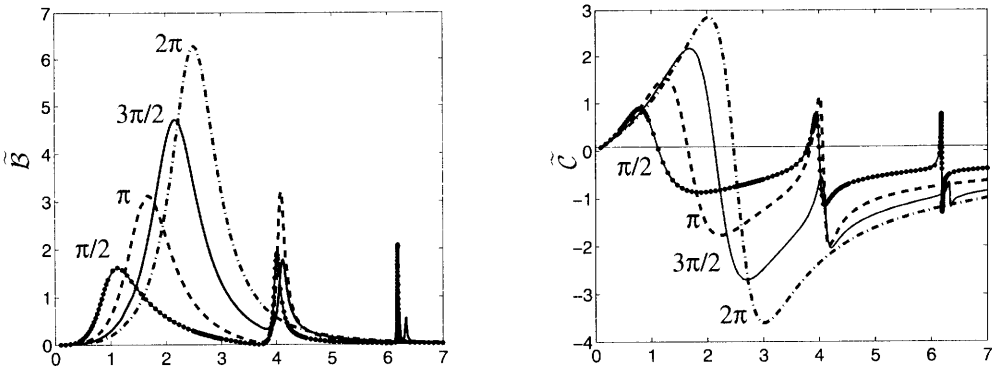

(a) Damping coefficient (b) Added mass

Figure 4-6: Damping coefficient and added mass function of kh for different value of ν. Plain with points markers: $\pi/2$, dashed: π, plain: $3\pi/2$, dash-dot: 2π. $a/h = 1/2$, $d/h = 0.2$

deplacement to the lower frequencies.

Now, similarly to the straight coastline, the added mass for the concave corner changes of sign several times for frequencies near the frequencies of the peak of resonance of $\widetilde{\mathcal{B}}$. With the exception of the thin breakwater, the shape of the curves of $\widetilde{\mathcal{C}}$ is similar to two N juxtaposed.

Variation of $\widetilde{\mathcal{B}}$ and $\widetilde{\mathcal{C}}$ with a/h.

Figure 4-7 presents the variation of $\widetilde{\mathcal{B}}$ and $\widetilde{\mathcal{C}}$ for d/h=0.2 and three values of a/h. As

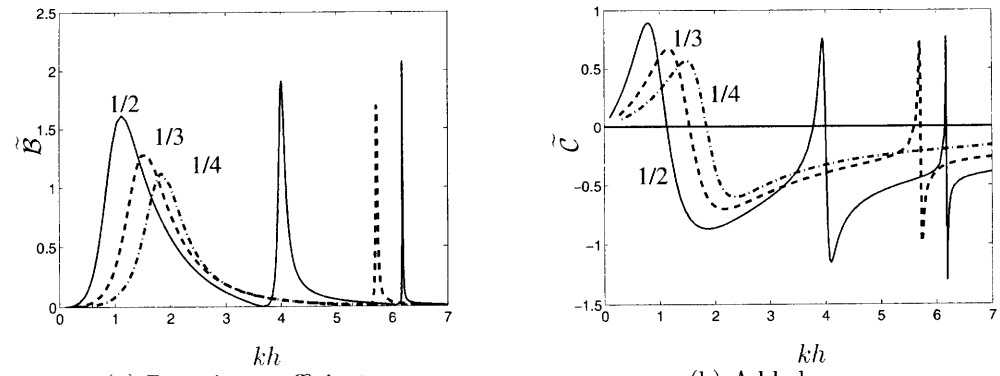

(a) Damping coefficient (b) Added mass

Figure 4-7: Variation of the damping coefficient and the added mass as kh increases. Plain: $a/h = 1/2$, dash: $a/h = 1/3$, dash-dot: $a/h = 1/4$. In every cases, $d/h = 0.2$

already seen in the previous section, as a/h decrases, the frequency of each peak of resonance is higher. The intensity of the first peak descreases with the decrease of a/h whereas the intensity of the second peak remains almost constant. The first peak corresponds to Helmholtz mode and the second one to sloshing mode. The later is shown on figure 4-8.

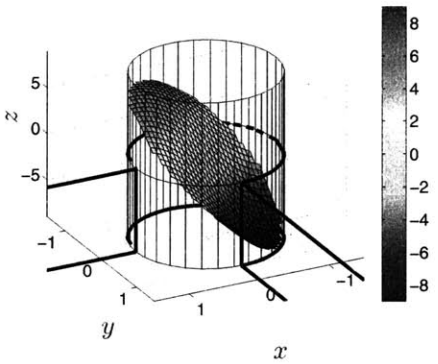

Figure 4-8: Free surface elevation inside the OWC at kh=4, a/h=1/2 and d/h=0.2. Radiation problem

4.4 Numerical results for energy extraction

4.4.1 Optimization for all frequencies

Combining diffraction and radiation problem we can now study the energy extraction rate of our device. We have applied first the same optimization strategy for all ω as developped in section 2.5.2.

Influence of a/h.

We fix d/h=0.2 and the volume of the chamber is equal to $V_0 = \pi a^2 h$. Figure 4-9 presents the capture length and the turbine coefficient χ for three values of the radius of the chamber a/h. As a/h increases, the capture length kL shows more local maxima and is less smooth. The value of these maxima does not depends strongly on the value of a/h and is equal 4 except for the third thin peak at kh=6.18 for a/h=1/2. Let us note that between the maxima of two different modes, there is a

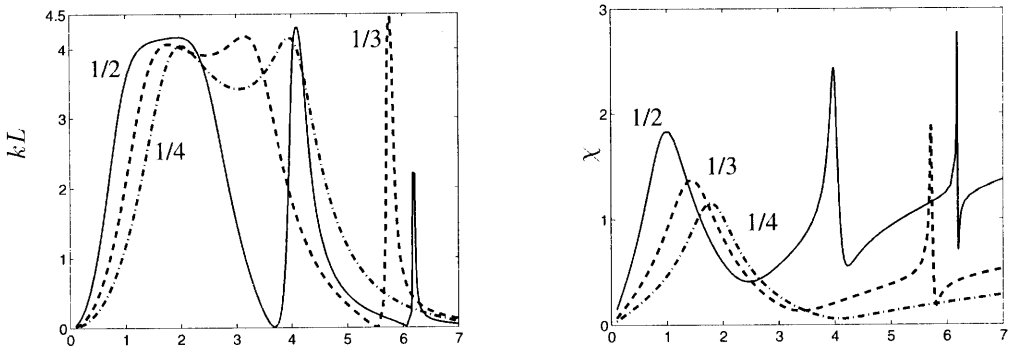

(a) Capture length (b) Turbine coefficient χ

Figure 4-9: Capture length and turbine coefficient function of kh. Plain: $a/h = 1/2$, dash: $a/h = 1/3$, dash-dot: $a/h = 1/4$. In every cases, $d/h = 0.2$, $\alpha = \pi/4$ and $V_0 = \pi a^2 h$.

frequency where no energy can be extracted: at $kh \approx 3.68$ ($ka \approx 1.84$) for $a/h = 1/2$ between the first and second mode and then at $kh \approx 6.06$ ($ka \approx 3.03$) between the second and the third mode, and at $kh \approx 5.55$ ($ka \approx 1.85$) for $a/h = 1/3$ between the first two modes. This frequency corresponds to a zero of $J_n'(ka)$ ($J_1'(ka = 1.84) = 0$, $J_2'(ka = 3.05) = 0$).

As a/h increases, the variation of the turbine coefficient χ are higher and more abrupt (see for example, $a/h = 1/2$ and $kh = 6.06$). If we compare figures 4-9b with 4-7 , we see that for a given value of a/h, the curve presents peaks for the same frequencies as the peak frequencies of $\widetilde{\mathcal{B}}$ and $\widetilde{\mathcal{C}}$ as it can be expected with the definition of $\chi = \sqrt{\widetilde{B}^2 + \left(\widetilde{C} - \beta\right)^2}$ and for these peaks, $\chi = \widetilde{B}$.

Influence of the size of the chamber.

Let us now examine the influence of the air compressibility on our system, that is the influence of the parameter β. As done in the previous chapter, we fix the size and geometry of the immersed part of the OWC but we consider different size of the air chamber volume V_0.

Figure 4-10 presents the curves of the capture length, the added mass and the parameter β for 4 values of V_0 and $a/h = 1/4$. For incompressible air ($V_0 = 0$), the

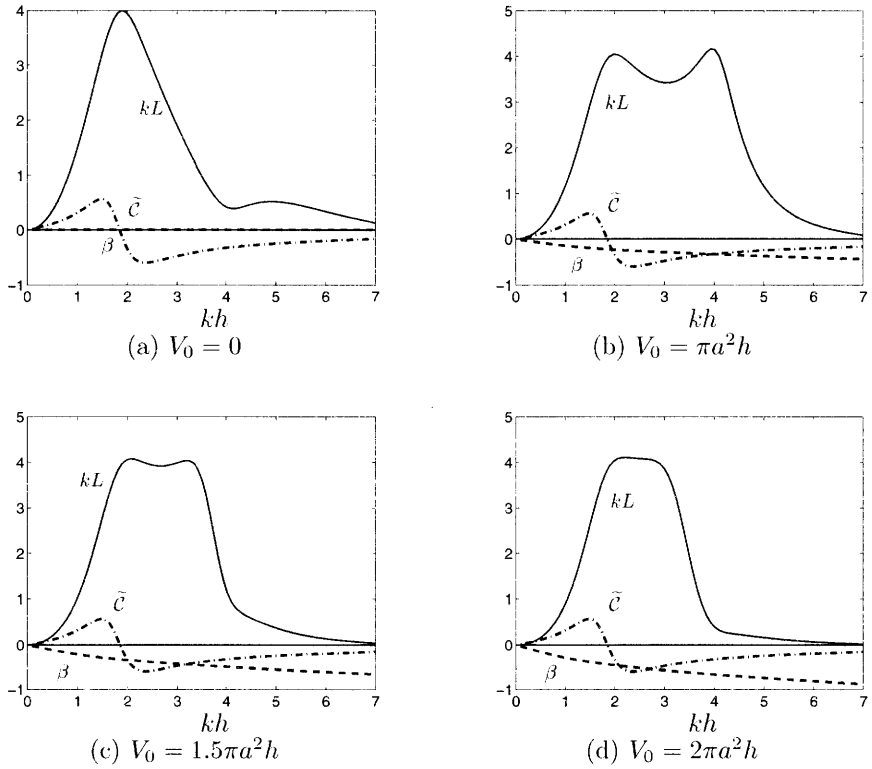

(a) $V_0 = 0$ (b) $V_0 = \pi a^2 h$

(c) $V_0 = 1.5\pi a^2 h$ (d) $V_0 = 2\pi a^2 h$

Figure 4-10: Capture length (plain), added mass (dashed-dotted) and coefficient β (dashed) for different pneumatic chamber volume V_0. a/h=1/4, d/h=0.2, $\alpha = \pi/4$.

curves of β and $\widetilde{\mathcal{C}}$ intersect only in one point and thus the capture length presents only one peak of resonance. As the volume of the air chamber increases, the capture length presents at most 2 distinct peaks of resonance (see figure 4-10b). Then as the volume continues to increase, the two points of intersection of β and $\widetilde{\mathcal{C}}$ move toward the minimum of the added mass (kh around 2.2) and as a consequence the two peaks of resonance of kL get confonded into one broad peak of resonance.

Now figure 4-11 presents the curves of the capture length, the added mass and the parameter β for 6 values of V_0 for $a/h = 1/2$. The curves of β and $\widetilde{\mathcal{C}}$ intersect at most 6 times (see figure 4-11b for $V_0 = 0.3\pi a^2 h$) which mean that the curve of the capture length presents at most 6 local extrema, that are grouped into 3 double peaks. The fist double peak is broader than the second one, which itself is broader than the third one. Each double peak is separated from the next one by a zero of the capture length that happens around zeros of $J_n'(ka)$. As V_0 increases, the curve is shifted downwards and the points of intersection with $\widetilde{\mathcal{C}}$ moves two by two towards the local minima of this function (at kh=1.89, 4.08 and 6.19). As a consequence, the distance between the intersection point reduces and each double peak becomes progressively a single peak as it can be observed in figure 4-11d. The limiting case is obtained around $V_0 = \pi a^2 h$ (see figure 4-11e). For this configuration, the curve of β is tangent to the curve of $\widetilde{\mathcal{C}}$ at the first minima. Then if V_0 continues to increase, there are no points of intersection for the two curves and the maxima of the capture length is smaller than before. A configuration where $V_0 > \pi a^2 h$ leads thus to poor efficiency. Situation where the volume chamber is comprised between $0.3\pi a^2 h$ and $0.8\pi a^2 h$ are the most interesting for the energy extraction. Let us recall that $V_0 = \pi a^2 h$ for the pilot station in Pico Island, Azores, Portugal, which corresponds to our limiting case for this configuration.

Influence of the incidence angle

As we have seen previously with figure 4-3, the dependance of the scattering coefficient with the incidence angle is extremely small in this case (less than 1%). As a consequence the capture length, that is proportionnal to the square of $|\Gamma|$, depends

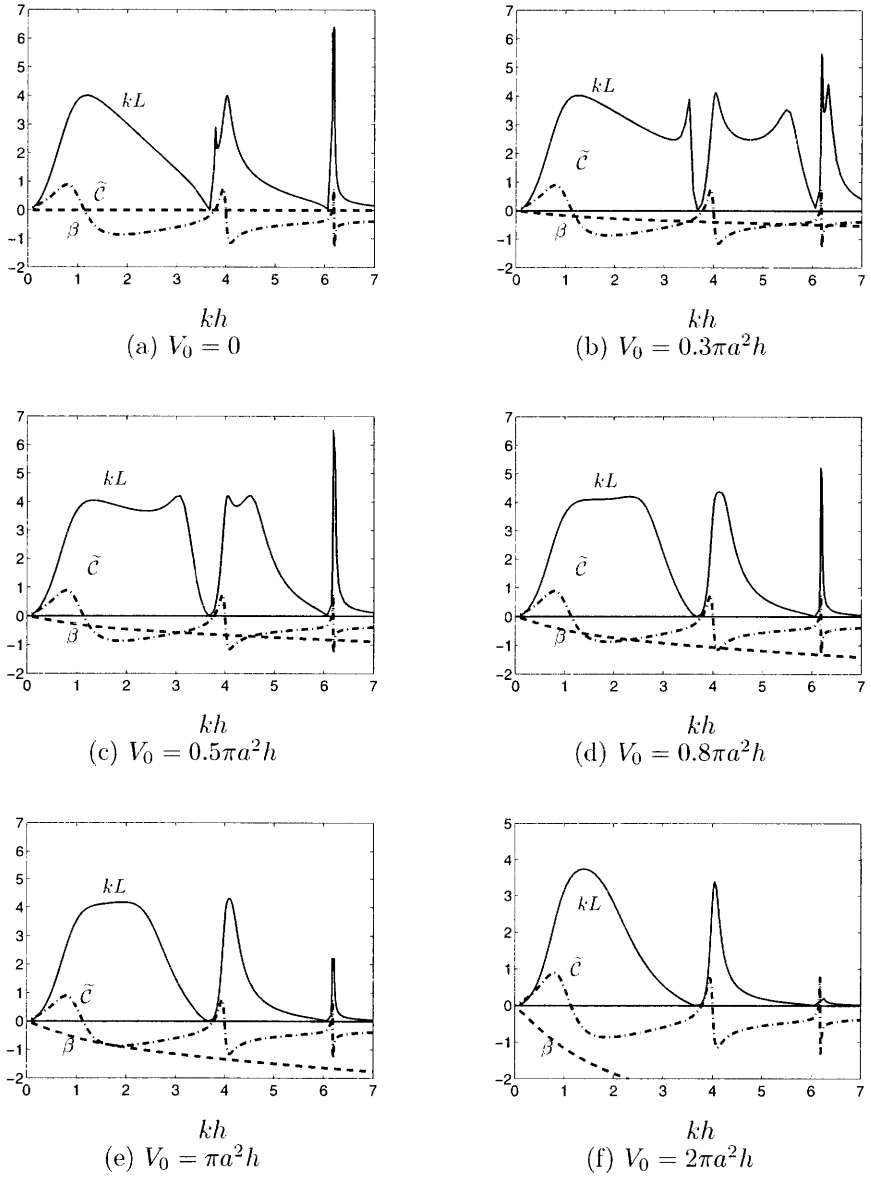

(a) $V_0 = 0$ (b) $V_0 = 0.3\pi a^2 h$

(c) $V_0 = 0.5\pi a^2 h$ (d) $V_0 = 0.8\pi a^2 h$

(e) $V_0 = \pi a^2 h$ (f) $V_0 = 2\pi a^2 h$

Figure 4-11: Capture length (plain), added mass (dashed-dotted) and coefficient β (dotted) for different pneumatic chamber volume V_0. a/h=1/2, d/h=0.2, $\alpha = \pi/4$.

also very few of the incidence angle. Figure 4-12 presents the capture length for incident angle equal to 0 and $\pi/4$ for $a/h = 1/2$. For low values of kh, we can con-

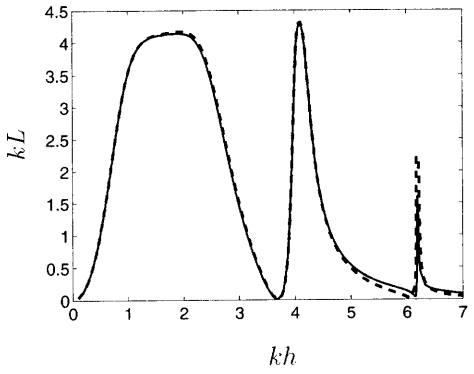

Figure 4-12: Capture length function of kh for $\alpha = 0$ (dashed) and $\alpha = \pi/4$ (plain). For each case a/h=1/2, d/h=0.2 and $V_0 = \pi a^2 h$.

sider that the capture length does not depends of the incident angle. As kh increases ($kh \geq 5$), this dependance becomes visible, even if it remains very small. Figure 4-13 presents the same curves for $a/h = 1/4$. We see that the angle of incidence has no visible influence on the capture length. This could have been predicted with figure 4-3b.

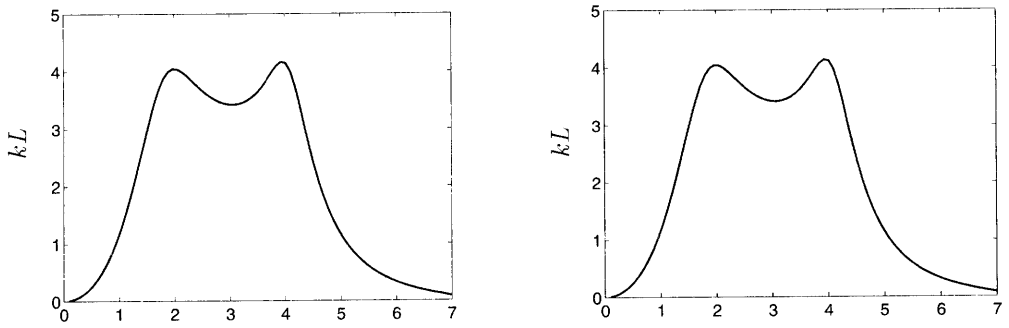

(a) $\alpha = 0$ (b) $\alpha = \pi/4$

Figure 4-13: Capture length function of kh for $\alpha = 0$ and $\alpha = \pi/4$. For each case a/h=1/4, d/h=0.2 and $V_0 = \pi a^2 h$.

Let us recall from section 2.5.2 that the angular average, i.e. average over all

angles of incidence, of the capture length is equal to

$$\overline{kL_{\text{opt}}} = \frac{1}{\nu\pi}\int_0^{\nu\pi} kL_{\text{opt}}(\alpha)\, d\alpha = \frac{2}{\nu} = 4 \tag{4.4.1}$$

Since the capture length is almost independant of α, with approximation the previous equality implies that the maximum capture length is around equal to 4. This can be verify on figure 4-12 and 4-13.

Comparison with other coastal geometries.

Figures 4-14a and 4-15a compare, respectively for $a/h = 1/4$ and $a/h = 1/2$, the capture length for the present situation with the case of a convexe corner of right angle, a thin breakwater (see Martin-Rivas and Mei (2008)) and a straight coastline (see Martin-Rivas and Mei (2009)) Figure 4-14d and 4-15d present the variation of the optimized turbine parameter χ. The capture length is significantly increased with this configuration. The efficiency at resonance is even four times bigger than for a thin breakwater and is, generally speaking, almost larger everywhere, except for $a/h = 1/2$ near the zeros of $J_n'(ka)$. The variation of the parameter χ is smaller for this configuration but is less smooth. It is an advantage since it means that the power-take does not need to be as versatile but also a disadvantage since it may require more to the control system.

4.4.2 Practical optimization

As in the previous chapter, let us now turn to a more practical optimization. We shall illustrate this strategy with two cases: a/h=1/4 and a/h=1/2. In every case d/h=0.2, the angle of incidence is 0 and the volume of the chamber is $V_0 = \pi a^2 h$.

We first concentrate on $a/h = 1/4$. Figures 4-17a and 4-17b present the curves of kL_s and χ_s. The two values of χ are $\chi_1 = 1.048$ and $\chi_1 = 0.06$ and $(kh)^* = 3.1$. Let us recall that for this two kh of resonance, $\chi = \widetilde{\mathcal{B}}$.

We see that the strategy is efficient. We are able to achieve almost as high as an efficient than the idealized case except around $(kh)^*$.

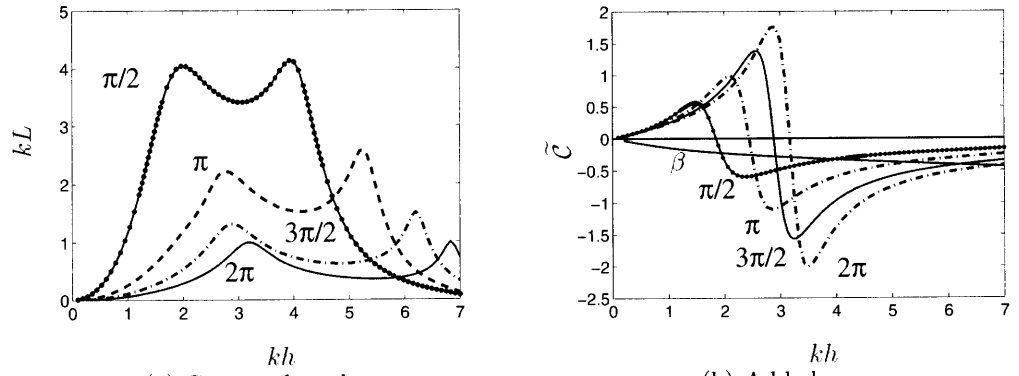

(a) Capture length (b) Added mass

(c) Free surface elevation (d) Turbine parameter χ

Figure 4-14: Comparison for different ν. Plain with point markers: $\nu = 1/2$, dash: $\nu = 1$, dash-dot: $\nu = 3/2$ and plain: $\nu = 2$. In every cases, d/h=0.2, a/h=1/4, α=$\pi/4$ and $V_0 = \pi a^2 h$.

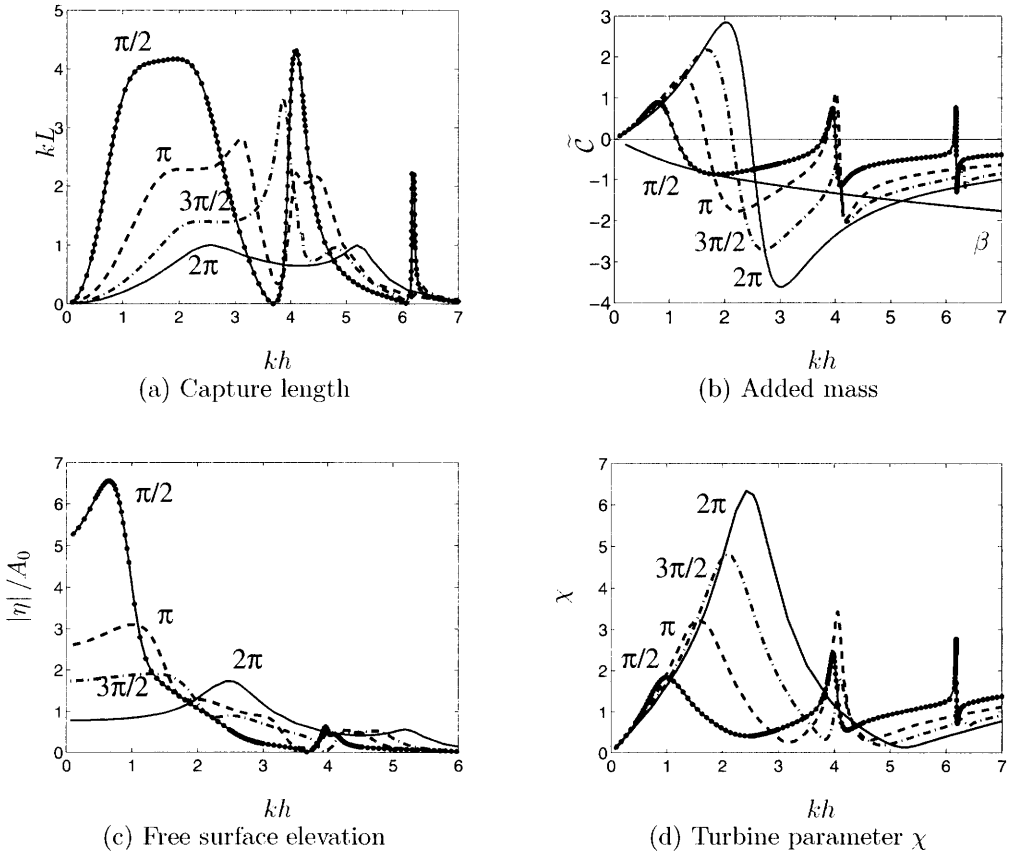

(a) Capture length (b) Added mass

(c) Free surface elevation (d) Turbine parameter χ

Figure 4-15: Comparison for different ν. Plain with point markers: $\nu = 1/2$, dash: $\nu = 1$, dash-dot: $\nu = 3/2$ and plain: $\nu = 2$. In every cases, d/h=0.2, a/h=1/2, α=0 and $V_0 = \pi a^2 h$.

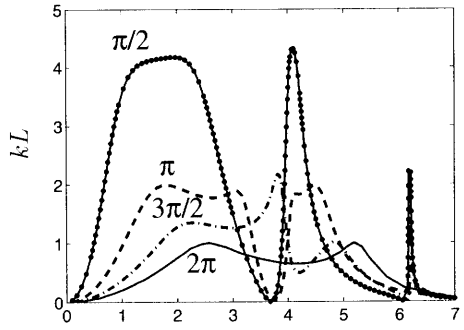

(a) Capture length

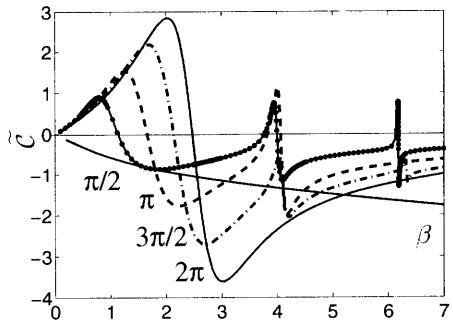

(b) Added mass

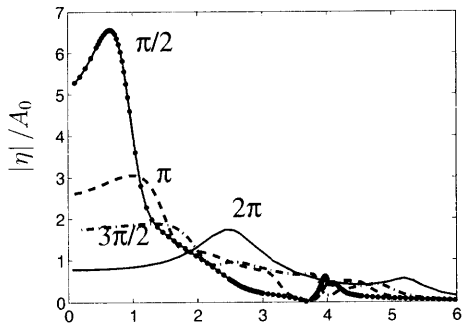

(c) Free surface elevation

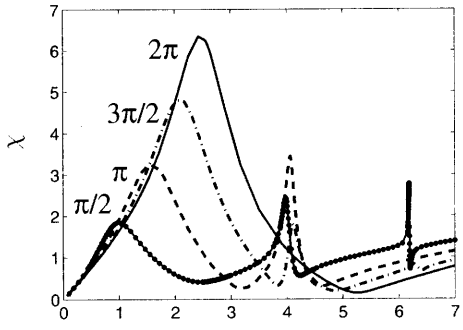

(d) Turbine parameter χ

Figure 4-16: Comparison for different ν. Plain with point markers: $\nu = 1/2$, dash: $\nu = 1$, dash-dot: $\nu = 3/2$ and plain: $\nu = 2$. In every cases, d/h=0.2, a/h=1/2, $\alpha = \pi/4$ and $V_0 = \pi a^2 h$.

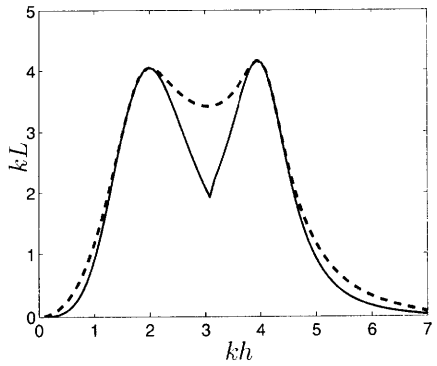

(a) Capture length

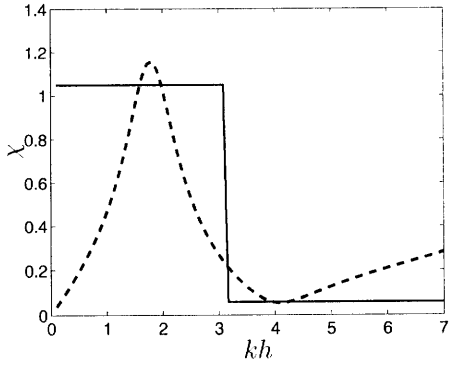

(b) Turbine parameter χ_s

Figure 4-17: Left: kL_s (plain) and kL (dashed) function of kh. Right: χ_s (plain) and χ (dashed) function of kh. a/h=1/4, d/h=0.2, $\alpha = \pi/4$ and $V_0 = \pi a^2 h$.

Figure 4-18 presents the same case but with only one value for the turbine parameter ($\chi = 1.048$). We see that in this case we miss the second maximum of the

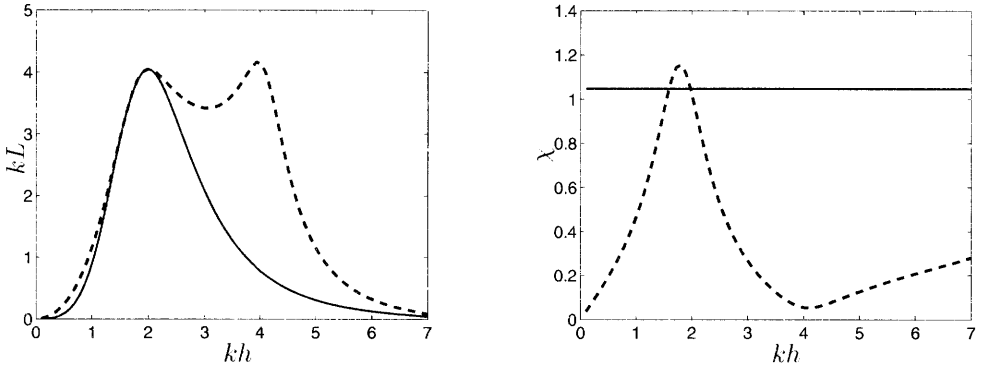

(a) Capture length (b) Turbine parameter χ_s

Figure 4-18: Left: kL_s (plain) and kL (dashed) function of kh. Right: χ_s (plain) and χ (dotted) function of kh. a/h=1/4, d/h=0.2, $\alpha = \pi/4$ and $V_0 = \pi a^2 h$.

capture length. We can note with this case that, as in the previous section, a small value of the turbine parameter χ can lead to a peak of frequency of the capture length. Indeed, as presented on figure 4-19, at the frequence of the second peak of resonance, both χ and Γ are small and thus their ratio is order unity.

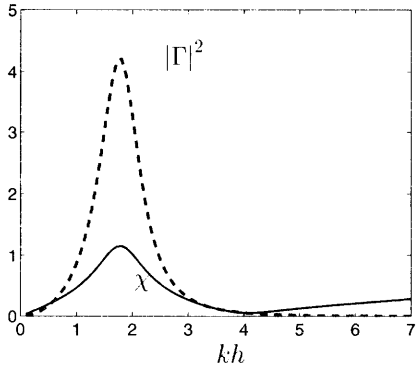

Figure 4-19: $|\Gamma|^2$ (dashed) and χ (plain) function of kh for a/h=1/4, d/h=0.2, $\alpha = \pi/4$ and $V_0 = \pi a^2 h$.

Let us finally consider the situation when a/h=1/2. The results are presented in figure 4-20. Here $\chi_1 = 0.604$, $\chi_2 = 1.181$ and $(kh)^* = 3.68$. The correspondence between the curve of kL and the curve of kL_s obtained with the new method is excellent. Indeed the two curves coincide for almost all frequencies, except for kh

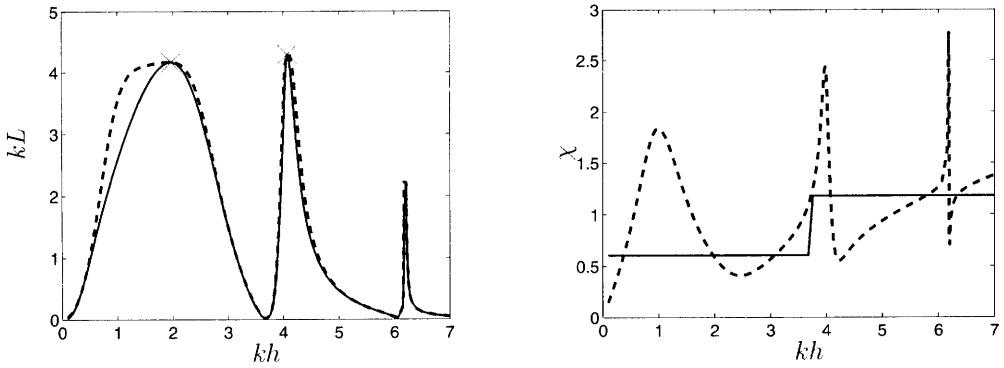

(a) Capture length (b) Turbine parameter χ_s

Figure 4-20: Practical optimization results for a/h=1/2, d/h=0.2, $\alpha = \pi/4$ and $V_0 = \pi a^2 h$. Left: Capture length and kL. Right: turbine parameter. Plain: practical optimization, dashed: optimization for all frequencies

between 0.5 and 2. This result can be explained by considering figure 4-20b that presents the curve of χ_{opt} and the curve of χ_s. We see that they have 6 points of intersection in addition to the two corresponding to the maxima of kL chosen. As a consequence the curves of kL_s merges prefectly with the one of kL not only at the two maxima but also at 6 other points. We see here then than our strategy is very efficient.

Chapter 5

Circular array of cylinders

Before studying an array of buoys, let us consider an array of vertical circular cylinders extending to the bottom as presented in figure 5-1a. We want to find an explicit analytical solution for this problem. The method can then be applied to a circular array of buoys. In this problem only normal incidence will be considered, that is the incident wave arrives from infinity, parallel to the x axis. Because of the symmetry of the problem, by the method of images it is formally equivalent to the one of three half cylinders in a rectangular channel as represented on figure 5-1b. The wall of the channel are vertical, along the z axis. Again the new problem can be decomposed as

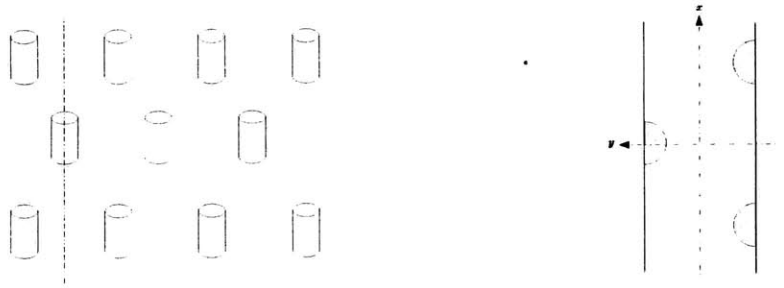

(a) Array in open sea (b) Array in a channel

Figure 5-1: Circular array of cylinders

the superposition of a symmetric and an antisymmetric problem as shown on figure 5-2. Each problem will be solved separetely. Then the solution to the general problem is given by the sum of the solution of the symmetric and antisymmetric problem. In

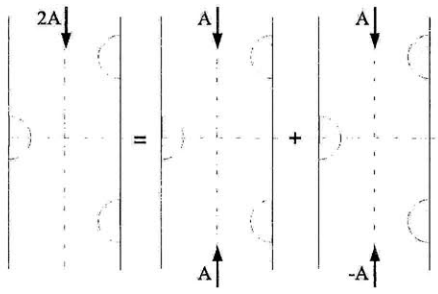

Figure 5-2: Decomposition of the problem into a symmetric and an antisymmetric problem

all this study we consider simple harmonic motion and symbol Re will be omitted for simplicity.

5.1 Symmetric problem

Let us consider the case of two plane incident waves arriving from $x = \infty$ and $x = -\infty$ with the same amplitude A_0.The problem is symmetric with respect to $x = 0$ and thus can be reduced to the study of half of the channel as presented on figure 5-3. The symmetry of the initial problem imposes that there is no flux on the vertical plan $x = 0$. The channel is infinite in the direction $x = +\infty$ and its width is $2c$.

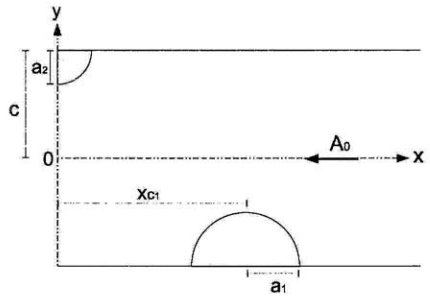

Figure 5-3: Symmetric problem

The half cylinder (called cylinder 1 from here on) has a radius a_1 and its center is located at $(x, y) = (x_{c1}, -c)$. The quarter of cylinder (called cylinder 2 from here on) has a radius a_2 and its center is located at $(x_2, y_2) = (0, c)$. Each cylinder has a local cartesian and polar coordinate system: (x_i, y_i) and (r_i, θ_i). The depth is assumed to

be constant and equal to h.

Equations Let us introduce the following notations:

- Ω_f is the fluid domain in the channel
- S_f is the free surface
- S_{c1} is the lateral surface of cylinder 1
- S_{c2} is the lateral surface of cylinder 2
- S_c are the lateral surfaces of the channel at $y = \pm c$
- S_0 is the vertical wall $x = 0$, $y \in [-c, c - a_2]$

The equations for the potential are:

$$\Delta\phi = 0, \qquad (x, y, z) \in \Omega_f \tag{5.1.1a}$$

$$\frac{\partial\phi}{\partial z} - \frac{\omega^2}{g}\phi = 0, \qquad \text{at} S_f \tag{5.1.1b}$$

$$\frac{\partial\phi}{\partial z} = 0, \qquad z = -h \tag{5.1.1c}$$

$$\frac{\partial\phi}{\partial y} = 0, \qquad \text{on} \quad S_c \tag{5.1.1d}$$

$$\frac{\partial\phi}{\partial n} = 0, \qquad \text{on} \quad S_{c1} \cup S_{c2} \tag{5.1.1e}$$

$$\frac{\partial\phi}{\partial x} = 0, \qquad \text{on} \quad S_0 \tag{5.1.1f}$$

where n is the normal to the vertical surface of cylinder 1 or 2. The potential of the plane incident wave is given by

$$\phi_i = \frac{-igA_0}{\omega} e^{-ikx} \frac{\cosh(k(z+h))}{\cosh(kh)} \tag{5.1.2}$$

Introduction of dimensionless variables Let us introduce the following dimensionless variables. We denote them by $'$.

$$\begin{aligned} x_i &= hx_i', \qquad & t &= t'\sqrt{\frac{h}{g}}, \quad & \eta &= A_0\eta' \\ \phi &= A_0\sqrt{gh}\phi', \quad & kh &= k', \qquad & a_i &= ha_i' \end{aligned} \tag{5.1.3}$$

And the incident potential is given by

$$\phi_i' = \frac{1}{i\omega'}e^{-ik'x'}\frac{\cosh(k'(z'+1))}{\cosh(k')} \tag{5.1.4}$$

Equations with dimensionless variables With the previous definitions we can rewrite the system of equations (5.1.1) as follow:

$$\Delta'\phi' = 0, \qquad \boldsymbol{x}' \in \Omega_f \tag{5.1.5a}$$

$$\frac{\partial\phi'}{\partial z'} - \omega'^2\phi' = 0, \qquad \text{at} S_f \tag{5.1.5b}$$

$$\frac{\partial\phi'}{\partial z'} = 0, \qquad z' = -1 \tag{5.1.5c}$$

$$\frac{\partial\phi'}{\partial y'} = 0, \qquad \text{on} \quad S_c \tag{5.1.5d}$$

$$\frac{\partial\phi'}{\partial n'} = 0, \qquad \text{on} \quad S_{c1} \cup S_{c2} \tag{5.1.5e}$$

$$\frac{\partial\phi'}{\partial x'} = 0, \qquad \text{on} \quad S_0 \tag{5.1.5f}$$

For simplicity we will omit the prime symbol from now on and if nothing is specified, all the variables are dimensionless.

Reduction to a 2D problem All the wall being vertical and extending to the bottom and the depth being constant and equal to h, we know that the problem can be reduced to a 2D problem and the scattered potential is of the form

$$\phi(x,y,z) = \frac{1}{i\omega'}(e^{-ikx}+\eta_s(x,y))\frac{\cosh(k'(z'+1))}{\cosh(k')} = \frac{1}{i\omega'}\eta(x,y)\frac{\cosh(k'(z'+1))}{\cosh(k')} \tag{5.1.6}$$

The function $\eta(x, y)$ corresponds to the free surface elevation. The new problem is then:

$$\Delta\eta = 0, \qquad \boldsymbol{x} \in \Omega_f \tag{5.1.7a}$$

$$\frac{\partial\eta}{\partial y} = 0, \qquad \text{at} \quad y = \pm c \tag{5.1.7b}$$

$$\frac{\partial\eta}{\partial n} = 0, \qquad \text{on} \quad S_{c1} \cup S_{c2} \tag{5.1.7c}$$

$$\frac{\partial\eta}{\partial x} = 0, \qquad \text{at} \quad x = 0 \tag{5.1.7d}$$

Solution We look for a solution using separation of variables. In order to satisfy (5.1.7a) and (5.1.7b), the solution must be of the following form (demonstration can be found in appendix C).

$$\eta = e^{-ikx} + \sum_{q=0}^{\infty} \alpha_q e^{-\nu_q x} V_q(y) \tag{5.1.8}$$

where

$$V_{2q}(y) = \cos\left(\frac{2q\pi}{2c}y\right) \tag{5.1.9a}$$

$$V_{2q+1}(y) = \sin\left(\frac{(2q+1)\pi}{2c}y\right) \tag{5.1.9b}$$

and

$$\nu_q = \begin{cases} -i\sqrt{k^2 - \left(\frac{q\pi}{2c}\right)^2}, & \text{if} \quad q < \dfrac{2kc}{\pi} \\ \sqrt{\left(\frac{q\pi}{2c}\right)^2 - k^2} & \text{otherwise} \end{cases} \tag{5.1.10}$$

The coefficients α_q are yet unknown and will be determined by applying the boundary conditions given by (5.1.7d) and (5.1.7c). In (5.1.8) the potential correponds to the sum of the incident wave and the scattered wave.

Boundary condition on S_0 Using the previous expression of the potential in equation (5.1.7d) leads to

$$-ik - \sum_{q=0}^{\infty} \alpha_q \nu_q V_q(y) = 0, \quad y \in [-c, c-a2] \tag{5.1.11}$$

Multiplying both side of the equation by $V_M(y)$ and integrating for $y \in [-c, c-a_2]$ we find that[1]

$$\forall M, \quad \sum_{q=0}^{\infty} \alpha_q \nu_q \langle V_q, V_M \rangle_{-c,c-a_2} = -ik \langle 1, V_M \rangle_{-c,c-a_2} \tag{5.1.12}$$

Boundary condition on cylinder 1 Equation (5.1.7c) imposes that

$$\left. \frac{\partial \eta}{\partial r_1} \right]_{r_1=a_1} = 0, \quad \theta_1 \in [0, \pi] \tag{5.1.13}$$

where (r_1, θ_1) is the local polar coordinate system of cylinder1. In order to apply this condition, the potential must be expressed with (r_1, θ_1) coordinates. The global cartesian coordinates and the local polar coordinates are related by

$$\begin{cases} x = x_{c1} + x_1 & = x_{c1} + r_1 \cos(\theta_1) \\ y = -c + y_1 & = -c + r_1 \sin(\theta_1) \end{cases} \tag{5.1.14}$$

Expression (5.1.8) can thus be written as

$$\eta(x_1, y_1) = e^{-ikx_{c1}} e^{-ikx_1} + \sum_{q=0}^{\infty} \alpha_q e^{-\nu_q x_{c1}} e^{-\nu_q x_1} V_q(-c + y_1) \tag{5.1.15}$$

[1]We denote the scalar product by

$$\langle f, g \rangle_{a,b} = \int_a^b f(y) g(y), \mathrm{d}y$$

Let us use the partial wave expansion for the plane waves (Mei et al. (2005), chapter 4, appendix 4.A):

$$e^{-ikx_1} = e^{-ikr_1\cos(\theta_1)} = \sum_{p=0}^{\infty} \epsilon_p \cos(p\theta_1)(-i)^p J_p(kr_1) \tag{5.1.16a}$$

$$e^{-\nu_q x_1} = e^{i\cdot i\nu_q r_1\cos(\theta_1)} = \sum_{p=0}^{\infty} \epsilon_p \cos(p\theta_1) i^p J_p(i\nu_q r_1) \tag{5.1.16b}$$

Let us also expand V_q in series of functions of local polar coordinates. We first consider q even. We have

$$\begin{aligned} V_{2q}(-c+y_1) &= \cos\left(\frac{\pi q}{c}(-c+y_1)\right) \\ &= (-1)^q \cos\left(\frac{\pi q}{c} y_1\right) \\ &= (-1)^q \cos\left(\frac{\pi q}{c} r_1 \sin\theta_1\right) \end{aligned} \tag{5.1.17}$$

Abramowitz and Stegun (1964), formula 9.1.42 gives the following identity

$$\cos(t\sin\theta) = \sum_{r=0}^{\infty} \epsilon_r J_{2r}(t) cos(2r\theta) \tag{5.1.18}$$

Applying this identity to (5.1.17) we finally obtain

$$V_{2q}(-c+y_1) = (-1)^q \sum_{r=0}^{\infty} \epsilon_r J_{2r}\left(\frac{2\pi q}{2c} r_1\right)\cos(2r\theta_1) \tag{5.1.19}$$

Let us now consider q odd.

$$\begin{aligned} V_{2q+1}(-c+y_1) &= \sin\left(-q\pi - \frac{\pi}{2} + \frac{(2q+1)\pi}{2c} y_1\right) \\ &= \cos\left(\frac{(2q+1)\pi}{2c} r_1 \sin\theta_1\right) \\ &= \sum_{r=0}^{\infty} \epsilon_r J_{2r}\left(\frac{(2q+1)\pi}{2c} r_1\right)\cos(2r\theta_1) \end{aligned} \tag{5.1.20}$$

Equations (5.1.19) and (5.1.20) can be summarized into the following way:

$$V_q(-c+y_1) = \sigma_q \sum_{r=0}^{\infty} \epsilon_r J_{2r}\left(\frac{q\pi}{2c} r_1\right) \cos(2r\theta_1) \tag{5.1.21}$$

with $\sigma_q = -1$ when $q \equiv 2$ [4] and $\sigma_q = 1$ otherwise. Substituting expressions (5.1.16) and (5.1.21) into (5.1.15), we obtain an expression for the potential as a sum of trigonometric functions and Bessel functions in the local polar coordinate system of cylinder 1:

$$\begin{aligned}\eta = & e^{-ikx_{c1}} \sum_{p=0}^{\infty} \epsilon_p \cos(p\theta_1)(-i)^p J_p(kr_1) \\ & + \sum_{q=0}^{\infty} \alpha_q e^{-\nu_q x_{c1}} \left(\sum_{p=0}^{\infty} \epsilon_p \cos(p\theta_1) i^p J_p(i\nu_q r_1)\right) \left(\sigma_q \sum_{r=0}^{\infty} \epsilon_r J_{2r}\left(\frac{\pi q}{c} r_1\right) \cos(2r\theta_1)\right)\end{aligned} \tag{5.1.22}$$

which can be rewritten as follows:

$$\begin{aligned}\eta = & e^{-ikx_{c1}} \sum_{p=0}^{\infty} \epsilon_p \cos(p\theta_1)(-i)^p J_p(kr_1) \\ & + \sum_{q=0}^{\infty} \sum_{p=0}^{\infty} \sum_{r=0}^{\infty} \alpha_q \epsilon_p \epsilon_r \sigma_q i^p e^{-\nu_q x_{c1}} \cos(p\theta_1) \cos(2r\theta_1) J_p(i\nu_q r_1) J_{2r}(\frac{\pi q}{c} r_1)\end{aligned} \tag{5.1.23}$$

The no flux condition given by (5.1.13) can now be applied, and leads to

$$\begin{aligned}0 = & e^{-ikx_{c1}} \sum_{p=0}^{\infty} \epsilon_p \cos(p\theta_1)(-i)^p k J_p'(ka_1) \\ & + \sum_{q=0}^{\infty} \sum_{p=0}^{\infty} \sum_{r=0}^{\infty} \alpha_q \epsilon_p \epsilon_r \sigma_q i^p e^{-\nu_q x_{c1}} \cos(p\theta_1) \cos(2r\theta_1) \cdot \\ & \left[i\nu_q J_p'(i\nu_q a_1) J_{2r}\left(\frac{\pi q}{c} a_1\right) + \frac{\pi q}{c} J_p(i\nu_q a_1) J_{2r}'\left(\frac{\pi q}{c} a_1\right)\right]\end{aligned} \tag{5.1.24}$$

This expression is valid for $\theta_1 \in [0, \pi]$. We will use the following orthogonality property:

$$\int_0^{\pi} \cos(p\theta) cos(M\theta) d\theta = \delta_{Mp} \frac{\pi}{\epsilon_p} \tag{5.1.25}$$

Let us use the following notations for simplicity[2]:

$$CC_1\left(p,2r,M\right)=\int_0^{\pi}\cos(p\theta)\cos(2r\theta)\cos(M\theta)d\theta \tag{5.1.26}$$

and

$$\mathcal{J}_1(p,q,r)=i\nu_q J_p'(i\nu_q a_1)J_{2r}\left(\frac{\pi q}{c}a_1\right)+\frac{\pi q}{c}J_p(i\nu_q a_1)J_{2r}'\left(\frac{\pi q}{c}a_1\right) \tag{5.1.27}$$

We multiply (5.1.24) by $\cos(M\theta_1)$ and integrate for $\theta_1\in[0,\pi]$. Making use of the previous relations we get for any M:

$$\begin{aligned}\sum_{q=0}^{\infty}\sum_{p=0}^{\infty}\sum_{r=0}^{\infty}\alpha_q\epsilon_p\epsilon_r\sigma_q i^p e^{-\nu_q x_{c1}}\mathcal{J}_1(p,q,r)CC_1\left(p,2r,M\right)=\\ -\pi(-i)^M k e^{-ikx_{c1}}J_M'(ka_1)\end{aligned} \tag{5.1.28}$$

which can be rewritten as

$$\sum_{q=0}^{\infty}\alpha_q A_q^{(1)}(M)=-\pi(-i)^M k e^{-ikx_{c1}}J_M'(ka_1) \tag{5.1.29}$$

with

$$A_q^{(1)}(M)=\sum_{p=0}^{\infty}\sum_{r=0}^{\infty}\epsilon_p\epsilon_r\sigma_q i^p e^{-\nu_q x_{c1}}\mathcal{J}_1(p,q,r)CC_1\left(p,2r,M\right) \tag{5.1.30}$$

Boundary condition on cylinder 2 Equation (5.1.7c) imposes that

$$\left.\frac{\partial\eta}{\partial r_2}\right]_{r_2=a_2}=0,\quad \theta_2\in[-\pi/2,0] \tag{5.1.31}$$

[2]An explicit result of this integral is given by Gradshteyn and Ryzhik (1965), formula 2.533:

$$\begin{aligned}\int\cos ax\cos bx\cos cx dx=\frac{1}{4}\left\{\frac{\sin(a+b+c)x}{a+b+c}+\frac{\sin(a+b-c)x}{a+b-c}+\right.\\ \left.+\frac{\sin(a-b+c)x}{a-b+c}+\frac{\sin(b+c-a)x}{b+c-a}\right\}\end{aligned}$$

where (r_2, θ_2) is the local polar coordinate system of cylinder2. We now have to express the potential with (r_2, θ_2). Using the following relation between the global cartesian system and the local polar coordinate system of cylinder 2,

$$\begin{cases} x = x_2 = r_2 \cos(\theta_2) \\ y = c + y_2 = c + r_2 \sin(\theta_2) \end{cases} \tag{5.1.32}$$

we get

$$\eta(x_2, y_2) = e^{-ikx_2} + \sum_{q=0}^{\infty} \alpha_q e^{-\nu_q x_2} V_q(c + y_2) \tag{5.1.33}$$

As before we write

$$e^{-ikx_2} = \sum_{p=0}^{\infty} \epsilon_p \cos(p\theta_2)(-i)^p J_p(kr_2) \tag{5.1.34a}$$

$$e^{-\nu_q x_2} = \sum_{p=0}^{\infty} \epsilon_p \cos(p\theta_2) i^p J_p(i\nu_q r_2) \tag{5.1.34b}$$

$$V_q(c + y_2) = \sigma_q \sum_{r=0}^{\infty} \epsilon_r J_{2r}(\frac{\pi q}{c} r_2) cos(2r\theta_2) \tag{5.1.34c}$$

Substituting (5.1.34a),(5.1.34b) and (5.1.34c) into (5.1.33) we obtain the free surface elevation in the local polar coordinates of cylinder 2:

$$\begin{aligned} \eta = & \sum_{p=0}^{\infty} \epsilon_p \cos(p\theta_2)(-i)^p J_p(kr_2) \\ & + \sum_{q=0}^{\infty} \sum_{p=0}^{\infty} \sum_{r=0}^{\infty} \alpha_q \epsilon_p \epsilon_r (-1)^q i^p \cos(p\theta_2) \cos(2r\theta_2) J_p(\tau_q r_2) J_{2r}\left(\frac{\pi q}{c} r_2\right) \end{aligned} \tag{5.1.35}$$

For simplicity let us denote:

$$\mathcal{J}_2(p, q, r) = i\nu_q J_p'(i\nu_q a_2) J_{2r}\left(\frac{\pi q}{c} a_2\right) + \frac{\pi q}{c} J_p(i\nu_q a_2) J_{2r}'\left(\frac{\pi q}{c} a_2\right) \tag{5.1.36}$$

Note that if the cylinders have the same radius ($a_1 = a_2$), $\mathcal{J}_1(p, q, r) = \mathcal{J}_2(p, q, r)$. Replacing the potential given by (5.1.35) into (5.1.31) and using the previous notation

lead to

$$0 = \sum_{p=0}^{\infty} \epsilon_p \cos(p\theta_1)(-i)^p k J_p'(ka_1) + \sum_{q=0}^{\infty}\sum_{p=0}^{\infty}\sum_{r=0}^{\infty} \alpha_q \epsilon_p \epsilon_r \sigma_q i^p \cos(p\theta_2)\cos(2r\theta_2)\mathcal{J}_2(p,q,r) \tag{5.1.37}$$

Let us denote[3]:

$$\mathcal{C}(p,M) = \int_{-\pi/2}^{0} \cos(p\theta_2)\cos(M\theta_2)\, d\theta_2 \tag{5.1.38}$$

Multiplying (5.1.37) by $\cos(M\theta_2)$ and integrating for $\theta_2 \in [-\pi/2, 0]$, we obtain for all n, M

$$\sum_{q=0}^{\infty}\sum_{p=0}^{\infty}\sum_{r=0}^{\infty} \alpha_q \epsilon_p \epsilon_r \sigma_q i^p \mathcal{J}_2(p,q,r) CC_2(p,2r,M) = -k\sum_{p=0}^{\infty} \epsilon_p (-i)^p \mathcal{C}(p,M) J_p'(ka_2) \tag{5.1.39}$$

which can be rewritten as

$$\sum_{q=0}^{\infty} \alpha_q A_q^{(2)}(M) = -k\sum_{p=0}^{\infty} \epsilon_p (-i)^p \mathcal{C}(p,M) J_p'(ka_2) \tag{5.1.40}$$

with

$$A_q^{(2)}(M) = \sum_{p=0}^{\infty}\sum_{r=0}^{\infty} \epsilon_p \epsilon_r \sigma_q i^p \mathcal{J}_2(p,q,r) CC_2(p,2r,M) \tag{5.1.41}$$

Linear system for the coefficients Let us summarize the result we have obtained so far. The unknown coefficients α_q are solution of the linear system of equation given by (5.1.12), (5.1.29) and (5.1.40) and rewritten below. For all M, M' and M'':

$$\sum_{q=0}^{\infty} \alpha_q \nu_q \langle V_q, V_M\rangle_{-c,c-a_2} = -ik\langle 1, V_M\rangle_{-c,c-a_2} \tag{5.1.42}$$

[3]An explicit result of this integral is given by Gradshteyn and Ryzhik (1965), formula 2.532:

$$\int \cos ax \cos bx dx = \frac{\sin(a+b)x}{a+b} + \frac{\sin(a-b)x}{a-b}$$

$$\sum_{q=0}^{\infty} \alpha_q A_q^{(1)}(M') = -\pi(-i)^{M'} k e^{-ikx_{c1}} J'_{M'}(ka_1) \tag{5.1.43}$$

$$\sum_{q=0}^{\infty} \alpha_q A_q^{(2)}(M'') = -k \sum_{p=0}^{\infty} \epsilon_p (-i)^p \mathcal{C}(p, M) J'_p(ka_2) \tag{5.1.44}$$

and $A_q^{(i)}$ are defined by equations (5.1.41) and (5.1.41). This is an infinite system of equations for the coefficients α_q. It will be further truncated after the Nth term and solved numerically.

5.2 Antisymmetric problem

Let us now consider a pair of incident waves, where the first arrives from $x = +\infty$ with amplitude A_0 and the second arrives from $x = -\infty$ with amplitude $-A_0$. The problem defined by (5.1.1) remains unchanged except the boundary condition (5.1.7d) which is replaced by

$$\phi = 0, \quad x = 0, y \in [-c, c - a_2] \tag{5.2.1}$$

The free surface elevation can again be written in the form given by (5.1.8). Since the boundary conditions on the two cylinders are unchanged, α_q are solution of (5.1.42) and (5.1.43).

$$1 + \sum_{q=0}^{\infty} \alpha_q V_q(y) = 0 \tag{5.2.2}$$

Multiplying by $V_M(y)$ and integrating for $y \in [-c, c - a_2]$ give finally

$$\langle 1, V_m \rangle_{-c,c-a_2} + \sum_{q=0}^{\infty} \alpha_q \langle V_q, V_M \rangle_{-c,c-a_2} = 0 \tag{5.2.3}$$

For a given n, α_q,$q = 0, 1, 2, ...$ are the solutions of the linear system defined by (5.2.3), (5.1.42) and (5.1.43) and rewritten below:

$$\langle 1, V_m \rangle_{-c,c-a_2} + \sum_{q=0}^{\infty} \alpha_q \langle V_q, V_M \rangle_{-c,c-a_2} = 0 \tag{5.2.4}$$

$$\sum_{q=0}^{\infty} \alpha_q A_q^{(1)}(M') = -\pi(-i)^{M'} k e^{-ikx_{c1}} J'_{M'}(ka_1) \tag{5.2.5}$$

$$\sum_{q=0}^{\infty} \alpha_q A_q^{(2)}(M'') = -k \sum_{p=0}^{\infty} \epsilon_p (-i)^p \mathcal{C}(p, M'') J'_p(ka_2) \tag{5.2.6}$$

This infinite system for the coefficients α_q will be truncated and solved numerically.

5.3 Energy conservation

For later checking the accuracy of numerical computations, let us consider a vertical surface at $x \sim \infty$. Green's formula gives

$$\int_{\partial S} \left(\phi \frac{\partial \eta^*}{\partial n} - \eta^* \frac{\partial \eta}{\partial n} \right) \mathrm{d}l = \int \int_{S_f} \left(\eta \nabla^2 \eta^* - \eta^* \nabla^2 \eta \right) \mathrm{d}S \tag{5.3.1}$$

where $\partial S = S_{c1} \bigcup S_{c2} \bigcup S_c \bigcup S_\infty \bigcup S_0$.

(5.1.7a) implies that the right-hand-side of (5.3.1) is equal to zero. The boundary conditions (5.1.7b)-(5.1.7d) implies that

$$\int \int_{S_{c1} \bigcup S_{c2} \bigcup S_c \bigcup S_0} \left(\phi \frac{\partial \phi^*}{\partial n} - \phi^* \frac{\partial \phi}{\partial n} \right) \mathrm{d}S = 0 \tag{5.3.2}$$

And thus (5.3.1) leads finally to

$$\int_{S_\infty} \left(\eta \frac{\partial \eta^*}{\partial n} - \eta^* \frac{\partial \eta}{\partial n} \right) \mathrm{d}l = 0 \tag{5.3.3}$$

which can also be written as

$$2i\mathrm{Im} \left(\int_{-c}^{c} \eta \frac{\partial \eta^*}{\partial x} \mathrm{d}x \right) = 0 \tag{5.3.4}$$

With (5.1.8) we have

$$\frac{\partial \eta^*}{\partial x} = ike^{ikx} + \sum_{q=0}^{\infty} \alpha_q^* \left(-\nu_q^* \right) e^{-\nu_q^* x} V_q^*(y) \tag{5.3.5}$$

Thus

$$\begin{aligned}\eta\frac{\partial\eta^*}{\partial x}dz =& \left\{e^{-ikx}+\sum_{q=0}^{\infty}\alpha_q e^{-\nu_q x}V_q(y)\right\}\cdot \\ & \left\{ike^{ikx}+\sum_{r=0}^{\infty}\alpha_r^*\left(-\nu_r^*\right)e^{-\nu_r^* x}V_r(y)\right\} \\ =& ik-e^{-ikx}\sum_{r=0}^{\infty}\alpha_r^*\nu_r^* e^{-\nu_r^* x}V_r(y)+ike^{ikx}\sum_{q=0}^{\infty}\alpha_q e^{-\nu_q x}V_q(y) \\ & -\sum_{q=0}^{\infty}\sum_{r=0}^{\infty}\alpha_q\alpha_r^*\nu_r^* e^{-\nu_q x}e^{-\nu_r^* x}V_r(y)V_q(y)\end{aligned} \tag{5.3.6}$$

Performing analytical integration we have:

$$\int_{-c}^{c}V_{2q}(y)V_{2r}(y)dy=\frac{2c}{\epsilon_q}\delta_{q,r} \tag{5.3.7a}$$

$$\int_{-c}^{c}V_{2q+1}(y)V_{2r+1}(y)dy=\frac{2c}{\epsilon_q}\delta_{q,r} \tag{5.3.7b}$$

$$\int_{-c}^{c}V_{2q}(y)V_{2r+1}(y)dy=0 \tag{5.3.7c}$$

$$\int_{-c}^{c}V_q(y)dy=\begin{cases}0, & \text{if} \quad q\neq 0\\ 2c & \text{if} \quad q=0\end{cases} \tag{5.3.7d}$$

(5.3.7e)

Integrating with respect to y (5.3.6) and making use of the two previous properties leads to

$$\begin{aligned}\int_{-c}^{c}\eta\frac{\partial\eta^*}{\partial x}dz =& i2kc-2ce^{-ikx}\alpha_0^*\nu_0^* e^{-\nu_0^* x}+2cike^{ikx}\alpha_0 e^{-\nu_0 x} \\ & -\sum_{q=0}^{\infty}\frac{2c}{\epsilon_{2q}}\alpha_{2q}\alpha_{2q}^*\nu_{2q}^* e^{-\nu_{2q}x}e^{-\nu_{2q}^* x}-\sum_{q=0}^{\infty}\frac{2c}{\epsilon_{2q+1}}\alpha_{2q+1}\alpha_{2q+1}^*\nu_{2q+1}^* e^{-\nu_{2q+1}x}e^{-\nu_{2q+1}^* x} \\ =& i2kc-2ce^{-ikx}\alpha_0^*\nu_0^* e^{-\nu_0^* x}+2cike^{ikx}\alpha_0 e^{-\nu_0 x}-\sum_{q=0}^{\infty}\frac{2c}{\epsilon_q}\alpha_q\alpha_q^*\nu_q^* e^{-\nu_q x}e^{-\nu_q^* x}\end{aligned} \tag{5.3.8}$$

Equation (5.1.10) gives

$$\nu_0=-\mathrm{i}k \tag{5.3.9}$$

As a result,

$$\begin{aligned}\int_{-c}^{c}\eta\frac{\partial\eta^*}{\partial x}dz =& i2kc + i2ck\left(e^{2ikx}\alpha_0 - e^{-2ikx}\alpha_0^*\right)\\ &-i\sum_{q=0}^{\infty}\frac{2c}{\epsilon_q}\left|\alpha_q\right|^2\tau_q^* e^{-\nu_q x}e^{--\nu_q^* x}\\ =& i2kc - 4ck\mathrm{Im}\left(e^{2ikx}\alpha_0\right)\\ &-\sum_{q=0}^{\infty}\frac{2c}{\epsilon_q}\left|\alpha_q\right|^2\nu_q^* e^{-\nu_q x}e^{-\nu_q^* x}\end{aligned} \tag{5.3.10}$$

We can now substitute this expression into (5.3.4) and obtain

$$2kc - \mathrm{Im}\left(\sum_{q=0}^{\infty}\frac{2c}{\epsilon_q}\left|\alpha_q\right|^2\nu_q^* e^{-\nu_q x}e^{-\nu_q^* x}\right) = 0 \tag{5.3.11}$$

According to (5.1.8), let us define q_0 such that

$$q_0 = \max\left\{q \;\middle|\; q < \frac{2ck}{\pi}\right\} \tag{5.3.12}$$

As a result q_0 has the following property:

$$q \le q_0 \Rightarrow \nu_q = -\mathrm{i}\sqrt{k^2 - \left(\frac{\pi q}{c}\right)^2} \tag{5.3.13a}$$

$$q > q_0 \Rightarrow \nu_q = \sqrt{\left(\frac{\pi q}{c}\right)^2 - k^2} \tag{5.3.13b}$$

(5.3.13c)

Thus we have

$$q \le q_0 \Rightarrow e^{-\nu_q^* x} = e^{\nu_q x} \tag{5.3.14a}$$

$$q > q_0 \Rightarrow e^{-\nu_q x} \approx 0, \quad k_0 x >> 1 \tag{5.3.14b}$$

(5.3.14c)

With this two previous properties, equation (5.3.11) can be rewritten as

$$\sum_{q=0}^{q_0} \frac{1}{\epsilon_q} |\alpha_q|^2 |\nu_q| = k \tag{5.3.15}$$

5.4 Numerical computation difficulties

All the numerical computation presented below have used the following inputs: a/h=5/30, c/h=30/30.

5.4.1 Condition number of the matrix of the system

As explained previously, equations (5.1.42), (5.1.43) and (5.1.44) define a linear infinite system of equations that determine the value of the unknown coefficients α_q. All the series must be truncated again after their N_i^{th} term, where i stand for the indexes of sommation: p, r or q. We obtain then the matrix of the system:

$$A = \begin{pmatrix} a_{11} & a_{12} & \cdots & a_{1N_q} \\ a_{21} & \cdots & \cdots & a_{1N_q} \\ \vdots & \ddots & \ddots & \vdots \\ a_{N_q1} & a_{N_q2} & \cdots & a_{N_qN_q} \end{pmatrix} \tag{5.4.1}$$

where the terms a_{ii} can easily be deduced from equations (5.1.42) to (5.1.44). This matrix is then inverted to find the solution. In order to find numerically an accurate solution, the system must be well-conditionned. A measure of this property is given by the condition number of the matrix A. Let us briefly describe the condition number by doing perturbation analysis. Suppose that A is perturbed by an amount δA, for example because of numerical roundoffs. We want to quantify the error on the solution. We have

$$(A + \delta A)(x + \delta x) = Ax + \delta Ax + A\delta x + \delta A\delta x = b \tag{5.4.2}$$

where b is the unperturbed right hand side. Since $Ax - b = 0$ we have

$$A\delta x = -\delta A(x + \delta x) \Rightarrow \delta x = -A^{-1}\delta A(x + \delta x) \tag{5.4.3}$$

Taking norms

$$\|\delta x\| \leq \left\|A^{-1}\right\| \|A\| \frac{1}{\|A\|} \|\delta A\| \|x + \delta x\| \tag{5.4.4}$$

and thus we find for the relative error that

$$\frac{\|\delta x\|}{\|x + \delta x\|} \leq \left\|A^{-1}\right\| \|A\| \frac{\|\delta A\|}{\|A\|} \tag{5.4.5}$$

The quantity $\|A^{-1}\| \|A\|$ is called the condition number of the matrix A and gives an estimation of the error of the solution. For example, suppose that the matrix has has a precision of 16 digits ($\frac{\|\delta A\|}{\|A\|} = 10^{-16}$) and assumme that the condition number is equal to 100, then $\frac{\|\delta x\|}{\|x+\delta x\|} \leq 10^{-14}$ wich means that 14 digits are accurate in the solution. Now if the condition number is equal to 10^{13} we have $\frac{\|\delta x\|}{\|x+\delta x\|} \leq 10^{-3} = 0.1\%$. Only 3 digits are accurate in the solution. Finally if the condition number is equal to 10^{20} we have $\frac{\|\delta x\|}{\|x+\delta x\|} \leq 10^{4} = 10^{6}\%$. The solution cannot be trusted at all. We see here that a big condition number leads to big error in the solution computed. Figure 5-4 presents a semilog plot of the condition number of A as the number of points N_q increases. As we have three type of equations, N_q is a multiple of 3. We see that

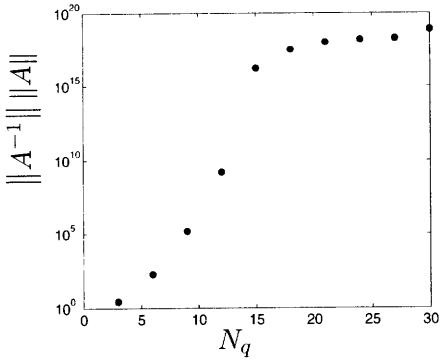

Figure 5-4: Condition number of A function of N_q

the condition number of A increases extremely fast with N_q and reaches the machine precision for q larger than 15. Thus the linear system cannot be solved at that point.

In order to investigate this problem, we have used collocation method, as described in the following section. Indeed this method requires less numerical operations and thus minimizes the risk of numerical roundoff errors. We now try a different method.

5.4.2 Collocation method

In this method we discretize the surface of the two cylinders and the surface S_0 into a finite number of points (x_i, y_i) as represented of figure 5-5. Then we require that the η satisfies the boundary conditions at these points, which leads to a finite linear sytem of equations that is solved numerically (see Hairer et al. (1993) or Iserles (1996) for more details on this method). The boundary conditions we have to imposed are

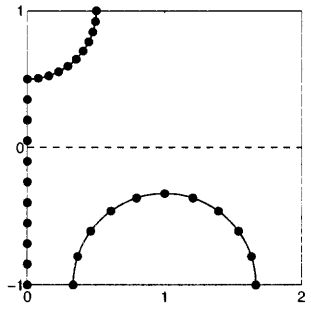

Figure 5-5: Discretization for the collocation method

defined by equations (5.1.7d) and (5.1.7c). The first one imposes (for the symmetric case):

$$\sum_{q=0}^{\infty} \alpha_q \nu_q V_q(y_i) = -ik \tag{5.4.6}$$

For the two cylinders

$$\frac{\partial \eta}{\partial \mathbf{n}} = \vec{n} \cdot \nabla \eta = n_x \frac{\partial \eta}{\partial x} + n_y \frac{\partial \eta}{\partial y} = 0 \tag{5.4.7}$$

where $\mathbf{n}$ is the normal to the surface of the cylinder. For cylinder 1 we have:

$$(x - x_{c1})^2 + (y + c)^2 = a_1^2 \tag{5.4.8}$$

and the normal is thus

$$\vec{n_1} = (x - x_{c1}, y + c) \qquad (x, y) \in \text{cylinder 1} \tag{5.4.9}$$

For cylinder 2 we have

$$x^2 + (y - c)^2 = a_2^2 \tag{5.4.10}$$

and the normal is thus

$$\vec{n_2} = (x, y - c) \qquad (x, y) \in \text{cylinder 2} \tag{5.4.11}$$

With these definition, the boundary condition for cylinder 1 becomes:

$$\sum_{q=0}^{\infty} \alpha_q \left(\mathrm{i}(x_i - x_{c1})\tau_q e^{\nu_q x_i} \cos\left(\frac{\pi q y_i}{c}\right) - (y_i + c)\frac{\pi q}{c} e^{\nu_q x_i} \sin\left(\frac{\pi q y_i}{c}\right)\right) = ik(x_i - x_{c1})e^{-\mathrm{i}kx_i} \tag{5.4.12}$$

and for cylinder 2

$$\sum_{q=0}^{\infty} \alpha_q \left(\mathrm{i}x_- \nu_q e^{\nu_q x_i} \cos\left(\frac{\pi q y_i}{c}\right) - (y_i - c)\frac{\pi q}{c} e^{\nu_q x_i} \sin\left(\frac{\pi q y_i}{c}\right)\right) = ikx_i e^{-\mathrm{i}kx_i} \tag{5.4.13}$$

We truncate the infinite series in (5.4.6), (5.4.12) and (5.4.13) and build the matrix B of the sytem. Figure 5-6a presents the condition number $c_B = \|B^{-1}\| \, \|B\|$ as a function of the number of points of collocations. This number is also equal to the number of terms in the series. As in the previous section the condition number reaches high values very fast. Figure 5-6b presents the condition number when we only take into account equations (5.4.6) and (5.4.13), i.e when we only consider cylinder 2 in the channel. The evolution of the condition number is similar. In order to investigate more the computation difficulties, we have consider the case with only cylinder 2 as represented on figure 5-7.

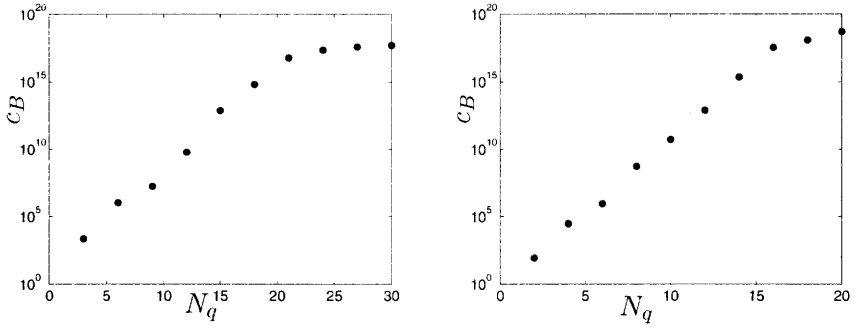

(a) With cylinder 1 and 2 (b) Only cylinder 2

Figure 5-6: Condition number of B function of N_q

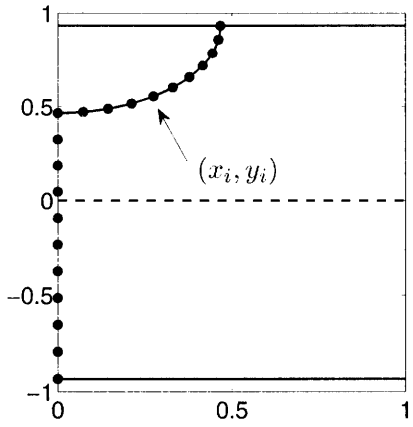

Figure 5-7: Collocation with only cylinder 2

5.4.3 Numerical and physical understanding of the computation difficulties

The matrix A of the system is composed of two block A_1 and A_2:

$$\begin{pmatrix} \cdots & \cdots & \cdots \\ \vdots & A & \vdots \\ \cdots & \cdots & \cdots \end{pmatrix} = \left(\begin{array}{ccc} \cdots & A_1 & \cdots \\ \hline \cdots & A_2 & \cdots \end{array}\right) \tag{5.4.14}$$

where A_1 corresponds to the system of equations given by applying boundary condition on the wall at $x = 0$ and A_2 corresponds to the system for the boundary condition on the cylinder. A quick estimation of equation (5.4.6) shows that the terms of the matrix A_1 are of order unity.

Let us now look at the terms of A_2. As x is larger than zero the evanescent mode $e^{-\nu_q x}$ in expression (5.1.8) decreases exponentially and are, with the exception of the first modes, almost equal to zero for x larger than zero. This is in particular true when we apply the boundary condition on the surface of the cylinder, near $x = a_2$. Let us look now turn to the physical situation. We expect the potential to be of order one on the free surface of the cylinder. As seen previously the evanescent mode are almost zero on this surface except for the first terms. As a consequence, we expect the coefficients α_q to be very large so that $\alpha_q e^{-\nu_q x} V_q(y) = O(1)$ on the cylinder. This intuition is verified numerically. We present below the matrix of the coefficient α_q for

$N_q = 14$ and $N_q = 22$. For brevity we only display the first 10 coefficients.

$$\alpha_{\{N_q=14\}} = \begin{pmatrix} 0.60 \\ 0.90 \\ 5.33 \\ 120 \\ 452 \\ 849 \\ 879 \\ 354 \\ 306 \\ 564 \end{pmatrix} \quad \alpha_{\{N_q=22\}} = \begin{pmatrix} 1.39 \\ 2.91 \\ 5.10 \\ 0.46 \\ 1076 \\ 8644 \\ 35444 \\ 94970 \\ 182403 \\ 262057 \end{pmatrix} \tag{5.4.15}$$

The numerical results confirm the physical intuition. In order to solve this problem one could try to renormalize the system. A potential renormalization is the following:

$$\eta = e^{-ikx} + \sum_{q=0}^{\infty} \left(\alpha_q e^{-\nu_q a_2}\right) \frac{e^{-\nu_q x}}{e^{-\nu_q a_2}} V_q(y) = e^{-ikx} + \sum_{q=0}^{\infty} \alpha'_q e^{-\nu_q (x-a_2)} V_q(y) \tag{5.4.16}$$

However this approach would fail too: it would indeed lead for α_q to a system where the coefficients are of order 1 on the part of the cylinder that is closed to $x = a_2$ but would be very large on the rest of the quarter of cylinder and on the wall $x = 0$. Thus, in order to keep the solution of order 1 on the wall, the coefficients α_q would have to be extremely small.

More generally any renormalization would just shift the problem to another place but would not solve it. Indeed normalization would be efficient on the two configurations presented on figure 5-8: either a boundary with x constant and a potential expressed in cartesian coordinates or a boundary with r constant and a potential defined in polar coordinates. For the present case, with the expression chosen for the potential, normalization cannot be used to solve the problem as the value of x varies as we apply the boundary condition along the surface of the cylinder.

From a numerical point of view, the serie $\sum \alpha_q e^{-\nu_q x} V_q(y)$ needs an infinite number

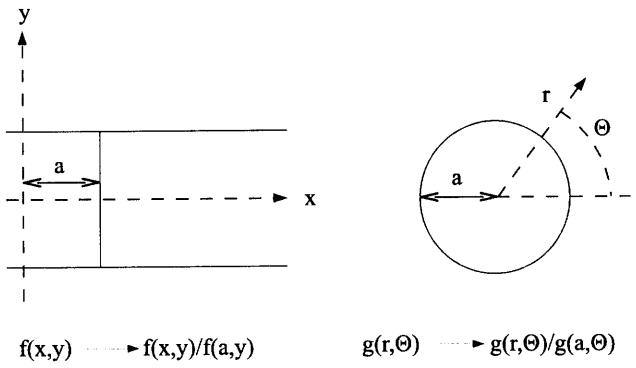

Figure 5-8: Two successfull case for normalization

of term to converge, which makes it numerically inefficient. As a consequence a new form of the potential has to be founded in order to deal with this problem.

Chapter 6

Circular array of buoys

Let us now consider the case of an array of buoys which are similarly aligned as the array of cylinders studied in chapter 5. The buoys are small cylinders of height H. Only normal incidence will be studied in this theory. Again the problem is equivalent of a half buoy in a channel as sketched in figure 5-1b of the previous chapter. The problem of the interaction of a wave with a floating body can be decomposed into a scattering and a radiation problem (see e.g. Mei et al. (2005)). We first consider the scattering problem.

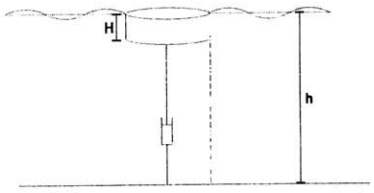

Figure 6-1: Pattern of a buoy

6.1 Scattering problem

The buoy is considered to be fixed and an incident wave is arriving from infinity. Similarly to the case of cylinder extending to the bottom, the scattering problem

can be decomposed into a symmetric and an antisymmetric problem and thus the problem is reduced to study hal of the channel as presented in the previosu chapter on figure 5-3. We decompose the fluid domain into three sub-domains:

- **Domain 1:** This domain comprised the water domain under the half buoy 1 and is defined in the polar coordinates of cylinder 1 by: $r_1 \leq a_1$, $0 \leq \theta_1 \leq \pi$.
- **Domain 2:** This domain comprised the water domain under the quarter of buoy 2 and is defined in the polar coordinates of cylinder 2 by: $r_2 \leq a_2$, $-\pi/2 \leq \theta_2 \leq 0$.
- **Outer domain:** This domain is defined by the fluid domain in the channel bereft of domains 1 and 2.

6.1.1 Symmetric problem

Equations Let us consider a plane incident wave arriving from $x = +\infty$. We denote by S_{B_j} and S_{L_j} the bottom and the lateral surface of the buoys j. Let us use the dimensionless parameters defined in the previous chapter in equation (5.1.3). With these parameters, the governing equations for the fluid are:

$$\Delta\phi = 0, \qquad \boldsymbol{x} \in \Omega_f \tag{6.1.1a}$$

$$\frac{\partial\phi}{\partial z} - \omega^2\phi = 0, \qquad \text{at} \quad S_f \tag{6.1.1b}$$

$$\frac{\partial\phi}{\partial z} = 0, \qquad z = -1 \tag{6.1.1c}$$

$$\frac{\partial\phi}{\partial y} = 0, \qquad \text{on} \quad S_c \tag{6.1.1d}$$

$$\frac{\partial\phi}{\partial n} = 0, \qquad \text{on} \quad S_{B_j} \cup S_{L_j} \tag{6.1.1e}$$

$$\frac{\partial\phi}{\partial x} = 0, \qquad \text{on} \quad S_0 \tag{6.1.1f}$$

and the incident wave is given by

$$\phi_i = \frac{1}{i\omega}\frac{f_0(z)}{f_0(0)}e^{-ikx} \tag{6.1.2}$$

The potential solution to the problem is the sum of the incident wave potential and the scattered wave potential: $\phi = \phi_i + \phi_s$.

Solution in the outer domain The form of the potential used in the previous section (equation (5.1.8)) can be easily extended in 3D with:

$$\phi_s = \frac{1}{i\omega} \sum_{n=0}^{\infty} \sum_{q=0}^{\infty} A_{nq} e^{i\tau_{nq} x} V_q(y) f_n(z) \tag{6.1.3}$$

where τ_{nq} is defined by

$$\tau_{nq} = i\sqrt{k_n^2 + \left(\frac{\pi q}{c}\right)^2}, \text{for} \quad n \geq 1 \tag{6.1.4a}$$

$$\tau_{0q} = \begin{cases} \sqrt{k^2 - \left(\frac{\pi q}{2c}\right)^2}, & \text{if} \quad q < ck/\pi \\ i\sqrt{\left(\frac{\pi q}{2c}\right)^2 - k^2} & \text{otherwise} \end{cases} \tag{6.1.4b}$$

$$\tag{6.1.4c}$$

Functions V_q are defined by

$$V_{2q}(y) = \cos\left(\frac{2q\pi}{2c} y\right) \tag{6.1.5a}$$

$$V_{2q+1}(y) = \sin\left(\frac{(2q+1)\pi}{2c} y\right) \tag{6.1.5b}$$

and f_n are the vertical eigenfunctions defined by

$$f_0(z) = \frac{\sqrt{2}\cosh(k(z+1))}{\sqrt{(1+\sinh^2(k)/\omega^2)}} \equiv c_0 \cosh(k(z+1)), \qquad k\tanh(k) = \omega^2 \tag{6.1.6a}$$

$$f_n(z) = \frac{\sqrt{2}\cos(k_n(z+1))}{\sqrt{(1-\sin^2(k_n)/\omega^2)}} \equiv c_n \cos(k_n(z+1)), \qquad k_n\tan(k_n) = -\omega^2 \tag{6.1.6b}$$

$$\tag{6.1.6c}$$

Coefficients A_{nq} are yet unknown. With this form, ϕ satisfies (6.1.1a), (6.1.1b), (6.1.1c) and (6.1.1d).

Boundary condition on the wall $x = 0$ for the outer potential By taking the derivative of the outer potential and using the scalar product in z and y, the calculation to satisfy the boundary condition (6.1.1f) leads to:

$$\forall n, M, \quad \sum_{q=0}^{\infty} \alpha_{nq} \tau_{nq} \langle V_q, V_M \rangle_{-c,c-a_2} = \frac{k}{f_0(0)} \delta_{n,0} \langle 1, V_M \rangle_{-c,c-a_2} \tag{6.1.7}$$

Solution in the inner domains The solution of the fluid domain under a buoy is given by Garnaud (2009) with the following result, that satisfies (6.1.1a), (6.1.1c) and (6.1.1e) on S_{B_j}:

$$\phi_s^j = \frac{1}{i\omega} \sum_{m=0}^{\infty} \cos(m\theta_j) \left(\phi_m^{P,j} + \sum_{n=0}^{\infty} B_{n,m}^j F_n(z) \psi_{n,m}(r_j) \right) \quad j = 1, 2 \tag{6.1.8}$$

$$\phi_m^{P,j} = -\frac{f_0(z)}{f_0(0)} \varepsilon_m \mathrm{i}^m J_m(kr_j) \tag{6.1.9}$$

where the eigenfunctions in this domain are given by:

$$F_0(z) = \frac{1}{\sqrt{1-H}} \tag{6.1.10a}$$

$$F_n(z) = \frac{\sqrt{2}\cos(K_n(z+1))}{\sqrt{1-H}} \qquad K_n = \frac{n\pi}{1-H} \tag{6.1.10b}$$

$$\Psi_{0,m}(r) = r^m \tag{6.1.10c}$$

$$\Psi_{n,m}(r) = I_m(K_n r) \tag{6.1.10d}$$

Matching domain 1 and outer domain The normal velocity and the pressure must be continuous across the interface between the domain 1 and the outer domain. Thus we need to match the value of the potential (pressure) and the value of its normal derivative across this surface. For this, let us express the incident wave potential and the outer potential in the local polar coordinate of cylinder 1. This has been done in the previous chapter with the following result:

$$\phi_i = \frac{1}{\mathrm{i}\omega} \frac{f_0(z)}{f_0(0)} e^{-\mathrm{i}kx_{c1}} \sum_{m=0}^{\infty} \epsilon_m \cos(m\theta_1)(-\mathrm{i})^p J_p(kr_1) \tag{6.1.11}$$

$$\phi_s = \frac{1}{i\omega}\sum_{n=0}^{\infty}\sum_{q=0}^{\infty}\sum_{p=0}^{\infty}\sum_{r=0}^{\infty} A_{nq} f_n(z)\epsilon_p\epsilon_r(-1)^q i^p e^{i\tau_{nq}x_{c1}}\cdots \\ \cos(p\theta_1)\cos(2r\theta_1)J_p(\tau_{nq}r_1)J_{2r}\left(\frac{\pi q}{c}r_1\right) \tag{6.1.12}$$

Continuity of the normal velocity We know that we must have at $r_1 = a_1$

$$\frac{\partial\phi_s}{\partial r_1} = \begin{cases} -\frac{\partial\phi_i}{\partial r_1} & -H \le z \le 0 \\ \frac{\partial\phi_s^1}{\partial r_1} & -1 \le z \le -H \end{cases} \tag{6.1.13}$$

Let us introduce the normal velocity U_m^1, $U_m^{P,1}$ and U_m^W respectively equal to

$$U_m^j = \sum_{n=0}^{\infty} B_{n,m}^j F_n(z)\Psi'_{n,m}(a_j) \tag{6.1.14a}$$

$$U_m^{P,j} = \left.\frac{\partial\phi_m^{P,j}}{\partial r_j}\right]_{r_j=a_j} \tag{6.1.14b}$$

$$U_m^{W,1} = \varepsilon_m(-\mathrm{i})^m k J'_m(ka_1)\frac{f_0(z)}{f_0(0)}e^{-ikx_{c1}} \tag{6.1.14c}$$

so that

$$\frac{\partial\phi_s^j}{\partial r_1} = \frac{1}{i\omega}\sum_{m=0}^{\infty}\cos(m\theta_j)\left(U_m^{P,j} + U_m^j\right) \tag{6.1.15a}$$

$$\frac{\partial\phi_i}{\partial r_1} = \frac{1}{i\omega}\sum_{m=0}^{\infty} U_m^{W,1}\cos(m\theta_1) \tag{6.1.15b}$$

Let us also introduce the following notation

$$\mathcal{G}_{n,q}^{r,p}(a_1) = \epsilon_p\epsilon_r(-1)^q i^p e^{i\tau_{nq}x_{c1}}\left(\tau_{np}J'_p(\tau_{np}a_1)J_{2r}\left(\frac{\pi q}{c}a_1\right) + \frac{\pi q}{c}J_p(\tau_{np}a_1)J'_{2r}\left(\frac{\pi q}{c}a_1\right)\right) \tag{6.1.16}$$

so that the normal derivative for (6.1.12) is given by:

$$\frac{\partial\phi_s}{\partial r_1} = \frac{1}{i\omega}\sum_{n=0}^{\infty}\sum_{q=0}^{\infty}\sum_{p=0}^{\infty}\sum_{r=0}^{\infty} A_{nq}\mathcal{G}_{n,q}^{r,p}(a_1)\cos(p\theta_1)\cos(2r\theta_1)f_n(z) \tag{6.1.17}$$

Combining (6.1.15) and (6.1.17), equation (6.1.13) can be written as

$$\sum_{n=0}^{\infty}\sum_{q=0}^{\infty}\sum_{p=0}^{\infty}\sum_{r=0}^{\infty} A_{nq}\mathcal{G}_{n,q}^{r,p}(a_1)\cos(p\theta_1)\cos(2r\theta_1)f_n(z) = \begin{cases} \sum_{m=0}^{\infty} U_m^{W,1}\cos(m\theta_1) & -H \le z \le 0 \\ \sum_{m=0}^{\infty}\left(U_m^1 + U_m^{P,1}\right)\cos(m\theta_1) & -1 \le z \le -H \end{cases} \tag{6.1.18}$$

Let us use the orthogonality of $\{f_n\}$, by taking the dot product of (6.1.18) with f_n. We get

$$\sum_{q=0}^{\infty}\sum_{p=0}^{\infty}\sum_{r=0}^{\infty} A_{nq}\mathcal{G}_{n,q}^{r,p}(a_1)\cos(p\theta_1)\cos(2r\theta_1) = \sum_{m=0}^{\infty}\left\langle U_m^{W,1}, f_n\right\rangle_{-H,0}\cos(m\theta_1) + \sum_{m=0}^{\infty}\left\langle U_m^1 + U_m^{P,1}, f_n\right\rangle_{-1,-H}\cos(m\theta_1) \tag{6.1.19}$$

We multiply by $\cos(M\theta)$ and integrate for $\theta \in [0,\pi]$. This lead to[1]

$$\sum_{q=0}^{\infty}\sum_{p=0}^{\infty}\sum_{r=0}^{\infty} A_{nq}\mathcal{G}_{n,q}^{r,p}(a_1)\,CC_1(p,2r,M) = \left\langle U_M^{W,1}, f_n\right\rangle_{-H,0}\frac{\pi}{\varepsilon_M} + \left\langle U_m^1 + U_m^{P,1}, f_n\right\rangle_{-1,-H}\frac{\pi}{\varepsilon_M} \tag{6.1.21}$$

We multiply now (6.1.14a) by f_n and integrate for $z \in [-1,-H]$ to obtain

$$\left\langle U_m^1, f_n\right\rangle_{-1,-H} = \sum_{p=0}^{\infty} B_{p,m}^1\Psi'_{p,m}(a_1)\left\langle F_p, f_n\right\rangle_{-1,-H} \tag{6.1.22}$$

[1]We keep the notation defined in chapter 5:

$$CC_1(p,2r,M) = \int_0^{\pi}\cos(p\theta)\cos(2r\theta)\cos(M\theta)d\theta \tag{6.1.20}$$

We can now substitute this expression into (6.1.21) to give,

$$\frac{\varepsilon_M}{\pi}\sum_{q=0}^{\infty}\sum_{p=0}^{\infty}\sum_{r=0}^{\infty}A_{nq}\mathcal{G}_{n,q}^{r,p}\left(a_1\right)CC_1\left(p,2r,M\right)-\sum_{p=0}^{\infty}B_{p,m}^{1}\Psi_{p,m}'(a_1)\left\langle F_p,f_n\right\rangle_{-1,-H}=\left\langle U_M^{W,1},f_n\right\rangle_{-H,0}+\left\langle U_m^{P,1},f_n\right\rangle_{-1,-H} \tag{6.1.23}$$

Continuity of the potential The continuity of the potential at the interface imposes that at $r_1 = a_1$

$$\phi_s = \phi_s^1, \quad z \in [-1, -H] \tag{6.1.24}$$

Let us introduce the notation:

$$\mathcal{D}_{n,q}^{r,p}(a_1) = \epsilon_p\epsilon_r(-1)^q i^p e^{i\tau_{nq}x_{c1}}J_p(\tau_{nq}a_1).J_{2r}\left(\frac{\pi q}{c}a_1\right) \tag{6.1.25}$$

Thus we equate (6.1.12) and (6.1.8) and take the dot product with F_n. Using the orthogonality of F_n's property we have:

$$\sum_{m=0}^{\infty}\cos\left(m\theta_1\right)\left(\left\langle\phi_m^{P,1},F_N\right\rangle_{-1,-H}+B_{N,m}^{1}\Psi_{N,m}(a_1)\right)=\sum_{n=0}^{\infty}\sum_{q=0}^{\infty}\sum_{p=0}^{\infty}\sum_{r=0}^{\infty}A_{nq}\mathcal{D}_{n,q}^{r,p}(a_1)\cos(p\theta_1)\cos(2r\theta_1)\left\langle f_n,F_N\right\rangle_{-1,-H} \tag{6.1.26}$$

We multiply by $\cos(M\theta)$ and integrate for $\theta \in [0, \pi]$:

$$\frac{\varepsilon_M}{\pi}\sum_{n=0}^{\infty}\sum_{q=0}^{\infty}\sum_{p=0}^{\infty}\sum_{r=0}^{\infty}\left(A_{nq}\mathcal{D}_{n,q}^{r,p}(a_1)\left\langle p,2r,M\right\rangle\left\langle_{0,\pi}f_n,F_N\right\rangle_{-1,-H}\right)-B_{N,M}^{1}\Psi_{N,M}(a_1)=\left\langle\phi_M^{P,1},F_N\right\rangle_{-1,-H} \tag{6.1.27}$$

Matching outer domain and domain 2 Continuity of the radial flux and the potential at the interface between the outer domain and the domain 2 must be assured. In the polar coordinate of cylinder 2 this interface is defined by $r_2 = a_2$ and $\theta_2 \in$

$[-\pi/2, 0]$ and the outer potential is given:

$$\phi_s = -\frac{1}{i\omega}\sum_{n=0}^{\infty} f_n(z) \sum_{q=0}^{\infty}\sum_{p=0}^{\infty}\sum_{r=0}^{\infty} A_{nq}\epsilon_p\epsilon_r(-1)^q i^p \cos(p\theta_2)\cos(2r\theta_2)J_p(\tau_{nq}r_2)J_{2r}\left(\frac{\pi q}{c}r_2\right) \tag{6.1.28}$$

$$\phi_i = \frac{1}{\mathrm{i}\omega}\frac{f_0(z)}{f_0(0)}\sum_{m=0}^{\infty}\varepsilon_m \cos(m\theta_2)(-\mathrm{i})^p J_p(kr_2) \tag{6.1.29}$$

In particular

$$\frac{\partial\phi_s}{\partial r_2}(a_2) = \frac{1}{i\omega}\sum_{n=0}^{\infty}\sum_{q=0}^{\infty}\sum_{p=0}^{\infty}\sum_{r=0}^{\infty} A_{nq}\mathcal{E}_{n,q}^{r,p}(a_2)\cos(p\theta_2)\cos(2r\theta_2)f_n(z) \tag{6.1.30}$$

with

$$\mathcal{E}_{n,q}^{r,p}(a_2) = \epsilon_p\epsilon_r(-1)^q i^p\left(\tau_{np}J_p'(\tau_{np}a_2)J_{2r}\left(\frac{\pi q}{c}a_2\right) + \frac{\pi q}{c}J_p(\tau_{np}a_2)J_{2r}'\left(\frac{\pi q}{c}a_2\right)\right) \tag{6.1.31}$$

Let us denote

$$U_m^{W,2} = \varepsilon_m(-\mathrm{i})^m k J_m'(ka_2)\frac{f_0(z)}{f_0(0)} \tag{6.1.32}$$

Continuity of the normal velocity We must have:

$$\frac{\partial\phi_s}{\partial r_2} = \begin{cases} -\frac{\partial\phi_i}{\partial r_2} & -H \le z \le 0 \\ \frac{\partial\phi_s^2}{\partial r_2} & -1 \le z \le -H \end{cases} \tag{6.1.33}$$

Using (6.1.30), (6.1.14a) and (6.1.14b), the previous condition imposes:

$$\sum_{n=0}^{\infty}\sum_{q=0}^{\infty}\sum_{p=0}^{\infty}\sum_{r=0}^{\infty} A_{nq}\mathcal{E}_{n,q}^{r,p}(a_2)\cos(p\theta_2)\cos(2r\theta_2)f_n(z) = \begin{cases} \sum_{m=0}^{\infty} U_m^{W,2}\cos(m\theta_2) & -H \le z \le 0 \\ \sum_{m=0}^{\infty}\left(U_m^2 + U_m^{P,2}\right)\cos(m\theta_2) & -1 \le z \le -H \end{cases} \tag{6.1.34}$$

As in the matching of the domain 1 with the outer domain, we multiply both side of the equality by f_n, integrate between -1 and 0 and make use of the orthogonality property of the $\{f_n\}$. Then we multiply by $\cos(M\theta_2)$ and integrate for $\theta_2 \in [-\pi/2, 0]$.

Unfortunatly orthogonality property is no longer available for this intergation. These steps lead to the result:

$$\begin{aligned}&\sum_{q=0}^{\infty}\sum_{p=0}^{\infty}\sum_{r=0}^{\infty} A_{nq}\mathcal{E}_{n,q}^{r,p}\left(a_2\right) CC_2\left(p,2r,M\right) = \\ &\sum_{m=0}^{\infty}\left\langle U_m^W, f_n\right\rangle_{-H,0}\mathcal{C}(m,M) + \sum_{m=0}^{\infty}\left\langle U_m^2 + U_m^{P,2}, f_n\right\rangle_{-1,-H}\mathcal{C}(m,M)\end{aligned} \tag{6.1.35}$$

The scalar product can be replaced by the expression given in (6.1.22), where we only need to change the superscript 1 to 2. This gives

$$\begin{aligned}&\sum_{q=0}^{\infty}\sum_{p=0}^{\infty}\sum_{r=0}^{\infty} A_{nq}\mathcal{E}_{n,q}^{r,p}\left(a_2\right) CC_2\left(p,2r,M\right) \\ &\qquad - \sum_{m=0}^{\infty}\sum_{p=0}^{\infty} B_{p,m}^1\Psi'_{p,m}(a_1)\left\langle F_p, f_n\right\rangle_{-1,-H}\mathcal{C}(m,M) \\ &\qquad\qquad = \sum_{m=0}^{\infty}\left\langle U_m^W + U_m^{P,2}, f_n\right\rangle_{-H,0}\mathcal{C}(m,M)\end{aligned} \tag{6.1.36}$$

Continuity of the potential At $r_2 = a_2$ we must impose

$$\phi_s = \phi_s^2, \quad z \in [-1,-H] \tag{6.1.37}$$

Let us introduce the notation

$$\mathcal{F}_{n,q}^{r,p}(a_2) = \epsilon_p\epsilon_r(-1)^q i^p J_p(\tau_{nq}a_2)J_{2r}\left(\frac{\pi q}{c}a_2\right) \tag{6.1.38}$$

The previous condition becomes

$$\begin{aligned}&\sum_{n=0}^{\infty}\sum_{q=0}^{\infty}\sum_{p=0}^{\infty}\sum_{r=0}^{\infty} A_{nq}\mathcal{F}_{n,q}^{r,p}(a_2)\cos(p\theta_2)\cos(2r\theta_2)f_n(z) = \\ &\qquad \sum_{m=0}^{\infty}\cos\left(m\theta_2\right)\left(\phi_m^{P,2} + \sum_{n}^{\infty} B_{n,m}^2\Psi_{n,m}(a_2)F_n(z)\right)\end{aligned} \tag{6.1.39}$$

As we did for cylinder 1, we multiply both side of the previsous equation by F_n and make use of their orthogonality property. Then we multiply by $\cos(M\theta)$ and integrate for $\theta_2 \in [-\pi/2, 0]$. We get

$$\sum_{n=0}^{\infty}\sum_{q=0}^{\infty}\sum_{p=0}^{\infty}\sum_{r=0}^{\infty} A_{nq}\mathcal{F}_{n,q}^{r,p}(a_2)CC_2(p,2r,M)\left\langle f_n, F_N\right\rangle_{-1,-H} = \sum_{m=0}^{\infty}\mathcal{C}(m,M)\left(\left\langle \phi_m^{P,2}, F_N\right\rangle_{-1,-H} + \sum_{n}^{\infty} B_{n,m}^2\Psi_{n,m}(a_2)\right) \quad (6.1.40)$$

Summary of the equations Let us summarize the results we have obtain so far. The unknown coefficients A_{nq}, $B_{n,m}^j$ are solution of the following linear infinite system of equations given by (6.1.7), (6.1.23), (6.1.27), (6.1.36) and (6.1.40) :

$$\forall n, M, \quad \sum_{q=0}^{\infty}\alpha_{nq}\tau_{nq}\langle V_q, V_M\rangle_{-c,c-a_2} = \frac{k}{f_0(0)}\delta_{n,0}\langle 1, V_M\rangle_{-c,c-a_2} \quad (6.1.41)$$

$$\frac{\varepsilon_M}{\pi}\sum_{q=0}^{\infty}\sum_{p=0}^{\infty}\sum_{r=0}^{\infty} A_{nq}\mathcal{G}_{n,q}^{r,p}(a_1)\,CC_1(p,2r,M) - \sum_{p=0}^{\infty} B_{p,m}^1\Psi'_{p,m}(a_1)\left\langle F_p, f_n\right\rangle_{-1,-H} = \left\langle U_M^{W,1}, f_n\right\rangle_{-H,0} + \left\langle U_m^{P,1}, f_n\right\rangle_{-1,-H} \quad (6.1.42)$$

$$\frac{\varepsilon_M}{\pi}\sum_{n=0}^{\infty}\sum_{q=0}^{\infty}\sum_{p=0}^{\infty}\sum_{r=0}^{\infty}\left(A_{nq}\mathcal{D}_{n,q}^{r,p}(a_1)CC_1(p,2r,M)\left\langle f_n, F_N\right\rangle_{-1,-H}\right) - B_{N,M}^1\Psi_{N,M}(a_1) = \left\langle \phi_M^{P,1}, F_N\right\rangle_{-1,-H} \quad (6.1.43)$$

$$\sum_{q=0}^{\infty}\sum_{p=0}^{\infty}\sum_{r=0}^{\infty} A_{nq}\mathcal{E}_{n,q}^{r,p}(a_2)\,CC_2(p,2r,M) - \sum_{m=0}^{\infty}\sum_{p=0}^{\infty} B_{p,m}^1\Psi'_{p,m}(a_1)\left\langle F_p, f_n\right\rangle_{-1,-H}\mathcal{C}(m,M) = \sum_{m=0}^{\infty}\left\langle U_m^W + U_m^{P,2}, f_n\right\rangle_{-H,0}\mathcal{C}(m,M) \quad (6.1.44)$$

$$\sum_{n=0}^{\infty}\sum_{q=0}^{\infty}\sum_{p=0}^{\infty}\sum_{r=0}^{\infty} A_{nq}\mathcal{F}_{n,q}^{r,p}(a_2)CC_2\left(p,2r,M\right)\left\langle f_n,F_N\right\rangle_{-1,-H} =$$

$$\sum_{m=0}^{\infty}\left\langle m,M\right\rangle_{-\pi/2,0}\left(\left\langle \phi_m^{P,2},F_N\right\rangle_{-1,-H}+\sum_{n}^{\infty}B_{n,m}^{2}\Psi_{n,m}(a_2)\right) \quad (6.1.45)$$

6.1.2 Antisymmetric problem

Let us now consider a pair of incident waves, where the first arrives from $x=+\infty$ with amplitude A_0 and the second from $x=-\infty$ with amplitude $-A_0$. The problem defined earlier by (6.1.1) remains unchanged except the boundary condition (6.1.1f) which is replaced by

$$\phi=0, \quad x=0, y\in[-c,c-a_2] \quad (6.1.46)$$

We look again for solution of the form 6.1.8 inside and of the form 6.1.3 outside. The boundary condition 6.1.46 and the scalar product in z and y give

$$\sum_{q=0}^{\infty}A_{nq}\left\langle V_q,V_M\right\rangle_{-c,-c-a_2}=0 \quad (6.1.47)$$

The calculation to match the potential and the normal velocity at the interfaces between the domains are identical to those of the previous section. Thus the unknown coefficients A_{nq} and $B_{n,m}^{j}$ are solution of the infinite linear system defined by (6.1.42), (6.1.43), (6.1.44) and (6.1.45) and (6.1.47).

6.2 Radiation problem

Let us now solve the radiation problem. The flow induced by the heaving movement of the buoy, is proportionnal to the velocity of the buoy $\dot{\zeta}$: $\phi=\phi_r\dot{\zeta}$. We shall use the following dimensioneless variable for the potential:

$$\phi_r=h\phi_r^* \quad (6.2.1)$$

6.2.1 Symmetric problem

With dimensioneless variables the equations for the flow are:

$$\Delta\phi = 0, \qquad \boldsymbol{x} \in \Omega_f \tag{6.2.2a}$$

$$\frac{\partial\phi}{\partial z} - \omega^2\phi = 0, \qquad \text{at} \quad S_f \tag{6.2.2b}$$

$$\frac{\partial\phi}{\partial z} = 0, \qquad z = -1 \tag{6.2.2c}$$

$$\frac{\partial\phi}{\partial y} = 0, \qquad \text{on} \quad S_c \tag{6.2.2d}$$

$$\frac{\partial\phi}{\partial z} = 1, \qquad \text{on} \quad S_{B_j} \tag{6.2.2e}$$

$$\frac{\partial\phi}{\partial r} = 0, \qquad \text{on} \quad S_{L_j} \tag{6.2.2f}$$

$$\frac{\partial\phi}{\partial x} = 0, \qquad \text{on} \quad S_0 \tag{6.2.2g}$$

$$\phi \quad \text{outgoing at} \quad +\infty \tag{6.2.2h}$$

We divide again the fluid domain into three subdomains identical to those defined for the scattering problem. For the outer domain we look for a solution of the form:

$$\phi_r = \sum_{n=0}^{\infty}\sum_{q=0}^{\infty} \alpha_{nq} e^{i\tau_{nq}x} V_q(y) f_n(z) \tag{6.2.3}$$

where V_q, τ_{nq} and f_n defined as previously. For the domains under the buoys, we follow Garnaud (2009) and look for a solution of the form:

$$\phi_r^j = \phi_r^{P,j} + \sum_{n=0}^{\infty} \beta_n^j F_n(z) \psi_{n,0}(r_j) \tag{6.2.4}$$

where $\phi_r^{P,j}$ is a particular solution of (6.2.2) defined by

$$\phi_r^{P,j} = \frac{1}{2(1-H)}\left((z+1)^2 - \frac{r_j^2}{2}\right) \tag{6.2.5}$$

We shall now apply the boundary condition (6.2.2g) and match the potential and the radial flux at the interfaces between the domains.

Boundary condition on S_0. We plug (6.2.3) into (6.2.2g), use the orthogonality property of the vertical eigenfunctions and then the scalar product in y. We get:

$$\sum_{q=0}^{\infty} \alpha_{nq}\tau_{nq} \langle V_q, V_M \rangle_{-c,c-a_2} = 0 \quad \forall\ M \tag{6.2.6}$$

Matching domain 1 and outer domain. As for the scattering problem, we express the outer potential in the local polar coordinate of cylinder 1:

$$\begin{aligned}\phi_r = \sum_{n=0}^{\infty}\sum_{q=0}^{\infty}\sum_{p=0}^{\infty}\sum_{r=0}^{\infty} \alpha_{nq} f_n(z)\epsilon_p\epsilon_r(-1)^q i^p e^{i\tau_{nq}x_{c1}} \ldots \\ \cos(p\theta_1)\cos(2r\theta_1) J_p(\tau_{nq}r_1) J_{2r}\left(\frac{\pi q}{c} r_1\right)\end{aligned} \tag{6.2.7}$$

Equaling the radial flux and taking the scalar product in z gives

$$\begin{aligned}\sum_{q=0}^{\infty}\sum_{p=0}^{\infty}\sum_{r=0}^{\infty} \alpha_{nq}\mathcal{G}_{n,q}^{r,p}(a_1)\cos(p\theta_1)\cos(2r\theta_1) = \\ \left\langle \frac{\partial \phi_r^{P,1}}{\partial r_1}(a_1), f_n \right\rangle_{-1,-H} + \sum_{n=0}^{\infty} \beta_n^1 \psi'_{n,0}(a_1) \langle F_n, f_n \rangle_{-1,-H}\end{aligned} \tag{6.2.8}$$

where $\mathcal{G}_{n,q}^{r,p}$ is defined by (6.1.16). We multiply by $\cos(M\theta)$ and integrate between 0 and π. We get finally:

$$\begin{aligned}\sum_{q=0}^{\infty}\sum_{p=0}^{\infty}\sum_{r=0}^{\infty} \alpha_{nq}\mathcal{G}_{n,q}^{r,p}(a_1)\langle p, 2r, M\rangle_{0,\pi} = \\ \delta_{M0}\pi\left\{\left\langle \frac{\partial \phi_r^{P,1}}{\partial r_1}(a_1), f_n \right\rangle_{-1,-H} + \sum_{n=0}^{\infty} \beta_n^1 \psi'_{n,0}(a_1)\langle F_n, f_n\rangle_{-1,-H}\right\}\end{aligned} \tag{6.2.9}$$

Let us now equate the potentials given by (6.2.4) and (6.2.7) and take the dot product with F_n. Using the orthogonality property of $\{F_n\}$ we have:

$$\begin{aligned}\sum_{n=0}^{\infty}\sum_{q=0}^{\infty}\sum_{p=0}^{\infty}\sum_{r=0}^{\infty} \alpha_{nq}\mathcal{D}_{n,q}^{r,p}(a_1)\cos(p\theta_1)\cos(2r\theta_1)\langle f_n, F_N\rangle_{-1,-H} = \\ \phi_r^{P,1}(a_1) + \beta_N^j \psi_{N,0}(a_1)\end{aligned} \tag{6.2.10}$$

where $\mathcal{D}_{n,q}^{r,p}$ is defined by (6.1.25). We next multiply by $\cos(M\theta)$ and integrate between 0 and π. We get finally:

$$\sum_{n=0}^{\infty}\sum_{q=0}^{\infty}\sum_{p=0}^{\infty}\sum_{r=0}^{\infty}\alpha_{nq}\mathcal{D}_{n,q}^{r,p}(a_1)CC_1\left(p,2r,M\right)\left\langle f_n,F_N\right\rangle_{-1,-H}=$$
$$\delta_{M0}\pi\left\{\left\langle\phi_r^{P,1}(a_1),F_N\right\rangle_{-1,-H}+\beta_N^1\psi_{N,0}(a_1)\right\} \tag{6.2.11}$$

Matching domain 2 and the outer domain. In the polar system of cylinder 2, the outer potential is given by

$$\phi_r=\sum_{n=0}^{\infty}f_n(z)\sum_{q=0}^{\infty}\sum_{p=0}^{\infty}\sum_{r=0}^{\infty}\alpha_{nq}\epsilon_p\epsilon_r(-1)^q i^p\cos(p\theta_2)\cos(2r\theta_2)J_p(\tau_{nq}r_2)J_{2r}\left(\frac{\pi q}{c}r_2\right) \tag{6.2.12}$$

Following the same method as before, we equate the radial flux, take the scalar product in z and make use of the orthogonality property of $\{f_n\}$. Then we multiply by $\cos(M\theta_2)$ and integrate for $\theta_2\in[-\pi/2,0]$. These steps lead to the result:

$$\sum_{q=0}^{\infty}\sum_{p=0}^{\infty}\sum_{r=0}^{\infty}\alpha_{nq}\mathcal{E}_{n,q}^{r,p}\left(a_2\right)CC_2\left(p,2r,M\right)=$$
$$\left\{\left\langle\frac{\partial\phi_r^{P,2}}{\partial r_1}(a_2),f_n\right\rangle_{-1,-H}+\sum_{n=0}^{\infty}\beta_n^2\psi'_{n,0}(a_2)\left\langle F_n,f_n\right\rangle_{-1,-H}\right\}\int_{-\pi/2}^{0}\cos\left(M\theta\right)\ \mathrm{d}\theta \tag{6.2.13}$$

where $\mathcal{E}_{n,q}^{r,p}\left(a_2\right)$ has been defined in (6.1.31).

We now equate the potentials given by (6.2.12) and (6.2.4). Again the scalar product with F_n is taken and the orthogonality property is used. Then we multiply by $\cos(M\theta_2)$ and integrate for $\theta_2\in[-\pi/2,0]$. We obtain for any M

$$\sum_{n=0}^{\infty}\sum_{q=0}^{\infty}\sum_{p=0}^{\infty}\sum_{r=0}^{\infty}\alpha_{nq}\mathcal{F}_{n,q}^{r,p}(a_2)CC_2\left(p,2r,M\right)\left\langle f_n,F_N\right\rangle_{-1,-H}=$$
$$\left\{\left\langle\phi_r^{P,2}(a_2),F_N\right\rangle_{-1,-H}+\beta_N^2\psi_{N,0}(a_2)\right\}\int_{-\pi/2}^{0}\cos\left(M\theta\right)\ \mathrm{d}\theta \tag{6.2.14}$$

where $\mathcal{F}_{n,q}^{r,p}$ has been defined in (6.1.38)

Summary of the equations. The unkonwn coefficients α_{nq} and β_n^j are solution of an infinite linear system of equation defined by (6.2.6), (6.2.9), (6.2.11), (6.2.13) and (6.2.14). This system must be truncated to be solve numerically. However we expect also computation difficulties, similar to the one we encountered for the cylinders extending to the bottom. Completion of the numerical task is left for the futur.

Chapter 7

Conclusions

In the forst part we have developed a general linear theory for an ocillating water column at the tip of a wedge-like coast of arbitrary apex angle. Numerical computations have been performed for two coastlines shaped as right-angle corners: one convex and one concave.

It has been found that the angle of incidence has some strong influence on the total vertical flux across the chamber surface and thus on the capture length, more so on the convex corner than on the concave corner. The influence of other parameters on the performance of the system has also been examined.

Our numerical simulations have been compared to the known situation of a thin breakwater and a straight coastline. It has been found that the most efficient configuration for energy extraction is the the concave corner, where all the incident wave energy is channeled to focus at the OWC.

Two strategies to optimize the energy extraction rate have been examined. We first assume a controllable multiple-turbine system which can be optimized over a wide range of frequencies. However in practice it may be difficult to adapt the turbine system for many frequencies. We have thus developed a simpler way of optimization, where the turbine parameter takes only two different values. Our comparison shows that the simpler scheme can achieve almost as high an efficiency as the idealized many-frequency optimization.

In the second part, we have formulated the problem of one or two cylinders or

buoys in a channel. Computational difficulties are discussed and firther investigation is needed to complete the numerical task.

Appendix A

Diffraction by a solid circular cylinder at the tip of a wedge

The theory of diffraction by a solid circular cylinder at the tip of a wedge in three dimension has been done by Martin-Rivas and Mei (2008), by extending the method of Stoker (1958) for the two-dimensional diffraction by a semi infinite screen. For convenience we describe here a circular cylinder of radius a, centered at the tip of a wedge of angle ν. The solid part of the wedge is comprised between $\theta = \nu\pi$ and $\theta = 2\pi$, for $r > a$ and the water occupies the region between $\theta = 0$ and $\theta = \nu\pi$ as represented on figure A-1. The depth is assumed constant and equal to h. Let us

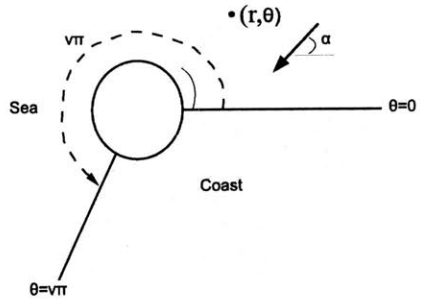

Figure A-1: Cylinder at the tip of a wedge

consider an incident plane wave, arriving from infinity with an angle α with respect

to the x axis ($\theta = 0$). The problem is the following:

$$\nabla^2 \varphi = 0 \tag{A.0.1a}$$

$$\frac{\partial \varphi}{\partial z} = 0 \quad \text{at} \quad z = -h \tag{A.0.1b}$$

$$\frac{\partial \varphi}{\partial z} - \frac{\omega^2}{g}\varphi = 0 \quad \text{at} \quad z = 0 \tag{A.0.1c}$$

$$\frac{\partial \varphi}{\partial \theta} = 0 \quad \text{for} \quad \theta = 2\pi, \nu\pi \quad \text{and} \quad r > a \tag{A.0.1d}$$

$$\frac{\partial \varphi}{\partial r} = 0 \quad \text{for} \quad r = a, \quad 0 \leq \theta \leq \nu\pi \tag{A.0.1e}$$

(A.0.1f)

We also imposed that the scattered potential is outgoing at infinity

$$\sqrt{r}\left(\frac{\partial \varphi^S}{\partial r} - ik\varphi^S\right) \to 0 \quad \text{as} \quad kr \to \infty \tag{A.0.2}$$

The velocity potential can be written as

$$\varphi(r, \theta, z) = -\frac{igA_0}{\omega}\eta(r, \theta)\frac{\cosh k(z + h)}{\cosh(kh)} \tag{A.0.3}$$

where the normalized free-surface displacement η satisfies the Helmotz equation

$$\nabla^2 \eta + k^2 \eta = 0 \tag{A.0.4}$$

We expand η in Fourier serie

$$\eta(r, \theta) = \frac{1}{\nu\pi}\tilde{\eta}_0(r) + \frac{2}{\nu\pi}\sum_{n=1}^{\infty}\tilde{\eta}_n(r)\cos\left(\frac{n\theta}{\nu}\right) \tag{A.0.5}$$

where $\tilde{\eta}_n(r)$ is the Fourier expansion coefficient of η defined by

$$\tilde{\eta}_n(r, \nu) = \int_0^{\nu\pi} \eta(r, \theta)\cos\left(\frac{n\theta}{\nu}\right) d\theta \tag{A.0.6}$$

All the coefficient of the sinus are equal to zero because η must satisfy the no-flux boundary condition at $\theta = 0$ and $\theta = \nu\pi$:

$$\frac{\partial \eta}{\partial \theta} = -\frac{2}{\nu\pi r}\sum_{n=1}^{\infty}\tilde{\eta}_n(r)\frac{n}{\nu}\sin\left(\frac{n\theta}{\nu}\right) = 0 \quad \text{for} \quad \theta = 0 \quad \text{and} \quad \theta = \nu\pi \tag{A.0.7}$$

From (A.0.4) it follows that Fourier coefficients of η must satisfy the Bessel differential equation

$$r^2\frac{d^2\tilde{\eta}_n}{dr^2} + r\frac{d\tilde{\eta}_n}{dr} + \left(k^2r^2 - \frac{n^2}{\nu^2}\right)\tilde{\eta}_n = 0, \quad r > a \tag{A.0.8}$$

Since the potential must satisfied the boundary condition on the cylinder given by (A.0.1e), each Fourier coefficient must satisfy it too. Thus the solution of the previous equation must be of the form

$$\tilde{\eta}_n(r) = a_n\left(J_{n/\nu}(kr) - \frac{J'_{n/\nu}(ka)}{Y'_{n/\nu}(ka)}Y_{n/\nu}(kr)\right) \tag{A.0.9}$$

where a_n are unknown coefficients.

The total potential φ is the sum of the incident potential φ^I and the scattered potential φ^S, thus in term of Fourier coefficient we can write:

$$\tilde{\eta}_n^S = \tilde{\eta}_n - \tilde{\eta}_n^I = \tilde{\eta}_n - \int_0^{\nu\pi}\eta^I(r,\theta)\cos\left(\frac{n\theta}{\nu}\right)d\theta \tag{A.0.10}$$

Each Fourier coefficient of the scattered potential must satisfy the radiation condition (A.0.2):

$$\sqrt{r}\left(\frac{\partial\tilde{\eta}_n^S}{\partial r} - ik\tilde{\eta}_n^S\right) \to 0 \quad \text{as} \quad kr \to \infty \tag{A.0.11}$$

With the two previous equations we have, for large kr

$$\sqrt{r}\left(\frac{\partial\tilde{\eta}_n^I}{\partial r} - ik\tilde{\eta}_n^I\right) \approx \sqrt{r}\left(\frac{\partial\tilde{\eta}_n}{\partial r} - ik\tilde{\eta}_n\right) \tag{A.0.12}$$

Let us now evaluate each side of this equality. Using the asymptotic expression of

Bessel functions, it follows from (A.0.9) that for large kr

$$\sqrt{r}\left(\frac{\partial\tilde{\eta}_n}{\partial r}-ik\tilde{\eta}_n\right)\ a_n\sqrt{\frac{2k}{\pi}}e^{-i(kr-n\pi/2\nu)}\left(e^{-i\pi/4}-e^{i\pi/4}\frac{J'_{n/\nu}(ka)}{Y'_{n/\nu}(ka)}\right) \tag{A.0.13}$$

For a plane incident wave from angle α with respect to the x axis, $\eta^I = e^{ikrcos(\theta-\alpha)}$. From the method of stationnary phase we obtain

$$\sqrt{r}\left(\frac{\partial\tilde{\eta}^I_n}{\partial r}-ik\tilde{\eta}^I_n\right)=\sqrt{r}\left(\frac{\partial}{\partial r}-ik\right)\tilde{\eta}^I_n\int_0^{\nu\pi}e^{ikrcos(\theta-\alpha)}\cos\frac{n\theta}{\nu}d\theta\approx 2\sqrt{2\pi k}\cos(n\alpha/\nu)e^{-i(kr+\pi/4)} \tag{A.0.14}$$

Equating the two previous asymptotic expression leads to

$$a_n\sqrt{\frac{2k}{\pi}}e^{-i(kr-n\pi/2\nu)}\left(e^{-i\pi/4}-e^{i\pi/4}\frac{J'_{n/\nu}(ka)}{Y'_{n/\nu}(ka)}\right)=2\sqrt{2\pi k}\cos(n\alpha/\nu)e^{-i(kr+\pi/4)} \tag{A.0.15}$$

It follows that

$$a_n=\frac{2\pi\cos(n\alpha/nu)e^{\frac{-in\pi}{2\nu}}Y'_{n/\nu}(ka)}{Y'_{n/\nu}(ka)-e^{i\pi/2}J'_{n/\nu}(ka)}=\frac{2i\pi\cos(n\alpha/nu)e^{\frac{-in\pi}{2\nu}}Y'_{n/\nu}(ka)}{H'_{n/\nu}(ka)} \tag{A.0.16}$$

where $H_{n/\nu}=H^1_{n/\nu}$. Finally the exact solution is

$$\eta=\sum_{n=0}^{\infty}\frac{\epsilon_n}{\nu\pi}\frac{2i\pi\cos(n\alpha/nu)e^{\frac{-in\pi}{2\nu}}Y'_{n/\nu}(ka)}{H'_{n/\nu}(ka)}\left(J_{n/\nu}(kr)-\frac{J'_{n/\nu}(ka)}{Y'_{n/\nu}(ka)}Y_{n/\nu}(kr)\right)\cos(n\theta\nu) \tag{A.0.17}$$

Appendix B

Numerical simulation

The linear infinite system of equations given by equations (2.2.45) and (2.3.22) must be solved with numerical computations. Two programs have been built to solve the diffraction and the radiation problems. The systems are solved by truncating the infinite series. Thus an important feature is the rate of convergence of each quantity (physical variables as damping coefficient, but also coefficients as A_{nl}, B_{nl}...). This study aims at finding the number of terms required to approximate the infinite series with a satisfying accuracy in a reasonnable time of computation. Afterwards our programs have been tested with limiting cases and known identities (energy conservation and reciprocal relation). Each test is presented in the second section. The study of the convergence, as well as the tests have been done for the case of a wedge making a right angle, that is $\nu = 3/2$.

B.1 Convergence

We will use for (3.2.1):

$$\varphi_C = -\frac{iP}{\rho\omega}\sum_{n=0}^{Nt}\sum_{l=0}^{Nl} D_{nl}\frac{I_n(k_l r)}{k_l a I_n'(k_l a)}\cos\left[n\left(\theta-\frac{3\pi}{4}\right)\right]Z_l(z) - \frac{iP}{\rho\omega} \qquad \text{(B.1.1)}$$

or for (3.2.5)

$$U(\theta, z) = \frac{-iPh}{\rho\omega} \sum_{m=0}^{Nm} \sum_{p=0}^{Np} \alpha_{mp} v_m(\theta) u_p(z) \tag{B.1.2}$$

Table B.1 presents the convergence of some coefficients in a test case when the number N_l of terms in the sum over eigenfunctions increases and table B.2 presents the relative error in percent. We see that a large number of terms is needed to get a satisfying

N_l	$\|A00\|$	$\|B01\|$	$\|C20\|$	$\|\eta/A_0\|$	$\|\Gamma\|$
200	0.321255	0.039874	0.033741	0.626502	3.108079
400	0.320445	0.039894	0.033782	0.625236	3.101798
600	0.320177	0.0399	0.033796	0.624816	3.099715
800	0.320043	0.039903	0.033803	0.624607	3.098676
1000	0.319963	0.039905	0.033807	0.624481	3.098053
1200	0.319909	0.039907	0.033809	0.624397	3.097638
1400	0.319871	0.039908	0.033811	0.624338	3.097341
1600	0.319842	0.039908	0.033813	0.624293	3.097119

Table B.1: Convergence of different coefficients as N_l increases. $\alpha = 0.1\pi$, $h/a = 2$, $d/a = 0.4$, $ka = 1.09$, $N_p = 3$, $N_m = 5$ and $N_t = 5$

accuracy. This is due to the fact that the flux has a discontinuity at $r = a$ and $z = -d$ whereas the eigenfunctions are continuous. However this is not restrictive since the computation time is not very long even for a very large number N_l. Table

N_l	$\|A00\|$	$\|B01\|$	$\|C20\|$	$\|\eta/A_0\|$	$\|\Gamma\|$
400	8.1E-04	2.0E-05	4.1E-05	1.3E-03	6.3E-03
600	2.7E-04	6.0E-06	1.4E-05	4.2E-04	2.1E-03
800	1.3E-04	3.0E-06	7.0E-06	2.1E-04	1.0E-03
1000	8.0E-05	2.0E-06	4.0E-06	1.3E-04	6.2E-04
1200	5.4E-05	2.0E-06	2.0E-06	8.4E-05	4.2E-04
1400	3.8E-05	1.0E-06	2.0E-06	5.9E-05	3.0E-04
1600	2.9E-05	0.0E+00	2.0E-06	4.5E-05	2.2E-04

Table B.2: Absolute error of different coefficients as N_l increases. $\alpha = 0.1\pi$, $h/a = 2$, $d/a = 0.4$, $ka = 1.09$, $N_p = 3$, $N_m = 5$ and $N_t = 5$

B.3 gives now the convergence of the same coefficients when the number N_p of terms $u_p(z)$ in the expansion for U increases. Table B.4 presents the absolute error between two consecutive terms. We can see that we only need a few term to get a excellent accuracy. In addition, the computation time is very fast as N_p increases. We took

$N_p = 5$ in our simulations. Now table B.5 gives now the convergence of the same

N_p	$\|A00\|$	$\|B01\|$	$\|C20\|$	$\|\eta/A_0\|$	$\|\Gamma\|$
2	0.319401	0.039408	0.033907	0.624976	3.100506
3	0.319856	0.039908	0.033812	0.624314	3.097223
4	0.319858	0.039909	0.033813	0.624322	3.097262
5	0.319858	0.039909	0.033813	0.624322	3.097263

Table B.3: Convergence of different coefficients as N_p increases. $\alpha = 0.1\pi$, $h/a = 2$, $d/a = 0.4$, $ka = 1.09$, $N_l = 1500$, $N_m = 5$ and $N_t = 5$

N_p	$\|A00\|$	$\|B01\|$	$\|C20\|$	$\|\eta/A_0\|$	$\|\Gamma\|$
3	4.55E-04	5.00E-04	9.50E-05	6.62E-04	3.28E-03
4	2.00E-06	1.00E-06	1.00E-06	8.00E-06	3.90E-05
5	0.00	0.00	0.00	0.00	1.00E-06

Table B.4: Absolute error of different coefficients as N_p increases of 1. $\alpha = 0.1\pi$, $h/a = 2$, $d/a = 0.4$, $ka = 1.09$, $N_l = 1500$, $N_m = 5$ and $N_t = 5$

coefficients when the number N_m of terms $v_m(z)$ in the expansion for U increases and table B.6 gives the absolute error between two consecutive terms. As in the case for the index p, the convergence is excellent and extremely fast. We only need 4 terms.

N_m	$\|A00\|$	$\|B01\|$	$\|C20\|$	$\|\eta/A_0\|$	$\|\Gamma\|$
2	0.611658	0.10657	0.458743	0.079927	0.372522
3	0.622723	0.110924	0.467042	0.083193	0.205379
4	0.622723	0.110924	0.467042	0.083193	0.204925

Table B.5: Convergence of different coefficients as N_m increases. $\alpha = 0.1\pi$, $h/a = 2$, $d/a = 0.4$, $ka = 1.09$, $N_l = 1500$, $N_p = 3$ and $N_t = 5$

And finally table B.7 presents now the convergence of the same coefficients when the number N_t of terms $\cos(n\theta)$ and $\sin(n\theta)$ in the expression of the potentials increases and table B.8 presents the absolute error between two consecutive terms. We can see that we need around 40 terms to get a satisfying accuracy.

N_m	$\|A00\|$	$\|B01\|$	$\|C20\|$	$\|\eta/A_0\|$	$\|\Gamma\|$
3	1.11E-02	4.35E-03	8.30E-03	3.27E-03	1.67E-01
4	0.00	0.00	0.00	0.00	4.54E-04

Table B.6: Absolute error of different coefficients as N_m increases of 1. $\alpha = 0.1\pi$, $h/a = 2$, $d/a = 0.4$, $ka = 1.09$, $N_l = 1500$, $N_p = 3$ and $N_t = 5$

N_t	$\|A00\|$	$\|B01\|$	$\|C20\|$	$\|\eta/A_0\|$	$\|\Gamma\|$
10	0.314349	0.052736	0.235762	0.039552	0.033232
20	0.312912	0.052636	0.234684	0.039477	0.033201
30	0.312706	0.052624	0.23453	0.039468	0.033232
35	0.312645	0.052621	0.234484	0.039466	0.033234
40	0.312613	0.05262	0.23446	0.039465	0.033238
45	0.312594	0.052619	0.234445	0.039464	0.033242

Table B.7: Convergence of different coefficients as N_t increases. $\alpha = 0.1\pi$, $h/a = 2$, $d/a = 0.4$, $ka = 1.09$, $N_l = 1500$, $N_p = 3$ and $N_m = 4$

N_t	$\|A00\|$	$\|B01\|$	$\|C20\|$	$\|\eta/A_0\|$	$\|\Gamma\|$
20	0.001437	1E-04	0.001078	7.5E-05	3.1E-05
30	0.000206	1.2E-05	0.000154	9E-06	3.1E-05
35	6.1E-05	3E-06	4.6E-05	2E-06	2E-06
40	3.2E-05	1E-06	2.4E-05	1E-06	4E-06
45	1.9E-05	1E-06	1.5E-05	1E-06	4E-06

Table B.8: Absolute error of different coefficients as N_m increases of 1. $\alpha = 0.1\pi$, $h/a = 2$, $d/a = 0.4$, $ka = 1.09$, $N_l = 1500$, $N_p = 3$ and $N_t = 5$

B.2 Tests of the accuracy

B.2.1 Energy conservation

First of all diffraction problem and radiation must satisfy the law of energy conservation.

Diffraction problem In this case, energy conservation is given by

$$2\mathrm{i}\cdot\mathrm{Im}\int\int_{S_\infty}\left(\phi_D\frac{\partial\phi_D^*}{\partial r}\right)dS=0 \tag{B.2.1}$$

Tables B.9 and B.10 gives the result for different test cases. As we can see, the energy is well conserved.

kh	4.94	3.17	2.24	1.72
$2\mathrm{i}\cdot\mathrm{Im}\int\int_{S_\infty}\left(\phi_D\frac{\partial\phi_D^*}{\partial r}\right)dS$	$3.21\cdot10^{-4}$	$-6.38\cdot10^{-7}$	$3.15\cdot10^{-3}$	$3.40\cdot10^{-3}$

Table B.9: Energy conservation for radiation problem. For all cases $h/a=2$ and $d/a=0.4$ and $\alpha=\pi/3$

kh	4.94	3.17	2.24	1.72
$2\mathrm{i}\cdot\mathrm{Im}\int\int_{S_\infty}\left(\phi_D\frac{\partial\phi_D^*}{\partial r}\right)dS$	$4.02\cdot10^{-4}$	$-1.03\cdot10^{-5}$	$4.43\cdot10^{-3}$	$4.62\cdot10^{-3}$

Table B.10: Energy conservation for radiation problem. For all cases $h/a=2$ and $d/a=0.4$ and $\alpha=\pi/4$

Radiation problem Energy conservation is given by equation (2.3.32). Taking $\nu=3/2$ gives in particular

$$\mathrm{Re}\left(\int\int_{S_\infty}-i\left(\phi_o\frac{\partial\phi_o^*}{\partial r}\right)rd\theta dz\right)=-\mathrm{Re}\left(\int_0^{3\pi/2}\int_0^a\left(\frac{P}{\rho\omega}\frac{\partial\phi_C}{\partial z}\right)\Big|_{z=0}rdrd\theta\right) \tag{B.2.2}$$

which can also be written in the form given in equation (2.3.40):

$$\tilde{\mathcal{B}}=3\frac{\sqrt{g/h}}{\omega}\sum_{n=0}^{\infty}\frac{|E_{n0}|^2}{\epsilon_n\left|k_0aK_{2n}'(k_0a)\right|^2} \tag{B.2.3}$$

Table B.11 summarizes the results for the test cases. It shows that the energy is well conserved.

kh	4.94	3.17	2.21	1.72
$\widetilde{B}$	0.1602	0.9454	4.6855	2.4375
$3\frac{\sqrt{g/h}}{\omega}\sum_{n=0}^{\infty}\frac{\lvert E_{n0}\rvert^2}{\epsilon_n\lvert k_0 a K'_{2n}(k_0 a)\rvert^2}$	0.1602	0.9454	4.6855	2.4375

Table B.11: Energy conservation for radiation problem. For all cases $a/h = 1/2$ and $d/a = 0.4$

B.2.2 Limiting cases

The diffraction problem can be tested in two limiting cases. First the analytical expression of the potential for the case of a cylinder extending to the bottom is known and given in appendix A. Thus the model can be tested for $d/h \rightarrow 1$.

Figure B-1a shows the comparison of the free surface elevation average along the cylinder outside the chamber for a value of d/h near to 1 with the theoretical solution. There is a very good agreement.

The program can also be tested as $ka \rightarrow 0$. Indeed the theoretical solution of a wedge of $\pi/2$ is also well known and is given by Stoker (1958). Figure B-1b presents the comparison of the free surface elevation along the cylinder outside the chamber for a small value of ka with the solution of a wedge with no cylinder. Agreement is excellent.

B.2.3 Reciprocity identity

As shown by Evans (Reference) for an OWC, the radiation damping coefficient can be related to the vertical flux inside the chamber due to diffraction by the following relation. The demonstration can be find in annexe 2.4.

$$B = \frac{k}{8\pi C_g \rho_\omega g}\int_0^{3\pi/2} \lvert\Gamma(\alpha)\rvert^2 \, d\alpha \tag{B.2.4}$$

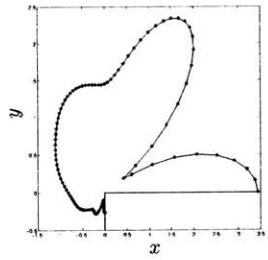

(a) Limiting case of a cylinder extending to the bottom

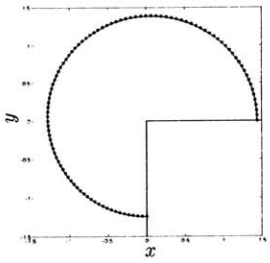

(b) Limiting case of a wedge with no cylinder

Figure B-1: Polar graph of the free surface elevation along the cylinder ($r = a$) outside the chamber. Left: convergence toward the theoretical solution of a cylinder extending to the bottom (plain) as d/h tends to 1: $d/h = 0.99$ (marquers), $ka = 3.23$. Right: convergence toward the theoretical solution of a wedge with no cylinder (plain) as ka tends to 0: $ka = 0.5$ (dots). In all cases $a/h = 2$ and $\alpha = \pi/3$

wich can be written with dimensionless variables as:

$$\widetilde{B} = \frac{kh^2\sqrt{g/h}}{8\pi C_g} \int_0^{3\pi/2} \left|\widetilde{\Gamma}(\alpha)\right|^2 d\alpha \tag{B.2.5}$$

Table B.12 shows the results for this relation for different random cases. We can notice that the relative error is always under 1%.

kh	8.77	6.45	4.94	2.24
$\widetilde{B}$	0.008475	0.1399	1.1283	4.6227
$\frac{kh^2\sqrt{g/h}}{8\pi C_g} \int_0^{3\pi/2} \left\|\widetilde{\Gamma}(\alpha)\right\|^2 d\alpha$	0.008464	0.1402	1.1290	4.6554
$\frac{\left\|\tilde{B} - \frac{kh^2\sqrt{g/h}}{8\pi C_g} \int_0^{3\pi/2} \left\|\widetilde{\Gamma}(\alpha)\right\|^2 d\alpha\right\|}{\tilde{B}} \cdot 100$	0.1256	0.224	0.0612	0.706

Table B.12: Reciprocal relation. For all cases $h/a = 2$ and $d/a = 0.4$

Appendix C

General form of the potential in a channel

We consider a rectangular channel along the axis x. The wall are vertical, and located at $y = \pm c$. Let us denote by Ω_f the fluid domain and S_f the free surface. We follow Malmo and Reitan (1985) and consider an incoming wave arriving from $x = +\infty$. Its potential can be written in the following form [1]:

$$\phi_i = \mathrm{Re}\left\{ -\frac{igA_0}{\omega} e^{-ikx} \frac{\cosh(k(z+h))}{\cosh(kh)} \right\} \tag{C.0.1}$$

We shall use the following dimensionless variables:

$$\begin{aligned} x_i &= hx_i', & t &= t'\sqrt{\frac{h}{g}}, & \eta &= A_0\eta' \\ \phi &= A_0\sqrt{gh}\phi', & kh &= k', & a_i &= ha_i' \end{aligned} \tag{C.0.2}$$

With this variables, the incident wave is given by

$$\phi_i' = \frac{1}{i\omega'} e^{-ik'x'} \frac{\cosh(k'(z'+1))}{\cosh(k')} \tag{C.0.3}$$

[1] In what follows, the symbol Re will be omitted.

For simplicity we will omit the prime symbol from now on and if nothing is specified, all the variables are dimensionless. The general equations for the fluid are:

$$\Delta\phi = 0, \qquad \boldsymbol{x} \in \Omega_f \tag{C.0.4a}$$

$$\frac{\partial\phi}{\partial z} - \omega^2\phi = 0, \qquad \text{on } S_f \tag{C.0.4b}$$

$$\frac{\partial\phi}{\partial z} = 0, \qquad z = -1 \tag{C.0.4c}$$

$$\frac{\partial\phi}{\partial y} = 0, \qquad y = \pm c \tag{C.0.4d}$$

The solution is the summ of the incident potential and the scattered potential: $\phi = \phi_i + \phi_s$. All the walls being vertical, the problem can be reduced to a 2-D problem by writing

$$\phi_s = \frac{1}{\mathrm{i}\omega}\eta(x,y)\frac{\cosh(k'(z'+1))}{\cosh(k')} \tag{C.0.5}$$

where $\eta(x,y)$ satisfies

$$\left(\frac{\partial^2}{\partial x^2} + \frac{\partial^2}{\partial y^2} + k^2\right)\eta = 0 \tag{C.0.6a}$$

$$\frac{\partial\phi}{\partial y} = 0, \qquad y = \pm c \tag{C.0.6b}$$

In order to find a solution to this problem, we proceed by separation of variables. Let us look for a solution of the form

$$\eta(x,y) = e^{-\nu x}V(y) \tag{C.0.7}$$

Equation (C.0.6a) implies thus that $V(y)$ verifies

$$V''(y) + (\nu^2 + k^2)V(y) = 0 \tag{C.0.8}$$

which implies

$$V(y) = A\cos\left(\sqrt{\nu^2+k^2}y\right) + B\sin\left(\sqrt{\nu^2+k^2}y\right) \tag{C.0.9}$$

Pluging this expression into (C.0.4d) imposes

$$-A\sin\left(\sqrt{\nu^2+k^2}c\right)+B\cos\left(\sqrt{\nu^2+k^2}c\right)=0 \tag{C.0.10a}$$

$$A\sin\left(\sqrt{\nu^2+k^2}c\right)+B\cos\left(\sqrt{\nu^2+k^2}c\right)=0 \tag{C.0.10b}$$

For this system to have a non trivial solution its determinant must be equal to zero.

$$\begin{vmatrix} -\sin\left(\sqrt{\nu^2+k^2}c\right) & \cos\left(\sqrt{\nu^2+k^2}c\right) \\ \sin\left(\sqrt{\nu^2+k^2}c\right) & \cos\left(\sqrt{\nu^2+k^2}c\right) \end{vmatrix}=0 \tag{C.0.11}$$

wich implies succesively

$$\sin\left(\sqrt{\nu^2+k^2}c\right)\cos\left(\sqrt{\nu^2+k^2}c\right)=0 \tag{C.0.12}$$

$$\Rightarrow \sin\left(2c\sqrt{\nu^2+k^2}\right)=0 \tag{C.0.13}$$

$$\Rightarrow 2c\sqrt{\nu_q^2+k^2}=q\pi, \quad q\in \tag{C.0.14}$$

Thus finally

$$\nu_q=\begin{cases} -i\sqrt{k^2-\left(\frac{q\pi}{2c}\right)^2}, & \text{if} \quad q<\frac{2kc}{\pi} \\ \sqrt{\left(\frac{q\pi}{2c}\right)^2-k^2} & \text{otherwise} \end{cases} \tag{C.0.15}$$

where the sign of the square root has be chosen so that $e^{-\nu_q x}$ is outgoing for x going to $+\infty$ if ν_q is real or corresponds to a plane wave progessing in the direction of positive x if ν_q is imaginary.

When q is even the system defined by equations (C.0.10) gives then $B=0$ and thus

$$V_q(y)=\alpha_q\cos\left(\frac{\pi q}{2c}y\right) \tag{C.0.16}$$

When q is odd, the system imposes $A=0$ and thus

$$V_q(y)=\alpha_q\sin\left(\frac{\pi q}{2c}y\right) \tag{C.0.17}$$

Expression of the solution Let us recall the result we have obatin so far. With the previous analysis we have found that the solution of the problem can be expressed in the following way:

$$\phi = -\frac{1}{\mathrm{i}\omega}\frac{\cosh(k(z+1))}{\cosh(k)}\left(e^{-ikx} + \sum_{q=0}^{\infty}\alpha_q e^{-\nu_q x}V_q(y)\right) \tag{C.0.18}$$

where

$$V_{2q}(y) = \cos\left(\frac{2q\pi}{2c}y\right) \tag{C.0.19a}$$

$$V_{2q+1}(y) = \sin\left(\frac{(2q+1)\pi}{2c}y\right) \tag{C.0.19b}$$

and

$$\nu_q = \begin{cases} -i\sqrt{k^2 - \left(\frac{q\pi}{2c}\right)^2}, & \text{if} \quad q < \frac{2kc}{\pi} \\ \sqrt{\left(\frac{q\pi}{2c}\right)^2 - k^2} & \text{otherwise} \end{cases} \tag{C.0.20}$$

Let us note that the sommation contains plane waves progessing in the direction of positive x. Let us also note that the y dependence of the scattered potential is a sum of functions either symmetric with respect to 0 for $V_q(y)$ or antisymmetric for $Y_q(y)$. This is represented on figure C-1.

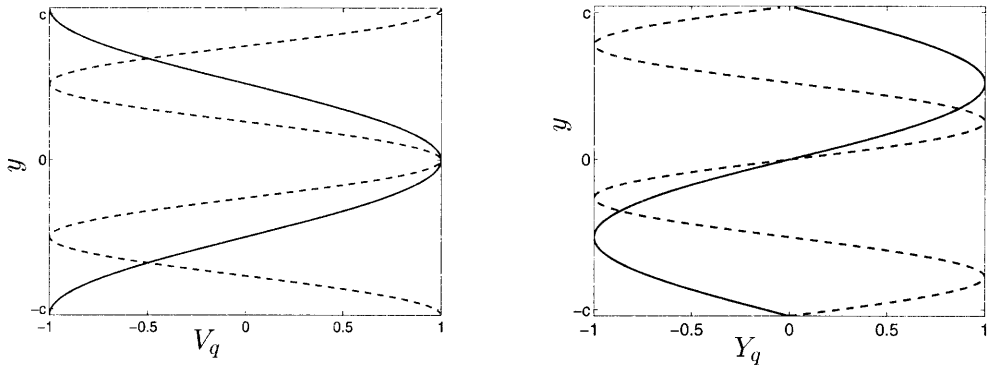

(a) V_2 (plain) and V_4 (dashed) (b) V_1 (plain) and V_3 (dashed)

Figure C-1: Function V_q for q=1,2,3,4

Bibliography

M. Abramowitz and I.A. Stegun. *Handbook of mathematical functions.* Dover Publications., 1964.

R. H. Charlier and C. W. Finkl. *Ocean Energy.* Springer Berlin Heidelberg, 2009.

D.V. Evans. Power from water waves. *Annual Review of Fluid Mechanics*, 13(1):157 – 187, 1981.

D.V. Evans. Wave-power absorption by systems of oscillating surface pressure ditributions. *Journal of Fluid Mechanics*, 114:481 – 499, 1982.

D.V. Evans. Maximum efficiency of wave-energy devices near coast lines. *Applied Ocean Research*, 10:162 – 164, 1988.

D.V. Evans and R. Porter. Hydrodynamic characteristics of an oscillating water column device. *Applied Ocean Research*, 17:155 – 164, 1995.

D.V. Evans and R. Porter. Efficient calculation of hydrodynamic properties of owc-type devices. *Journal of Offshore Mechanics and Arctic Engineering*, 119:210 – 218, 1997.

A.F. Falcão. The shoreline owc power plant at the azores. In 4^{th} *European Wave Energy Conference*, Aalbord, Denmark, 2000.

A.C. Fernandes. *Analysis of an Axisymmetric Pneumatic Buoy by Reciprocity Relations and a Ring-source Method.* PhD thesis, Massachusetts Institute of Technology, Department of Ocean Engineering, 1983.

X. Garnaud. Wave emergy extraction from buoys. Master's thesis, Massachusetts Institute of Technology, 2009.

I.S. Gradshteyn and I.M. Ryzhik. *Table of Integrals, Series and Products.* Academic Press, 1965.

E. Hairer, S.P. Norsett, and G. Wanner. *Solving ordinary differential equations I: Nonstiff problems.* Springer, 1993.

P. Haren. Optimal design of hagen-cockerell raft. Master's thesis, Massachusetts Institute of Technology, 1978.

A. Iserles. *A First Course in the Numerical Analysis of Differential Equations.* Cambridge University Press, 1996.

D.C. Handscomb J.C. Mason. *Chebyshev polynomials.* Chapman & Hall/CRC, 2003.

C.M. Linton and D.V. Evans. The interaction of waves with arrays of vertical circular cylinders. *Journal of Fluid Mechanics*, 215:549 – 569, 1990.

C.M. Linton and D.V. Evans. The radiation and scattering of surface waves by a vertical circular cylinder in a channel. *Philosophical Transactions: Physical Sciences and Engineering*, 338:325 – 357, 1992a.

C.M. Linton and D.V. Evans. Integral equations for a class of problems concerning obstacles in waveguides. *Journal of Fluid Mechanics*, 245:349–365, 1992b.

O. Malmo and A. Reitan. Wave-power absorption by an oscillating water column in a channel. *Journal of Fluid Mechanics*, 158:153 – 175, 1985.

H. Martin-Rivas and C.C. Mei. Wave power extraction from an oscillating water column at the tip of a breakwater. *Journal of Fluid Mechanics*, 626:395–414, 2008.

H. Martin-Rivas and C.C. Mei. Wave power extraction from an oscillating water column along a straight coast. *Ocean Engineering*, 36:426–433, 2009.

E. Martins, F. Siveira Ramos, L. Carrilho, P. Justino, L. Gato, L. Trigo, and F. Neumann. Ceodouros project: overall design of an owc in the new oporto breakwater. In 6^{th} *European Wave and Tidal Energy Conference*, Glasgow, UK, 2005.

M.E. McCormick. *Ocean Wave Energy Conversion.* New York, Wiley-Interscience, 1981.

C.C. Mei, M. Stiassnie, and D.K.P. Yue. *Theory and applications of ocean surface waves. Part 1: Linear Aspects.* World Scientific, 2005.

F. Neumann, V. Winands, and A.J.N.A. Sarmento. Pico shoreline owc: status and new perspectives. In *2nd International Conference on Ocean Energy (ICOE 2008)*, Brest, France, 2008.

R. Porter and D.V. Evans. Complementary approximations to wave scattering by vertical barriers. *Journal of Fluid Mechanics*, 294:155 – 180, 1995.

S.H. Salter. The architecture of nodding duck wave power generators. *The Naval Architect*, January:21 – 24, 1976.

A.J.N.A. Saramento and A.F.de O. Falcao. Wave generation by an oscillating surface-pressure and its application in wave-energy extraction. *Journal of Fluid Mechanics*, 150:467 – 485, 1985.

C.M. Smith. *Some problems in linear water waves.* PhD thesis, University of Bristol, 1958.

B.H. Spring and P.L. Monkmeyer. Interaction of plane waves with vertical cylinders. *Proc. 14th Intl Conf. on Coastal Engineering*, pages 1828–1845, 1974.

J.J. Stoker. *Water waves.* Wiley-Interscience, 1958.

R.C. Thorne. Multipole expansions in the theory of surface waves. *Proc. Cambridge. Phil.Soc.*, 49:707–716, 1953.